MALATYA TURGUT ÖZAL UNIVERSITY

NATURENGS

MTU Journal of Engineering and Natural Sciences

Volume: 2 Issue: 1 - June 2021

https://dergipark.org.tr/tr/pub/naturengs

www.naturengs.com

MALATYA TURGUT ÖZAL UNIVERSITY

NATURENGS

MTU Journal of Engineering and Natural Sciences

Volume: 2 / Issue: 1 / June - 2021

We are delighted to present the second volume of the journal NATURENGS owned by Malatya Turgut Özal University. MTU Journal of Engineering and Natural Sciences – NATURENGS is a double- blind peer-reviewed, open-access international journal which will publish electronically two times in a year by the Malatya Turgut Özal University from June 2020.

We set out with the desire to create an environment where scientific and/or technological studies carried out in universities, industry and other research institutions will be shared. We aim to advance by giving priority to studies involving scientific and / or technological originality.

Manuscripts submitted for publication are analyzed in terms of scientific quality, ethics and research methods in terms of its compliance by the Editorial Board representatives of the relevant areas. Then, the abstracts of the appropriate articles are sent to at least two different referees with a well-known in scientific area. If the referees agree to review the article, full text in the framework of the privacy protocol is sent. By the decisions of referees, either directly or corrected article is published or rejected. Confidential reports of the referees in the journal archive will be retained for ten years. All post-evaluation process is done electronically on the internet.

In the journal's publication policy, we would like to state that we will not compromise on quality. In this process, we know that we have undertaken important tasks, especially the selection of referees and monitoring of evaluations. Our journal is indexed in *Index Copernicus, CiteFactor, Scientific Indexing Services, ASOS, DRJI, ESJI* and *ASI* international databases. We will work with the devotion to get our journal into the TR-Index and then the Science Citation Index database as soon as possible.

We would like to thanks our Rector, Prof. Dr. Aysun Bay KARABULUT, who encouraged and supported the establishment of our journal. In addition, we would like to thank all the Authors and Referees who contributed to this issue.

Assist. Prof. Aydan AKSOĞAN KORKMAZ
On behalf of the Editorial Board

MALATYA TURGUT ÖZAL UNIVERSITY

NATURENGS

MTU Journal of Engineering and Natural Sciences

Volume: 2 / Issue: 1 / June- 2021

ISSN: 2717-8013

Contact Information

MTU Journal of Engineering and Natural Sciences – NATURENGS,

Malatya Turgut Özal University, 44210, Battalgazi/Malatya, TURKEY

Phone: +90-422 846 12 55, Fax: +90-422 846 12 25,

e-mail: naturengs@ozal.edu.tr

web: https://dergipark.org.tr/tr/pub/naturengs

MALATYA TURGUT ÖZAL UNIVERSITY

NATURENGS

MTU Journal of Engineering and Natural Sciences

Volume: 2 / Issue: 1 / June- 2021

ISSN: 2717-8013

MTU Journal of Engineering and Natural Sciences – NATURENGS
Volume: 2 / Issue: 1 / June - 2021

CONTENTS

Some Inequalities on Half Lightlike Submanifolds of a Lorentzian Manifold with Semi-Symmetric Metric Connection
Nergiz (ÖNEN) POYRAZ, Burçin DOĞAN……. 1

Determination of Breakfast Habits of Health School Students and the Factors Affecting Them: Bitlis Eren University Example
Mustafa Şamil ARGUN, Betül ZANLIER……. 15

A Computational Method Based on Interval Length for Fuzzy Time Series Forecasting
Özlem AKAY……. 22

Numerical Analysis of Geotechnical Seismic Isolation System for High-Rise Buildings
Özgür YILDIZ……..... 34

Attitudes Towards Vaccines And Intention to Vaccinate Against Covid-19: A Statistical Analysis
Burcu Özcan, Edanur Yıldırak, Zeynep Aksoy…….. 44

The Usage of Mg - Metal Chlorides in Hydrogen Generation
Begüm Esra AYTAŞ, Sevim YOLCULAR KARAOĞLU……. 60

Microfluidic Technology and Biomedical Field
Zülfü TÜYLEK…….. 74

Non-linear and Equivalent Linear Site Response Analysis of Istanbul Soils
Özgür YILDIZ……. 88

NATURENGS
MTU Journal of Engineering and Natural Sciences
https://dergipark.org.tr/tr/pub/naturengs
DOI: 10.46572/naturengs.881981

Research Article

Some Inequalities on Half Lightlike Submanifolds of a Lorentzian Manifold with Semi-Symmetric Metric Connection

Nergiz (ÖNEN) POYRAZ[1], Burçin DOĞAN[2*]

[1] Department of Mathematics, Faculty of Arts and Sciences, Çukurova University, Adana, Turkey.
[2*] Department of Engineering Basic Science, Faculty of Engineering and Natural Sciences, Malatya Turgut Özal University, Malatya, Turkey.

(**Received:** 17.02.2021; **Accepted:** 24.02.2021)

ABSTRACT: In this paper, we introduce some inequalities for screen homothetic half lightlike submanifolds of a real space form $\tilde{M}(c)$ of constant sectional curvature c, endowed with the semi-symmetric metric connection. Using these inequalities, we derive some characterizations for such half lightlike submanifolds. Finally, Chen-Ricci inequalities are calculated. Moreover, the equality cases are considered and we get some results.

Keywords: Chen inequalities, Half lightlike submanifold, Lorentzian manifold, Semi-symmetric metric connection.

1. INTRODUCTION

Lightlike geometry has applications in mathematical physics and because of this, it is an important research field in differential geometry. Kupeli initiated the geometry of lightlike submanifolds in [1]. Then Duggal and Bejancu developed it [2]. Moreover, many authors studied it [3,4].

A semi-symmetric linear connection on a differentiable manifold is presented in [5], the geometers studied it in [6] and [7]. Then, in [8] and [9], the geometry of a Riemannian manifold and a hypersurface of a Riemannian manifold with a semi-symmetric metric connection was investigated by Imai. The studies on Riemannian, semi-Riemannian, and Lorentzian manifolds with semi-symmetric metric connections belong to Nakao [10], Duggal-Sharma [11], and Konar-Biswas [12], respectively. Lightlike hypersurfaces of a semi-Riemannian manifold with a semi-symmetric metric connection were introduced in [13]. Later, Akyol, Vanlı, and Fernandez investigated the geometry of such connection on S manifolds in [14].

In addition to these, Chen introduced Chen inequalities and defined new types of curvature invariants in [15], and then, many authors worked on this topic [16-23]. Chen inequalities on submanifolds with constant and quasi-constant curvature with a semi-symmetric metric connection were studied in [24] and [25], respectively.

Firstly Chen inequalities on lightlike geometry were worked by Gülbahar, Kılıç, and Keleş in

*Corresponding Author: burcin.dogan@ozal.edu.tr
ORCID number of authors: [1] 0000-0002-8110-712X, [2] 0000-0001-8386-213X

[26] and [27]. Then Poyraz, Doğan, and Yaşar studied Chen inequalities on the lightlike hypersurface of a Lorentzian manifold with a semi-symmetric metric connection in [28]. Some inequalities for screen conformal half lightlike submanifolds were established by Gülbahar and Kılıç in [29].

In this study, we introduce some inequalities for screen homothetic half lightlike submanifolds of a real space form $\tilde{M}(c)$ endowed with the semi-symmetric metric connection. Using these inequalities, we derive some characterizations for such half lightlike submanifolds. Finally, Chen-Ricci inequalities are calculated. Moreover, the equality cases are considered and we get some results.

2. PRELIMINARIES

Let $(\tilde{M},\tilde{g})$ be a semi-Riemannian manifold. A connection $\tilde{\nabla}$ $\tilde{M}$ is called a semi-symmetric metric connection if it is metric, i.e., $\tilde{\nabla}\tilde{g}=0$ and its torsion tensor $\tilde{T}$ satisfies

$$\tilde{T}(\tilde{X},\tilde{Y})=\tilde{\pi}(\tilde{Y})\tilde{X}-\tilde{\pi}(\tilde{X})\tilde{Y} \tag{2.1}$$

for any vector fields $\tilde{X}$ and $\tilde{Y}$ of $\tilde{M}$, where $\tilde{\pi}$ is a 1-form defined by

$\tilde{g}(\tilde{P},\tilde{X})=\tilde{\pi}(\tilde{X})$

and $\tilde{P}$ is a vector field on $\tilde{M}$, which is called the torsion vector field.

Let $\tilde{M}$ be a semi-Riemannian manifold admits a semi-symmetric metric connection which is given by

$$\tilde{\nabla}_{\tilde{X}}\tilde{Y}=\overset{\circ}{\tilde{\nabla}}_{\tilde{X}}\tilde{Y}+\tilde{\pi}(\tilde{Y})\tilde{X}-\tilde{g}(\tilde{X},\tilde{Y})\tilde{P} \tag{2.2}$$

for any $\tilde{X},\tilde{Y}\in\Gamma(T\tilde{M})$, where $\overset{\circ}{\tilde{\nabla}}$ is the Levi-Civita connection concerning the semi-Riemannian metric $\tilde{g}$ [7].

Let $(\tilde{M},\tilde{g})$ be a $(n+3)-$dimensional semi-Riemannian manifold of the index $q\geq 1$ and M be a lightlike submanifold of codimension 2 of $\tilde{M}$. Then the radical distribution $Rad(TM)=TM\cap TM^{\perp}$ M is a vector subbundle of TM and the $TM^{\perp}$ of rank 1 or 2. If $rank(Rad(TM))=1$, then M is called half lightlike submanifold of $\tilde{M}$. Then there exist complementary non-degenerate distributions $S(TM)$ and $S(TM^{\perp})$ of $Rad(TM)$ in TM and $TM^{\perp}$, which are named the screen and the screen transversal distribution on M, respectively. Hence we derive

$$TM=Rad(TM)\perp S(TM),\ TM^{\perp}=Rad(TM)\perp S(TM^{\perp}). \tag{2.3}$$

Consider the orthogonal complementary distribution $S(TM)^{\perp}$ to $S(TM)$ in $T\tilde{M}$. Then ξ and L belong to $\Gamma(S(TM)^{\perp})$. Hence we obtain

$$S(TM)^{\perp}=S(TM^{\perp})\perp S(TM^{\perp})^{\perp}, \tag{2.4}$$

where $S(TM^{\perp})^{\perp}$ is the orthogonal complementary to $S(TM^{\perp})$ in $S(TM)^{\perp}$. For any null section $\xi\in Rad(TM)$ on a coordinate neighborhood $U\subset M$, there exists a uniquely determined null vector field $N\in\Gamma(ltr(TM))$ holding

$$\tilde{g}(N,\xi)=1,\quad \tilde{g}(N,N)=\tilde{g}(N,X)=\tilde{g}(N,L)=0,\ \forall X\in\Gamma(TM). \tag{2.5}$$

We say $ltr(TM)$ and $tr(TM) = S(TM^{\perp}) \perp ltr(TM)$ the lightlike transversal vector bundle and transversal vector bundle M for $S(TM)$, respectively. Hence we have

$$\begin{aligned} T\tilde{M} &= TM \oplus tr(TM) \\ &= \{Rad(TM) \oplus ltr(TM)\} \perp S(TM) \perp S(TM^{\perp}). \end{aligned} \tag{2.6}$$

Using (2.6) we define the projection morphism $Q : \Gamma(TM) \to \Gamma(S(TM))$. Hence we have

$$\tilde{\nabla}_X Y = \nabla_X Y + B(X,Y)N + D(X,Y)L, \tag{2.7}$$

$$\tilde{\nabla}_X U = -A_U X + \nabla^t_X U, \tag{2.8}$$

$$\tilde{\nabla}_X N = -A_N X + \tau(X)N + \rho(X)L, \tag{2.9}$$

$$\tilde{\nabla}_X L = -A_L X + \psi(X)N, \tag{2.10}$$

$$\nabla_X QY = \nabla^*_X QY + C(X,QY)\xi, \tag{2.11}$$

$$\nabla_X \xi = -A^*_\xi X - \tau(X)\xi, \tag{2.12}$$

for any $X, Y \in \Gamma(TM)$, $\xi \in \Gamma(Rad(TM))$, $U \in \Gamma(tr(TM))$, $N \in \Gamma(ltr(TM))$ and $L \in \Gamma(S(TM^{\perp}))$.

Then ∇ and ∇^* are named induced linear connections on TM and $S(TM)$ respectively, B and D are named the local second fundamental forms of M, C is named the local second fundamental form on $S(TM)$. A_N, A^*_ξ and A_L are named linear operators on TM. Also τ, ρ and ψ are named $1-$forms on TM.

This ∇ is not a metric connection and holds

$$(\nabla_X g)(Y,Z) = B(X,Y)\eta(Z) + B(X,Z)\eta(Y), \tag{2.13}$$

for any $X, Y, Z \in \Gamma(TM)$, where η is a $1-$form defined by

$$\eta(X) = \tilde{g}(X,N), \ \forall X \in \Gamma(TM). \tag{2.14}$$

But ∇^* is a metric connection. Using (2.1) and (2.13), we see that

$$T(X,Y) = \pi(Y)X - \pi(X)Y \tag{2.15}$$

and B and D are symmetric, where T is the torsion tensor for ∇. From (2.13) and (2.15), we see that ∇ is a semi-symmetric non-metric connection of M. Moreover, B and D are independent of the choice of $S(TM)$ and hold

$$B(X,\xi) = 0, \ D(X,\xi) = -\varepsilon\psi(X), \forall X \in \Gamma(TM). \tag{2.16}$$

Therefore one obtains

$$B(X,Y) = g(A^*_\xi X, Y), \quad g(A^*_\xi X, N) = 0, \tag{2.17}$$

$$C(X,QY) = g(A_N X, QY), \quad g(A_N X, N) = 0, \tag{2.18}$$

$$D(X,QY) = g(A_L X, QY), \quad g(A_L X, N) = \rho(X), \tag{2.19}$$

$$D(X,Y) = g(A_L X, Y) - \psi(X)\eta(Y), \ \forall X, Y \in \Gamma(TM). \tag{2.20}$$

By (2.17) and (2.18), A^*_ξ and A_N are $\Gamma(S(TM))-$valued shape operators related to B and E, respectively and $A^*_\xi \xi = 0$.

Using (2.7), (2.12), and (2.16), one derives

$$\tilde{\nabla}_X \xi = -A^*_\xi X - \tau(X)\xi - \varepsilon\psi(X)L, \tag{2.21}$$

for any $X \in \Gamma(TM)$.

Definition 1. *A half lightlike submanifold* (M,g) *of a semi-Riemannian manifold* $(\tilde{M},\tilde{g})$ *is named irrotational [1] if* $\tilde{\nabla}_X\xi\in\Gamma(TM)$ *for any* $X\in\Gamma(TM)$. *From (2.16) and (2.21), the definition of irrotational is equivalent to the condition* $\psi(X)=0$, *that is,* $D(X,\xi)=0$ *for any* $X\in\Gamma(TM)$.

Definition 2. *A half lightlike submanifold* (M,g) *of a semi-Riemannian manifold* $(\tilde{M},\tilde{g})$ *is called umbilical in* $\tilde{M}$ *if there is a smooth vector field* $H\in\Gamma(tr(TM))$ *on any coordinate neighborhood* U *such that*

$$h(X,Y)=Hg(X,Y) \tag{2.22}$$

for any $X,Y\in\Gamma(TM)$, *where*

$$h(X,Y)=B(X,Y)N+D(X,Y)L \tag{2.23}$$

is the global second fundamental form tensor of M. *In the case of* $h=0$ *on* U, *we call that* M *is totally geodesic [30].*

Besides, M is totally umbilical iff, on each coordinate neighborhood U, there exist smooth vector functions λ and δ such that

$$B(X,Y)=\lambda g(X,Y), D_2(X,Y)=\delta g(X,Y), \tag{2.24}$$

for any $X,Y\in\Gamma(TM)$.

Definition 3. *[30] The screen distribution* $S(TM)$ *of* M *is named totally umbilical if there is a smooth function* γ *on any coordinate neighborhood* $U\subset M$ *such that*

$$E(X,QY)=\gamma g(X,Y), \tag{2.25}$$

for any $X,Y\in\Gamma(TM)$. *If* $\gamma=0$ *on* U, *then we say that* $S(TM)$ *is totally geodesic in* M.

Furthermore, $(M,g,S(TM))$ is named minimal if $\psi(X)=0$ and

$$trace_{S(TM)}h=0, \tag{2.26}$$

where $trace_{S(TM)}$ denotes the trace restricted to $S(TM)$ concerning the degenerate metric g [31].

Let $(M,g,S(TM))$ be a $(n+1)-$dimensional half-lightlike submanifold and $\{e_1,...,e_n\}$ be an orthonormal basis of $\Gamma(S(TM))$. Let us consider

$$\mu_1=\frac{1}{n}\sum_{j=1}^{n}B(e_j,e_j),\ \mu_2=\frac{1}{n}\sum_{j=1}^{n}D(e_j,e_j). \tag{2.27}$$

Then it is clear from (2.26) and (2.27) that M is minimal iff $\mu_1=\mu_2=0$.

A lightlike hypersurface (M,g) of a semi-Riemannian manifold $(\tilde{M},\tilde{g})$ is called *screen locally conformal* if the shape operators A_N and A_ξ^* of M and $S(TM)$, respectively, are related by

$$A_N=\phi A_\xi^*, \tag{2.28}$$

i.e.,

$$C(X,PY)=\phi B(X,Y),\ \forall X,Y\in\Gamma(TM), \tag{2.29}$$

where ϕ is a non-vanishing smooth function on a neighborhood U in M. If ϕ is a non-zero constant, M is named screen homothetic [32].

We denote $\tilde{R}$, R and R^* the curvature tensors of the semi-symmetric metric connection of $\tilde{\nabla}$, ∇ and ∇^*, respectively.

Using (2.7)-(2.12) for M and $S(TM)$, we derive:

$$\begin{aligned}\tilde{g}(\tilde{R}(X,Y)Z,QW) &= g(R(X,Y)Z,QW)\\ &\quad +B(X,Z)C(Y,QW)-B(Y,Z)C(X,QW)\\ &\quad +D(X,Z)D(Y,QW)-D(Y,Z)D(X,QW),\end{aligned} \tag{2.30}$$

$$\begin{aligned}\tilde{g}(\tilde{R}(X,Y)Z,\xi) &= (\nabla_X B)(Y,Z)-(\nabla_Y B)(X,Z)\\ &\quad +[\tau(X)-\pi(X)]B(Y,Z)-[\tau(Y)-\pi(Y)]B(X,Z)\\ &\quad +\psi(X)D(Y,Z)-\psi(Y)D(X,Z),\end{aligned} \tag{2.31}$$

$$\begin{aligned}\tilde{g}(\tilde{R}(X,Y)Z,N) &= g(R(X,Y)Z,N)\\ &\quad +\rho(Y)D(X,Z)-\rho(X)D(Y,Z),\end{aligned} \tag{2.32}$$

$$\begin{aligned}\tilde{g}(\tilde{R}(X,Y)\xi,N) &= g(A^*_\xi X,A_N Y)-g(A^*_\xi Y,A_N X)\\ &\quad -2d\tau(X,Y)+\rho(X)\psi(Y)-\rho(Y)\psi(X),\end{aligned} \tag{2.33}$$

$$\begin{aligned}g(R(X,Y)QZ,QW) &= g(R^*(X,Y)Z,QW)+B(Y,QW)C(X,QZ)\\ &\quad -B(X,QW)C(Y,QZ),\end{aligned} \tag{2.34}$$

$$\begin{aligned}\tilde{g}(R(X,Y)QZ,N) &= (\nabla_X C)(Y,QZ)-(\nabla_Y C)(X,QZ)\\ &\quad +[\tau(Y)+\pi(Y)]C(X,QZ)-[\tau(X)+\pi(X)]C(Y,QZ),\end{aligned} \tag{2.35}$$

for any $X,Y,Z\in\Gamma(TM)$ [33].

Now let us choose a $2-$dimensional non-degenerate plane section

$$\Pi = Span\{X,Y\}, \tag{2.36}$$

in T_pM, $p\in M$. Then the sectional curvature at p is expressed by [34]

$$K(\Pi)=\frac{g(R(X,Y)Y,X)}{g(X,X)g(Y,Y)-g(X,Y)^2}. \tag{2.37}$$

Let $p\in M$ and ξ be the null vector of T_pM. A plane Π of T_pM is said to be null plane if it contains ξ and e_i such that $g(\xi,e_i)=0$ and $g(e_i,e_i)=\varepsilon_i=\pm 1$. The null sectional curvature of Π is defined by

$$K_i^{null}=\frac{g(R_p(e_i,\xi)\xi,e_i)}{g_p(e_i,e_i)}.$$

The Ricci tensor $\tilde{Ric}$ of $\tilde{M}$ and the induced Ricci type tensor $R^{(0,2)}$ of M are given by

$$\begin{aligned}\tilde{Ric}(X,Y) &= trace\{Z\to\tilde{R}(Z,X)Y\},\ \forall X,Y\in\Gamma(T\tilde{M}),\\ R^{(0,2)}(X,Y) &= trace\{Z\to R(Z,X)Y\},\ \forall X,Y\in\Gamma(TM),\end{aligned} \tag{2.38}$$

where

$$R^{(0,2)}(X,Y)=\sum_{i=1}^{n}\varepsilon_i g(R(e_i,X)Y,e_i)+\tilde{g}(R(\xi,X)Y,N) \tag{2.39}$$

for the quasi-orthonormal frame $\{e_1,...,e_n,\xi\}$ of T_pM. From the equations (2.30)-(2.33), it can be shown that the Ricci type tensor doesn't need to be symmetric as the sectional curvature map. This tensor is called Ricci tensor if it is symmetric.

One defines scalar curvature τ by

$$\tau(p)=\sum_{i,j=1}^{n}K_{ij}+\sum_{i=1}^{n}K_i^{null}+K_{iN}, \tag{2.40}$$

where $K_{iN} = \tilde{g}(R(\xi, e_i)e_i, N)$ for $i \in \{1,...,n\}$.

3. CHEN RICCI INEQUALITIES

Let M be a $(n+1)-$dimensional half lightlike submanifold of a $(n+3)-$dimensional of a Lorentzian manifold $\tilde{M}$ with a semi-symmetric metric connection and $\{e_1,....,e_n,\xi\}$ be a basis of $\Gamma(TM)$ where $\{e_1,....,e_n\}$ be an orthonormal basis of $\Gamma(S(TM))$. For $k \le n$, we establish $\pi_{k,\xi} = sp\{e_1,....,e_k,\xi\}$ is a $(k+1)-$dimensional degenerate plane section and $\pi_k = sp\{e_1,....,e_k\}$ is $k-$dimensional non-degenerate plane section. The $k-$degenerate Ricci curvature and the $k-$Ricci curvature are defined by

$$Ric_{\pi_{k,\xi}}(X) = R^{(0,2)}(X,X) = \sum_{j=1}^{k} g(R(e_j,X)X,e_j) + \widehat{g}(R(\xi,X)X,N), \tag{3.1}$$

$$Ric_{\pi_k}(X) = R^{(0,2)}(X,X) = \sum_{j=1}^{k} g(R(e_j,X)X,e_j), \tag{3.2}$$

respectively for a unit vector $X \in \Gamma(TM)$. Also, $k-$degenerate scalar curvature and $k-$scalar curvature at $p \in M$ are given by

$$\tau_{\pi_{k,\xi}}(p) = \sum_{i,j=1}^{k} K_{ij} + \sum_{i=1}^{k} K_i^{null} + K_{iN}, \tag{3.3}$$

$$\tau_{\pi_k}(p) = \sum_{i,j=1}^{k} K_{ij}, \tag{3.4}$$

respectively. For $k = n, \quad \pi_n = sp\{e_1,....,e_n\} = \Gamma(S(TM)),$ we have the screen Ricci curvature and the screen scalar curvature given by

$$Ric_{S(TM)}(e_1) = Ric_{\pi_n}(e_1) = \sum_{j=1}^{n} K_{1j} = K_{12} + ... + K_{1n}, \tag{3.5}$$

and

$$\tau_{S(TM)} = \sum_{i,j=1}^{n} K_{ij}, \tag{3.6}$$

respectively.

Let $\tilde{M}(c)$ be a real space form of constant sectional curvature c endowed with a semi-symmetric metric connection $\tilde{\nabla}$. The curvature tensor $\overset{\circ}{\tilde{R}}$ to the Levi-Civita connection $\overset{\circ}{\tilde{\nabla}}$ on $\tilde{M}(c)$ is defined by

$$\tilde{g}(\overset{\circ}{\tilde{R}}(X,Y)Z,QW) = c\{g(X,W)g(Y,Z) - g(Y,W)g(X,Z)\}. \tag{3.7}$$

Using (2.2), we derive

$$\begin{aligned}\tilde{g}(\tilde{R}(X,Y)Z,QW) = \tilde{g}(\overset{\circ}{\tilde{R}}(X,Y)Z,QW) - \alpha(Y,Z)g(X,W) + \alpha(X,Z)g(Y,W) \\ -\alpha(X,W)g(Y,Z) + \alpha(Y,W)g(X,Z),\end{aligned} \tag{3.8}$$

for any $X,Y,Z,W \in \Gamma(TM)$, where α is a $(0,2)$ tensor field defined by

$$\alpha(X,Y) = (\overset{\circ}{\tilde{\nabla}}_X \pi)Y - \pi(X)\pi(Y) + \frac{1}{2}\pi(Q)g(X,Y) \tag{3.9}$$

[8].

From (2.30), (3.6), (3.7), and (3.8), we can write

$$\tau_{S(TM)}(p) = n(n-1)c - 2(n-1)\lambda + \sum_{i,j=1}^{n} B_{ii}C_{jj} - B_{ij}C_{ji} + \sum_{i,j=1}^{n} D_{ii}D_{jj} - D_{ij}D_{ji}, \tag{3.10}$$

where λ is the trace of α and $B_{ij} = B(e_i, e_j)$, $C_{ij} = C(e_i, e_j)$, $D_{ij} = D(e_i, e_j)$ for $i, j \in \{1,...,n\}$.

Let M be a screen homothetic half lightlike submanifold of a $(n+3)-$dimensional Lorentzian space form $\tilde{M}(c)$. Using (2.29) and (3.10) we get

$$\tau_{S(TM)}(p) = n(n-1)c - 2(n-1)\lambda + \phi n^2\mu_1^2 + n^2\mu_2^2 - \sum_{i,j=1}^{n}[\phi(B_{ij})^2 + (D_{ij})^2]. \tag{3.11}$$

Lemma 4. *[35] Let $a_1,...,a_n$ be $n-$ real numbers and define $A = \sum_{i<j}(a_i - a_j)^2$. Then*

(1) $A \geq \frac{n}{2}(a_1 - a_2)^2$ and equality holds iff

$\frac{1}{2}(a_1 + a_2) = a_3 = ... = a_n.$

(2) Let k, ℓ be integers such that $1 \leq k < \ell \leq n$ and $(k,\ell) \neq (1,2)$. If $A = \frac{n}{2}(a_1 - a_2)^2 = \frac{n}{2}(a_k - a_1)^2$ then $a_1 = a_2 = ... = a_n$.

Theorem 5. *Let M be a $(n+1)-$dimensional screen homothetic half lightlike submanifold with $\phi > 0$ of a $(n+3)-$dimensional Lorentzian space form $\tilde{M}(c)$ endowed with a semi-symmetric metric connection $\tilde{\nabla}$. Then we obtain*

$$\begin{aligned}\tau_{S(TM)}(p) \leq\ & n(n-1)c - 2(n-1)\lambda + \frac{n^3}{n+1}\phi\mu_1^2 \\ & - \frac{\phi n}{2(n+1)}\sum_{i,j=1}^{n}(B_{11} - B_{22})^2 + \frac{n^3}{n+1}\mu_2^2 \\ & - \frac{n}{2(n+1)}\sum_{i,j=1}^{n}(D_{11} - D_{22})^2.\end{aligned} \tag{3.12}$$

The equality case of (3.12) satisfies at $p \in M$ iff

$$\mu_1 = \frac{n}{2}(B_{11} + B_{22})^2, \mu_2 = \frac{n}{2}(D_{11} + D_{22})^2 \tag{3.13}$$

and

$$B_{ij} = D_{ij} = 0, \text{ for } i \neq j \in \{1,...,n\}. \tag{3.14}$$

Proof. From the Binomial theorem, we can write

$$\begin{aligned}&(B_{11} - B_{22})^2 + ... + (B_{11} - B_{nn})^2 + (B_{22} - B_{33})^2 + ... + (B_{22} - B_{nn})^2 \\ &\quad + ... + (B_{n-1n-1} - B_{nn})^2 = n\sum_{i=1}^{n}(B_{ii})^2 - 2\sum_{i\neq j}^{n} B_{ii}B_{jj}.\end{aligned} \tag{3.15}$$

By Lemma 4 and (3.15) we obtain

$$\sum_{i=1}^{n}(B_{ii})^2 \geq \frac{1}{n}\sum_{i\neq j} B_{ii}B_{jj} + \frac{1}{2}(B_{11} - B_{22})^2. \tag{3.16}$$

We also can derive

$$\frac{2}{n}\sum_{i\neq j} B_{ii}B_{jj} = n\mu_1^2 - \frac{1}{n}\sum_{i=1}^{n}(B_{ii})^2. \tag{3.17}$$

Using (3.16) and (3.17) we get

$$\sum_{i=1}^{n}(B_{ii})^2 \geq \frac{n^2}{n+1}\mu_1^2 + \frac{n}{2(n+1)}(B_{11}-B_{22})^2. \tag{3.18}$$

Similarly, we obtain

$$\sum_{i=1}^{n}(D_{ii})^2 \geq \frac{n^2}{n+1}\mu_2^2 + \frac{n}{2(n+1)}(D_{11}-D_{22})^2. \tag{3.19}$$

Finally, using (3.18) and (3.19) in (3.11), we obtain (3.12).

Taking consideration of case (1) of Lemma 4, the equality of (3.12) holds at $p \in M$ iff (3.13) and (3.14) hold. The converse part of the theorem is straightforward.

Considering Theorem 5, we derive Corollary 6 and Corollary 7.

Corollary 6. *Let M be a $(n+1)-$dimensional screen homothetic half lightlike submanifold with $\phi > 0$ of a $(n+3)-$dimensional Lorentzian space form $\tilde{M}(c)$ endowed with a semi-symmetric metric connection $\tilde{\nabla}$. Then we have*

$$\begin{aligned}\tau_{S(TM)}(p) \leq\ & n(n-1)c - 2(n-1)\lambda + \frac{n^3}{n+1}\phi\mu_1^2 - \frac{\phi n}{2(n+1)}\sum_{i,j=1}^{n}(B_{ii}-B_{jj})^2 \\ & + \frac{n^3}{n+1}\mu_2^2 - \frac{n}{2(n+1)}\sum_{i,j=1}^{n}(D_{ii}-D_{jj})^2.\end{aligned} \tag{3.20}$$

The equality case of (3.20) satisfies for all $p \in M$ iff $S(TM)$ is a totally umbilical in M.

Corollary 7. *Let M be a $(n+1)-$dimensional irrotational screen homothetic half lightlike submanifold with $\phi > 0$ of a $(n+3)-$dimensional Lorentzian space form $\tilde{M}(c)$ endowed with a semi-symmetric metric connection $\tilde{\nabla}$. Then we have*

$$\begin{aligned}\tau_{S(TM)}(p) \leq\ & n(n-1)c - 2(n-1)\lambda + \frac{n^3}{n+1}\phi\mu_1^2 \\ & - \frac{\phi n}{2(n+1)}\sum_{i,j=1}^{n}(B_{ii}-B_{jj})^2 + \frac{n^3}{n+1}\mu_2^2 - \frac{n}{2(n+1)}\sum_{i,j=1}^{n}(D_{ii}-D_{jj})^2.\end{aligned} \tag{3.21}$$

The equality case of (3.21) holds for all $p \in M$ iff M is totally umbilical.

Lemma 8. *[15] If $n \geq 2$ and $a_1,...,a_n \in \mathbb{R}$ are real numbers such that*

$$\left(\sum_{i=1}^{n}a_i\right)^2 = (n-1)\left(\sum_{i=1}^{n}a_i^2 + a\right),$$

then

$2a_1a_2 \geq a$

with equality holding iff

$a_1 + a_2 = a_3 = ... = a_n.$

Theorem 9. *Let M be a $(n+1)-$dimensional screen homothetic half lightlike submanifold with $\phi > 0$ of a $(n+3)-$dimensional Lorentzian space form $\tilde{M}(c)$ endowed with a semi-symmetric metric connection $\tilde{\nabla}$ such that the vector field P is tangent to M and $\Pi = Span\{e_1, e_2\}$ be a $2-$dimensional non-degenerate plane section of T_pM, $p \in M$. Then we have*

$$\tau_{S(TM)}(p)-\tau(\Pi)\le(n-2)\left(\frac{\phi n^2}{n-1}\mu_1^2+(n+1)c-2\lambda\right)$$
$$-2trace(\lambda|_{\Pi^\perp})+B(\Pi^\perp)^2+^2 n^2\mu_2^2(\Pi^\perp) \tag{3.22}$$
$$+\sum_{j>2}^{n}D_{11}D_{jj}+D_{22}D_{jj}$$

where

$$B(\Pi^\perp)^2=\sum_{i=3}^{n}(B_{ii})^2 \text{ and } n^2\mu_2^2(\Pi^\perp)=\sum_{i,j=3}^{n}D_{ii}D_{jj}. \tag{3.23}$$

The equality case of (3.22) holds for all $p\in M$ *if* $\mu_1=0$, $\mu_2=D_{11}+D_{22}$ *and the shape operator* A_ξ^* *of* M

$$A_\xi^*=\begin{pmatrix}B_{11} & B_{12} & \dots & 0\\ B_{21} & B_{22} & \dots & 0\\ \\ 0 & 0 & \dots & 0\end{pmatrix}. \tag{3.24}$$

Proof. If

$$\delta=\tau_{S(TM)}(p)-n(n-1)c+2(n-1)\lambda-\phi n^2\frac{(n-2)}{n-1}\mu_1^2$$
$$-n^2\mu_2^2+\sum_{i,j=1}^{n}(D_{ij})^2 \tag{3.25}$$

is said, we derive

$$\delta=\phi\frac{n^2}{n-1}\mu_1^2-\phi\sum_{i,j=1}^{n}(B_{ij})^2. \tag{3.26}$$

Thus, we can derive

$$\left(\sum_{i=1}^{n}B_{ii}\right)^2=(n-1)\left(\frac{\delta}{\phi}+\sum_{i=1}^{n}(B_{ii})^2+\sum_{i\neq j=1}^{n}(B_{ij})^2\right). \tag{3.27}$$

From Lemma 8, we obtain

$$2B_{11}B_{22}\ge\frac{\delta}{\phi}+\sum_{i\neq j=1}^{n}(B_{ij})^2. \tag{3.28}$$

Let choose $\Pi=Sp\{e_1,e_2\}$. Then, we get

$$\begin{aligned}\tau(\Pi)&=2c-2(\alpha_{11}+\alpha_{22})+\phi\sum_{i,j=1}^{2}B_{ii}B_{jj}-(B_{ij})^2+\sum_{i,j=1}^{2}D_{ii}D_{jj}-(D_{ij})^2\\ &\ge 2c-2(\alpha_{11}+\alpha_{22})+\delta+\phi\sum_{i\neq j=1}^{n}(B_{ij})^2-\phi\sum_{i\neq j=1}^{2}(B_{ij})^2\\ &\quad+\sum_{i,j=1}^{2}D_{ii}D_{jj}-(D_{ij}{}^2)\\ &=2c-2(\alpha_{11}+\alpha_{22})+\delta+\phi\sum_{i,j=1}^{n}(B_{ij})^2-\phi\sum_{i=1}^{n}(B_{ii})^2\\ &\quad-\phi\sum_{i,j=1}^{2}(B_{ij})^2-\phi\sum_{i=1}^{2}(B_{ii})^2+\sum_{i,j=1}^{2}D_{ii}D_{jj}-(D_{ij}{}^2)\\ &\ge 2c-2(\alpha_{11}+\alpha_{22})+\delta-\phi\sum_{i=3}^{n}(B_{ii})^2+2D_{11}D_{22}-\sum_{i\neq j}^{2}(D_{ij})^2\end{aligned} \tag{3.29}$$

We remark that

$$\alpha(e_1,e_1)+\alpha(e_2,e_2)=\lambda-trace(\lambda|_{\Pi^\perp}). \tag{3.30}$$

Using (3.26), (3.29), and (3.30) we derive

$$\begin{aligned}\tau(\Pi)\geq&-(n-2)(n+1)c+2(n-1)\lambda-2(\lambda-trace(\lambda|_{\Pi^\perp}))+\tau_{S(TM)}(p)\\&-\phi n^2\frac{(n-2)}{(n-1)}\mu_1^2-\sum_{i,j=3}^{n}D_{ii}D_{jj}-\sum_{j>2}^{n}(D_{11}D_{jj}+D_{22}D_{jj})\\&+\sum_{i,j=3}^{n}(D_{ij})^2-\phi\sum_{i=3}^{n}(B_{ii})^2.\end{aligned} \tag{3.31}$$

Thus we obtain (3.22).

The equality case of (3.22) holds for all $p\in M$ iff for all $i,j\in\{3,...,n\}$

$B_{ij}=D_{ij}=0,$

$B_{11}+B_{22}=B_{33}=0.$

Thus the proof is completed.

For the sectional curvature of screen conformal half lightlike submanifold is symmetric, the screen scalar curvature $r_{S(TM)}$ can be denoted by

$$r_{S(TM)}(p)=\sum_{1\leq i<j\leq n}K_{ij}=\frac{1}{2}\sum_{i,j=1}^{n}K_{ij}=\frac{1}{2}\tau_{S(TM)}(p). \tag{3.32}$$

By using (3.32), the equality (3.11) can be rewritten as follows:

$$\begin{aligned}2r_{S(TM)}(p)=&n(n-1)c-2(n-1)\lambda+\phi n^2\mu_1^2+n^2\mu_2^2\\&-\sum_{i,j=1}^{n}[\phi(B_{ij})^2+(D_{ij})^2].\end{aligned} \tag{3.33}$$

Lemma 10. *[36] Let $a_1,a_2,....,a_n$, be n-real number $(n>1)$, then*

$$\frac{1}{n}(\sum_{i=1}^{n}a_i)^2\leq\sum_{i=1}^{n}a_i^2$$

with equality if $a_1=a_2=....=a_n$.

Theorem 11. *Let M be a $(n+1)-$dimensional screen conformal half lightlike submanifold with $\phi>0$ of a $(n+3)-$dimensional Lorentzian space form $\tilde{M}(c)$ endowed with a semi-symmetric metric connection $\tilde{\nabla}$. Then we get*

$$2r_{S(TM)}(p)\leq n(n-1)(c+\phi\mu_1^2+\mu_2^2)-2(n-1)\lambda. \tag{3.34}$$

The equality of (3.34) satisfies for all $p\in M$ iff $S(TM)$ is a totally umbilical in M.

Proof. From (3.33), we have

$$\begin{aligned}2r_{S(TM)}(p)=&n(n-1)c-2(n-1)\lambda+\phi n^2\mu_1^2-\phi\sum_{i=1}^{n}(B_{ii})^2\\&-\phi\sum_{i\neq j=1}^{n}(B_{ij})^2+n^2\mu_2^2+\sum_{i=1}^{n}(D_{ii})^2+\sum_{i\neq j=1}^{n}(D_{ij})^2.\end{aligned} \tag{3.35}$$

Using Lemma 10 in (3.35) we find (3.34).

The equality of (3.34) holds for all $p\in M$ iff

$B_{11}=...=B_{nn},\ B_{ij}=0,$

$D_{11}=...=D_{nn},\ D_{ij}=0,\ \text{for } i\neq j\in\{1,...,n\}.$

Thus $S(TM)$ is a totally umbilical in M.

The following corollary is obtained from the previous theorem.

Corollary 12. *Let M be a $(n+1)-$dimensional irrational screen conformal half lightlike submanifold with $\phi>0$ of a $(n+3)-$dimensional Lorentzian space form $\tilde{M}(c)$ endowed with a semi-symmetric metric connection $\tilde{\nabla}$. Then we have*

$$2r_{S(TM)}(p)\le n(n-1)(c+\phi\mu_1^2+\mu_2^2)-2(n-1)\lambda. \tag{3.36}$$

The equality of (3.36) holds for all $p\in M$ iff M is totally umbilical.

One obtains the following equation from the Binomial theorem:

$$\begin{aligned}\sum_{i,j=1}^{n}(B_{ij})^2=&\frac{1}{2}n^2\mu_1^2+\frac{1}{2}(B_{11}-B_{22}-\ldots-B_{nn})^2\\&+\sum_{j=2}^{n}(B_{1j})^2-\sum_{2\le i<j\le n}^{m}(B_{ii}B_{jj}-(B_{ij})^2).\end{aligned} \tag{3.37}$$

Theorem 13. *Let M be a $(n+1)-$dimensional screen homothetic half lightlike submanifold with $\phi>0$ of a $(n+3)-$dimensional Lorentzian space form $\tilde{M}(c)$ endowed with a semi-symmetric metric connection $\tilde{\nabla}$ such that the vector field P is tangent to M. Then, the followings are true.*

(i) For $X\in S^1(TM)=\{X\in S(TM):\langle X,X\rangle=1\}$

$$Ric_{S(TM)}(X)\le\frac{1}{4}(\phi n^2\mu_1^2+n^2\mu_2^2)+(n-1)c-\lambda+(n-2)\alpha(X,X). \tag{3.38}$$

(ii) The equality case of (3.38) is held by $X\in S^1(TM)$ iff

$$\begin{aligned}&B(X,Y)=D(X,Y)=0,\ \text{for all } Y\in T_p(M) \text{ orthogonal to } X,\\&B(X,X)=\frac{n}{2}\mu_1,\ D(X,X)=\frac{n}{2}\mu_2\end{aligned} \tag{3.39}$$

(iii) The equality case of (3.38) *holds for all $X\in S^1(TM)$ if either $S(TM)$ is totally geodesic in M or $n=2$ and $S(TM)$ is totally umbilical in M.*

Proof. From (3.33) and (3.37), we get

$$\begin{aligned}\frac{1}{4}(\phi n^2\mu_1^2+n^2\mu_2^2)=&r_{S(TM)}(p)-\frac{n(n-1)}{2}c+(n-1)\lambda\\&+\frac{1}{4}\phi(B_{11}-B_{22}-\ldots-B_{nn})^2+\phi\sum_{j=2}^{n}(B_{1j})^2\\&-\phi\sum_{2\le i<j\le n}B_{ii}B_{jj}-(B_{ij})^2+\frac{1}{4}(D_{11}-D_{22}-\ldots-D_{nn})^2\\&+\sum_{j=2}^{n}(D_{1j})^2-\sum_{2\le i<j\le n}D_{ii}D_{jj}-(D_{ij})^2.\end{aligned} \tag{3.40}$$

Moreover,

$$\begin{aligned}&\phi\sum_{2\le i<j\le n}B_{ii}B_{jj}-(B_{ij})^2+\sum_{2\le i<j\le n}D_{ii}D_{jj}-(D_{ij})^2\\&=\sum_{2\le i<j\le n}K_{ij}-\frac{(n-2)(n-1)}{2}c+(n-2)\big(\lambda-\alpha(e_1,e_1)\big)\end{aligned} \tag{3.41}$$

is obtained. Using the two last equations, we have

$$Ric_{S(TM)}(e_1)=\frac{1}{4}(\phi n^2\mu_1^2+n^2\mu_2^2)+(n-1)c-\lambda-(n-2)\alpha(e_1,e_1)$$
$$-\frac{1}{4}\phi(B_{11}-B_{22}-...-B_{nn})^2-\phi\sum_{j=2}^{n}(B_{1j})^2 \tag{3.42}$$
$$-\frac{1}{4}(D_{11}-D_{22}-...-D_{nn})^2-\sum_{j=2}^{n}(D_{1j})^2.$$

Choosing $e_1=X$ as any vector of $T_p^1(M)$ in (3.42) we get (3.38).

Equality holds in (3.38) for $X\in T_p^1(M)$ iff

$$B_{12}=B_{13}=...=B_{1n}=0 \text{ and } B_{11}=B_{22}+...+B_{nn}. \tag{3.43}$$

From (3.43) we obtain

$$n\mu_1=B_{11}+...+B_{nn}=2B_{11}. \tag{3.44}$$

Similarly, we get

$$n\mu_2=D_{11}+...+D_{nn}=2D_{11}. \tag{3.45}$$

From (3.44) and (3.45), we obtain (3.39).

Supposing the equality case of (3.38) for all $X\in T_p^1(M)$, considering (3.43), we derive

$$B_{ij}=0, \quad i\neq j. \tag{3.46}$$
$$2B_{ii}=B_{11}+B_{22}+...+B_{nn}, \ \ i\in\{1,...,n\}. \tag{3.47}$$

From (3.47), we have $2B_{11}=2B_{22}=...=2B_{nn}=B_{11}+B_{22}+...+B_{nn}$, which implies that

$$(n-2)\sum_{i=1}^{n}B_{ii}=0.$$

Similarly, we get

$$(n-2)\sum_{i=1}^{n}D_{ii}=0.$$

Thus, either $\sum_{i=1}^{n}B_{ii}=\sum_{i=1}^{n}D_{ii}=0$ or $n=2$. If $\sum_{i=1}^{n}B_{ii}=\sum_{i=1}^{n}D_{ii}=0$, then from (3.47) we get

$$B_{ii}=D_{ii}=0,\forall\ i\in\{1,...,n\}. \tag{3.48}$$

From (3.46) and (3.48), we derive $B_{ij}=D_{ij}=0$, $\forall i,j\in\{1,...,n\}$. Hence, $S(TM)$ *is totally geodesic in* M. If $n=2$, then from (3.47),

$2B_{11}=2B_{22}=B_{11}+B_{22}$,

$2D_{11}=2D_{22}=D_{11}+D_{22}$,

that is, $S(TM)$ *is totally umbilical in* M. The converse of proof is trivial.

REFERENCES

[1] Kupeli, D. N., (1996). *Singular semi-Riemannian Geometry*, Kluwer Academic Publishers, Dordrecht.

[2] Duggal, K. L., Bejancu, A., (1996). *Lightlike Submanifolds of Semi-Riemannian Manifolds and Applications*, Kluwer Academic Publishers, Dordrecht.

[3] Duggal, K. L., Jin, D. H. (2007). *Null curves and Hypersurfaces of Semi-Riemannian Manifolds*, World Scientific.

[4] Duggal, K. L. and Sahin, B., (2010). *Differential Geometry of Lightlike Submanifolds*, Birkhäuser, Basel.

[5] Friedmann, A and Schouten, J. A., (1924). Über die Geometrie der halbsymmetrischen Übertragungen, *(German) Math. Z.*, 1(21): 211-223.

[6] Hayden, H. A., (1932). *Subspace of a space with torsion*, *Proceedings of the London Mathematical Society II Series*, 34, 27-50.

[7] Yano, K., (1970). On Semi-Symmetric Metric Connection*, Rev. Roum. Math. Pures Et Appl.,* 15: 1579-1586.

[8] Imai, T., (1972). Hypersurfaces of a Riemannian Manifold with Semi-Symmetric Metric Connection, *Tensor, N.S.,* 23: 300-306.

[9] Imai, T., (1972). Notes on Semi-Symmetric Metric Connection, *Tensor, N.S.,* 24: 293-296.

[10] Nakao, Z., (1976). Submanifolds of a Riemannian manifold with semi-symmetric metric connections, *Proc. Amer. Math. Soc.,* 54: 261-266.

[11] Duggal, K. L., and Sharma, R., (1986). Semi-Symmetric metric connection in a Semi-Riemannian Manifold, *Indian J. Pure appl Math.,* 17: 1276-1283.

[12] Konar, A. and Biswas, B., (2001). Lorentzian Manifold that Admits a type of Semi-Symmetric Metric Connection, *Bull. Cal. Math., Soc.*, 93(5): 427-437.

[13] Yaşar, E., Çöken, A. C., Yücesan, A., (2007). Lightlike Hypersurfaces of Semi-Riemannian Manifold with Semi-Symmetric Metric Connection*, Kuwait Journal of Science and Engineering*, 34(2A): 11-24.

[14] Akyol, M. A., Vanlı, A. T. And Fernandez, L. M., (2013). Curvature properties of a semi symmetric metric connection on S manifolds., *Annales Polonici Mathematici*, 107(1): 71-86.

[15] Chen, B. Y., (1993). Some pinching and classification theorems for minimal submanifolds, *Arch. math.,* (Basel), 60(6): 568-578.

[16] Chen, B. Y., (1998). *Strings of Riemannian invariants, inequalities, ideal immersions and their applications*, *The Third Pacific Rim Geometry Conference* (Seoul, 1996), 7-60, *Monogr. Geom. Topology*, 25, Int. Press, Cambridge, MA.

[17] Chen, B. Y., (2000). Some new obstructions to minimal and Lagrangian isometric immersions, *Japanese J. Math.*, 26: 105-127.

[18] Chen, B. Y., (2008). $\delta-$*invariants, Inequalities of Submanifolds and Their Applications, in Topics in Differential Geometry,* Eds. A. Mihai, I. Mihai, R. Miron, *Editura Academiei Romane*, Bucuresti, 29-156.

[19] Chen, B. Y., Dillen, F., Verstraelen, L. and Vrancken, V., (2000). Characterizations of Riemannian space forms, Einstein spaces and conformally flat spaces, *Proc. Amer. Math. Soc.,* 128: 589-598.

[20] Hong, S., Matsumoto K. and Tripathi, M. M., (2005). Certain basic inequalities for submanifolds of locally conformal Kaehlerian space forms*, SUT J. Math.,* 4(1): 75-94.

[21] Kim, J. S., Choi, J., (2003). A basic inequality for submanifolds in a cosymplectic space form, *Int. J. Math. Math. Sci.,* 9: 539-547.

[22] Matsumoto, K., Mihai, I., Oiaga, A., (2001). Ricci curvature of submanifolds in complex space forms, *Rev. Roumaine Math. Pures Appl.,* 46: 775-782.

[23] Oiaga, A., Mihai, I., Chen, B. Y., (1999). Inequalities for slant submanifolds in complex space forms, *Demonstratio Math.,* 32: 835-846.

[24] Mihai, A. and Özgür, C., (2010). Chen inequalities for submanifolds of real space form with a semi-symmetric metric connection*, Taiwanese Journal of Mathematics*, 14(4): 1465-1477.

[25] Zhang, P., Zhang, L. and Song, W., (2014). Chen's inequalities for submanifolds of a Riemannian manifold of quasi-constant curvature with a semi-symmetric metric connection, *Taiwanese Journal of Mathematics*, 18(6): 1841-1862.

[26] Gülbahar, M., Kılıç, E. and Keleş, S., (2013). Chen-like inequalities on lightlike hypersurfaces of a Lorentzian manifold*, J. Inequal. Appl.,* 266.

[27] Gülbahar, M., Kılıç, E. and Keleş, S., (2013). Some inequalities on screen homothetic lightlike hypersurfaces of a Lorentzian manifold*, Taiwanese Journal of Mathematics*, 17(6): 2083-2100.

[28] Poyraz, N. Ö., Doğan, B. and Yaşar, E., (2017). Chen Inequalities on Lightlike Hypersurface of a Lorentzian manifold with semi-symmetric metric connection*, Int. Electronic Journal of Geometry*, 10(1): 1-14.

[29] Gülbahar, M., Kılıç, E., (2017). Some optimal inequalities for screen conformal half-lightlike submanifolds, *Acta Mathematica Academiae Paedagogicae Nyíregyháziensis*, 33(2): 315-329.

[30] Duggal, K. L. and Jin, D. H., (1999). Half lightlike submanifolds of codimension 2, *Math. J. Toyama Univ*, 22: 121-161.

[31] Bejan, C. L. and Duggal, K. L., (2005). Global lightlike manifolds and harmonicity*, Kodai Math. J.,* 28(1): 131-145.

[32] Duggal, K. L. and Sahin, B., (2004). Screen conformal half-lightlike submanifolds, *Int. J. Math. and Math. Sci.,* 68: 3737-3753.

[33] Jin, D. H., (2011). Geometry of half lightlike submanifolds of a semi-Riemannian space form with a semi-symmetric metric connection*, J. Chungcheong Math. Soc.,* 24(4): 769-780.

[34] Beem, J. K., Ehrlich, P. E. and Easley, K. L., (1996). *Global Lorentzian Geometry*, *Volume 202 of Monographs and Textbooks in Pure and Applied Mathematics*, Marcel Dekker, Inc., New York.

[35] De Smet, P. J., Dillen, F., Verstraelen, L. and Vrancken, V., (1999). A pointwise inequality in submanifold theory, *Arch. Math. (Brno)*, 5(2): 115-128.

[36] Tripathi, M. M., (2003). *Certain Basic Inequalities for Submanifolds in (;) Space*, *Recent Advances in Riemannian and Lorentzian Geometries*, Baltimore, 187-202.

NATURENGS
MTU Journal of Engineering and Natural Sciences
https://dergipark.org.tr/tr/pub/naturengs
DOI: 10.46572/naturengs.880845

Research Article

Determination of Breakfast Habits of Health School Students and the Factors Affecting Them: Bitlis Eren University Example

Mustafa Şamil ARGUN[1*], Betül ZANLIER[2]

[1] Department of Food Engineering, Akşehir Faculty of Engineering and Architecture, Selçuk University, Konya, Turkey.
[2] Department of Nutrition and Dietetics, School of Health, Bitlis Eren University, Bitlis, Turkey.

(**Received:** 15.02.2021; **Accepted:** 07.03.2021)

ABSTRACT: In this study, it was aimed to determine the breakfast habits of Health School students and the factors affecting them. The research was conducted with 120 students representing Bitlis Eren University Health School students. The questionnaire form was used as a data collection tool. As a result of the study, it was observed that 35.8% of the students had a regular breakfast every day, and 3.3% did not have breakfast. It was determined that 48.3% of the students who skipped breakfast skipped because of waking up late, 24.2% due to lack of appetite in the mornings, 10% because of not caring, 5% because of dislike to eat breakfast, 2.5% for economic insufficiency, and 2.5% for fear of gaining weight. They reported that the most common situations encountered by students when they did not eat breakfast were the feeling of hunger, weakness, fatigue, and decreased attention. The majority of the students think that breakfast enables a fresh start to the day, breakfast is the most important meal of the day and breakfast helps regulate blood sugar. It was observed that students whose fathers were public employees skip breakfast more ($p < 0.001$). As the monthly income of the students' families increased, the rate of skipping breakfast increased ($p < 0.05$). The effect of the smoking status on skipping breakfast was found to be significant ($p < 0.01$).

Keywords: School of health, Healthy eating, Skip meals, Breakfast habit.

1. INTRODUCTION

A healthy breakfast has positive effects on providing school-age children with essential nutrients for their activities and long-term health throughout life. Skipping breakfast, many health problems, and cognitive and psychosocial function in addition to poor performance could negatively impact learning and academic success. Children who skip breakfast have difficulty concentrating in the afternoon and feel tired at the end of the day due to reduced energy levels [1]. Parents' breakfast habits are strongly associated with their children's breakfast consumption from birth to adolescence, so parents have important responsibilities in this regard. It is recommended to eat a healthy breakfast every day, consisting of a variety of foods, especially high-fiber and nutrient-rich whole grains, fruits, and dairy products [2]. Current nutritional behaviors and practices observed in children and adolescents can have detrimental consequences on their health. Adverse health consequences that may result from excessive soda and sugary beverage intake; fast food consumption; insufficient intake of fresh fruits, vegetables, fiber-rich foods, and dairy products, and other calcium-rich foods; reduced levels

*Corresponding author: msargun@selcuk.edu.tr
ORCID number of authors: [1] 0000-0001-8209-3164, [2] 0000-0002-0358-6508

of physical activity; the increasing rates of obesity point to the need to review the diet and lifestyle characteristics of this age group [3, 4]. Studies are showing that regular breakfast habits also make adults feel healthier and contribute to their daily activities [5]. In the research conducted about the eating habits of university students in Turkey, the students' not pay attention to a regular and balanced diet, skip meals, including primarily breakfast were reported [6-10]. This study was aimed to determine the breakfast habits of the students studying at Bitlis Eren University School of Health and the influencing factors.

2. MATERIAL AND METHODS

2.1. Research Type

This research is a descriptive cross-sectional study designed to determine the breakfast habits of students studying in the first, second, third, and fourth grades of Bitlis Eren University Health School Departments.

2.2. Research Universe and Sampling

The universe of the research consists of 480 students studying in the first, second, third, and fourth grades of Bitlis Eren University School of Health. The sample size, population size was determined at a 95% confidence level by using the formula used for a certain population (taking d = 0.08), and the research sample consists of 120 students with the participation of 40 students from the Nutrition and Dietetics Department, 40 from the Nursing department and 40 from the Social Work department. The students were selected by a simple random sampling method.

2.3. Data Collection Tools Used in the Study

In collecting the data, a questionnaire was used, which was created by scanning the necessary literature and containing questions about the students' socio-demographic characteristics and determination of breakfast consumption habits. The questionnaires were filled in face to face with the students. The students were asked about their height and weight. The body mass index (BMI) of the students was calculated using the [weight / (height)^2] formula. In the evaluation of BMIs, reference values of World Health Organization (WHO) 18 years and over standards were used [11]. 18.5 and below were weak, 18.5-24.9 normal, 24.9-29.9 slightly obese, 30- 39.9 intervals were classified as obese, values 40 and above as morbidly obese.

2.4. Statistical Analysis

The data obtained as a result of the research were evaluated using the "SPSS 22.0 for Windows" statistical package program. Qualitative variables are expressed as number (n) and percentage (%). Quantitative variables are given as mean ± standard deviation. The Chi-square test was used to evaluate qualitative data. In all statistical evaluations, a value of $p<0.05$ was considered significant.

2.5. Ethical Aspect of the Research

To conduct the study, necessary permission was obtained from Bitlis Eren University Ethical Principles and Ethics Committee with the decision dated 13.12.2016 and numbered 2016/16-X.

3. RESULTS AND DISCUSSION

The distribution of the students participating in the study according to their anthropometric measurements is shown in Table 1. The average height of the students was found to be 168.75 ± 8.50 in the range. The average weight of the students is in the range of 60.76 ± 10.27. The average BMI of the students is in the range of 21.24 ± 2.48. When the BMI values of the students were examined, it was found that 14.2% were included in the classification of weak, 76.6% of normal weight, and 9.2% of slightly obese.

Table 1. Anthropometric measurements of the students participating in the study

Variables	**Number (n)**	**(%)**
Height (mean ± sd)	**168.75±8.50**	
Weight (mean ± ss)	**60.76±10.27**	
BMI (mean ± sd)	**21.24±2.48**	
BMI Classification		
Weak (<18.5)	17	14.2
Normal (18.5-24.9)	92	76.6
Slightly obese (24.9-29.9)	11	9.2
Obese (30-39.9)	0	0
Morbidly obese (>40)	0	0
Total	**120**	**100**

52.5% of the students are female and 47.5% are male. 40% of the students are in the age range of 18-20, 56.9% in the age range of 21-23, and 4.1% in the age range of 24 and above. The average age of the students is 20.96 ± 1.82. When the monthly income of the students' families is examined, it is seen that 12.5% of them are less than 1000 TL, 45.8% are between 1000-2000 TL, and 41.8% are more than 2000 TL. Fathers of 10.8% of students are workers, 18.3% are public servants and 20.8% are retired (Table 2).

Table 2. Socio-Demographic characteristics of the students participating in the study

Variables	**Number (n)**	**%**
Gender		
Female	63	52.5
Male	57	47.5
Age (mean ± sd)	20.96 ±1.82	
Age Classification		
18-20 years	48	40
21-23 years	66	56.9
24 years and over	6	4.1
Monthly Income (Turkish Lira)		
Less than 1000	15	12.5
Between 1000-2000	55	45.8
More than 2000	50	41.7
Father's Profession		
Has no father	9	7.5
Public servant	22	18.3
Worker	13	10.8
Retired	25	20.8
Self-employment	18	15
Tradesman	11	9.1
Private sector	3	2.5
Driver	6	5
Farmer	13	10.8

The distribution of the students participating in the study according to the number of daily main meals and snacks, the meals they skip the most, and the reasons for skipping breakfast are shown in Table 3. When the number of daily main meals of the students is examined, it is seen that 4.2% of the students have one, 54.2% two, 41.6% three main meals. Looking at the number of daily snacks, it is seen that 36.2% of the one, 26.7% two, 11.7% three, 25% four, 22.5% did not eat any snacks. It is observed that the most frequently skipped meals are lunch (47.5%) and breakfast (40%), with 7.5% of those who never skipped a meal.

Arslan et al. (1994) reported that the most skipped meal among higher education students was breakfast (51.9%) [12].

It was determined that 48.3% of the students' reasons for skipping breakfast were waking up late, 5% did not like having breakfast, 24.2% had no appetite in the morning, 2.5% was economically inadequate, and 10% did not care.

Table 3. Number of daily main and snack meals, the most often skipped meal, and the reasons for skipping breakfast of the students participating in the study

Variables	Number (n)	%
Number of Main Meals		
1 main meal	5	4.2
2 main meals	65	54.2
3 main meals	50	41.6
Number of Snacks		
No snacks	27	22.5
1 Snack	44	36.2
2 Snacks	32	26.7
3 Snacks	14	11.7
4 Snacks	3	2.5
The Most Frequently Missed Main Meal		
Breakfast	48	40
Lunch	57	47.5
Dinner	6	5
Not skipping meals	9	7.5
Reason for skipping breakfast		
Waking up late in the morning 58 48.3	58	48.3
Dislike to have breakfast	6	5
Lack of appetite in the morning	29	24.2
Economic insufficiency	3	2.5
Not to give importance	12	10
Fear of weight gain	3	2.5
Never skips meals	9	7.5

It was determined that 35.8% of the students had a regular breakfast every day, and 3.3% did not have breakfast. The most common situations encountered by students when they do not eat breakfast were the feeling of hunger (82.5%), weakness (74.2%), fatigue (71.7%), and decreased attention (71.7%), and the least common situation they encountered was palpitations (36.7%). 89.2% of the students consider breakfast as the most important meal of the day (Table 4).

Faydaoğlu et al. (2013) reported in a study they conducted that 27.2% of university students had breakfast every day and 1.4% did not have breakfast [10]. They found that 61.2% of the students did not have breakfast because they could not catch the class or did not have time.

Çetik Yıldız (2020), in his study examining the breakfast habits of university students, reported that the most skipped meal (47.9%) was breakfast [13]. In the same study, as the cause of students skipping meals, lack of time (37.0%), get up late in the morning (24.0%) and lack of breakfast habits (19.0%) were identified as. Çinibulak (2018) stated in his study that there is a statistically strong, significant, and positive relationship between having breakfast and lesson motivation [14].

Table 4. The answers of the students participating in the study to the frequency of having breakfast, how long they have breakfast after waking up, and the information about breakfast

Variables	**Number (n)**		**%**	
Frequency of Having Breakfast in the Morning				
Regular every day	43		35.8	
Sometimes	58		48.3	
Weekend only	15		12.5	
Never	4		3.3	
How long after waking up do you have breakfast?				
<30 minutes	28		23.3	
30 minutes -1hour	60		50	
1 hour- 2 hours	21		17.5	
>2 hours	11		9.2	
The Situation Encountered When Not Having Breakfast	**Yes**		**No**	
	Number (n)	**%**	**Number (n)**	**%**
Fatigue	86	71.7	34	28.3
Weakness	89	74.2	31	25.8
Feeling of hunger	99	82.5	21	17.5
Dizziness	65	54.2	55	45.8
Decreased attention	86	71.7	34	28.3
Staggers	67	55.8	53	44.2
Palpitations	44	36.7	76	63.3
Unrest	72	60	48	40
Feel cold	48	40	72	60
Headache	77	64.2	43	35.8
Breakfast is the most important meal of the day	107	89.2	13	10.8

The relationship between the meals skipped by students according to their father's profession was found to be statistically significant ($p < 0.001$). The relationship between the meals skipped by the students according to their family's monthly income ($p < 0.05$) and smoking status ($p < 0.01$) was found to be statistically significant (Table 5). It was observed that students whose fathers were public servants skip breakfast more often. It was observed that students who smoke more often skip breakfast, while non-smokers skip lunch. As the family income of the students increased, the rate of skipping breakfast increased.

Table 5. Distribution of which meals were skipped by the students participating in the study according to father's occupation, family's monthly income, and smoking status

	Skipped Meal								
	Breakfast		**Lunch**		**Dinner**		**I don't skip meals**		**χ^2 and p-Value**
Father's Profession	(n)	(%)	(n)	(%)	(n)	(%)	(n)	(%)	
Public servants	16	13.3	4	3.3	1	0.8	1	0.8	
Retired	11	9.2	10	8.3	1	0.8	3	2.5	
Self-employment	4	3.3	12	10	1	0.8	1	0.8	
Tradesman	3	2.5	7	5.8	0	0	1	0.8	χ^2=59.700 p=0.000
Private sector	0	0	1	0.8	2	1.7	0	0	
Farmer	1	2.1	12	21.1	0	0	0	0	
Worker	6	5	6	5	0	0	0	0	
Driver	2	1.7	2	1.7	0	0	2	1.7	
Has no father	5	4.2	3	2.5	1	0.8	0	0	
Family's monthly income(Turkish Lira)									
<1000	1	0.8	11	9.2	2	1.7	1	0.8	χ^2=15.481 p=0.017
1000-2000	19	15.8	28	23.3	2	1.7	6	5	
>2000	28	23.3	18	15	2	1.7	2	1.7	
Smoking Status									
Yes	17	14.2	8	6.7	3	2.5	0	0	χ^2=11.797 p=0.008
No	31	25.8	49	40.8	3	2.5	9	7.5	
Total (n)					**120**				
Total (%)					**100**				

4. CONCLUSIONS

It was determined that students skip breakfast and lunch as the main meal most frequently. It was observed that the most common situations encountered by students when they did not eat breakfast were the feeling of hunger (82.5%), weakness (74.2%), fatigue (71.7%), and decreased attention (71.7%). It was understood that the most important reasons for students to skip breakfast were waking up late, lack of appetite in the morning, and not caring.

As a result, students do not eat breakfast regularly, although they see its negative effects. In addition to the role of parents in the acquisition of breakfast habits, it has been understood that bad habits such as sleep patterns and smoking have an important role. The great task falls to parents in acquiring the habit of regular breakfast and meals.

Conflict of Interest

The authors declare that there are no conflicts of interest.

REFERENCES

[1] ALBashtawy, M. (2017). Breakfast Eating Habits among Schoolchildren, *Journal of Pediatric Nursing*, 36: 118-123.

[2] Rampersaud, G.C., Pereira, M.A., Girard, B.L., Adams, J. and Metzl, J.D. (2005). Breakfast Habits, Nutritional Status, Body Weight, and Academic Performance in Children and Adolescents, *Journal of the American Dietetic Association*, 105(5): 743-760.

[3] Johnson, R.K. (2000). Changing Eating and Physical Activity Patterns of US Children, *Proceedings of the Nutrition Society*, 59(2): 295-301.

[4] St-Onge, M.P., Keller, K.L. and Heymsfield, S.B. (2003). Changes in Childhood Food Consumption Patterns: A Cause For Concern in Light of Increasing Body Weights, *The American Journal of Clinical Nutrition*, 78(6): 1068-1073.

[5] Reeves, S., Halsey, L.G., McMeel, Y. and Huber, J.W. (2013). Breakfast Habits, Beliefs and Measures of Health and Wellbeing in a Nationally Representative UK Sample, *Appetite*, 60: 51-57.

[6] Heşeminia, T., Çalışkan, D. ve Işık, A. (2002). Ankara'da Yüksek Öğretim Öğrenci Yurtlarında Kalan Öğrencilerin Beslenme Sorunları, *İbni Sina Tıp Dergisi*, 7: 155-167.

[7] Mazıcıoğlu, M.M. ve Öztürk, A. (2003). Üniversite 3 ve 4. Sınıf Öğrencilerinde Beslenme Alışkanlıkları ve Bunu Etkileyen Faktörler, *Erciyes Tıp Dergisi*, 25(4): 172-178.

[8] Özkurt, Ö., Nural, N. ve Hindistan, S. (2006). KTÜ Trabzon Sağlık Yüksekokulu Hemşirelik Öğrencilerinin Beslenme Alışkanlıklarının ve Malnütrisyon Prevelansının Saptanması, *5. Ulusal Hemşirelik Öğrencileri Kongresi*, Şanlıurfa, Türkiye.

[9] Güleç, M., Yabancı, N., Göçgeldi, E. ve Bakır, B. (2008). Ankara'da İki Kız Öğrenci Yurdunda Kalan Öğrencilerin Beslenme Alışkanlıkları, *Gülhane Tıp Dergisi*, 50(2): 102-109.

[10] Faydaoğlu, E., Energin, E. ve Sürücüoğlu, M.S. (2013). Ankara Üniversitesi Sağlık Bilimleri Fakültesinde Okuyan Öğrencilerin Kahvaltı Yapma Alışkanlıklarının Saptanması, *Gümüşhane Üniversitesi Sağlık Bilimleri Dergisi*, 2(3): 299-311.

[11] WHO Expert Committee (1995). Physical Status: The Use and Interpretation of Anthropometry, *WHO Technical Report Series,* no. 854. Geneva: WHO.

[12] Arslan, P., Karaağaoğlu, N., Duyar, İ. ve Güleç, E. (1993). Yüksek Öğrenim Gençlerinin Beslenme Alışkanlıklarının Puanlandırma Yöntemi ile Değerlendirilmesi, *Beslenme ve Diyet Dergisi*, 22(2): 195-208.

[13] Çetik Yıldız, S. (2020). Üniversite Öğrencilerinde Kahvaltı Yapma Alışkanlığının Saptanması ve Çözüm Önerileri, *Iğdır Üniversitesi Fen Bilimleri Enstitüsü Dergisi*, 10(2): 819-827.

[14] Çinibulak, S. (2018). *Düzenli Sabah Kahvaltısı Yapmanın Öğrenci Motivasyonuna Etkisinin Belirlenmesi*, Kırklareli Üniversitesi Sağlık Bilimleri Enstitüsü, Yüksek Lisans Tezi, Kırıkkale.

NATURENGS
MTU Journal of Engineering and Natural Sciences
https://dergipark.org.tr/tr/pub/naturengs
DOI: 10.46572/naturengs.882203

Research Article

A Computational Method Based on Interval Length for Fuzzy Time Series Forecasting

Özlem AKAY

Department of Statistics, Faculty of Science and Letters, Çukurova University, Adana, Turkey

(**Received:** 17.02.2021; **Accepted:** 26.03.2021)

ABSTRACT: In the literature, there have been a good many different forecasting methods related to forecasting problems of fuzzy time series. The main issue of fuzzy time series forecasting is the accuracy of the forecasted values. The forecasting accuracy rate is affected by the length of each interval in the universe of discourse. Thus, it is substantial to determine the length of each interval. In this study, a new computational method based on class width to determine interval length is proposed and also used the coefficient of variation for time series forecasting. After the intervals are formed, the historical time series data set is fuzzified according to fuzzy time series theory. The proposed model has been tested on the student enrollments, University of Alabama, and a real-life problem of rice production for containing higher uncertainty. This method was compared with existent methods to determine the effectiveness in terms of the mean square error (MSE) and the average forecasting (AFE). The results are shown that the proposed model can achieve a higher forecasting accuracy rate than the existing models.

Keywords: Interval length, Coefficient of variation, Fuzzified, Fuzzy time series, Forecasting.

1. INTRODUCTION

Forecasting activities are very important in daily life. If things such as earthquakes, stock markets, weather can be predicted by people in advance, people take the necessary precautions and make their plans according to the situation that will occur [1]. Regression analysis and moving average methods are constantly used for forecasting [2]. However, these methods are not attending the forecasting problems in which the historical data are in linguistic terms [3]. Zadeh (1965) [4] developed the concept of linguistic variables, fuzzy set theory, and its application to approximate reasoning. Song and Chissom (1993) [5] have successfully employed this in fuzzy time series forecasting. Many researchers have recommended various forecasting methods based on fuzzy time series to cope with forecasting problems, in recent years. Fuzzy time series forecasting appeared as a method for predicting the future values in a situation in which neither a pattern in variations of time series are visualized nor a trend is viewed and also the information is vague and imprecise [5].

Hwang et al. (1998) [1] suggested a model based on time-variant fuzzy time series to cope with the forecasting problems. The opinion of this model is that the variation of enrollment of this year is related to the trend of the enrollments of the past years. Huarng (2001) [6] recommended

Corresponding Author: oakay@cu.edu.tr
ORCID number of authors: 0000-0002-9539-7202

heuristic models to improve forecasting by integrating problem-specific heuristic knowledge with Chen's model. Huarng (2001) [7] proposed distribution-and average-based length to approach the issue of how to determine effective lengths of intervals. Distribution-based length is the largest length smaller than at least half the first differences of data. The average-based length is set to one-half the average of the first differences of data. Singh (2007) [8] offered a new method which is a simplified computational approach for fuzzy time series forecasting. The new model is included different parameters. Singh (2007) [9] recommended a simple time-variant model by using the difference operator for time series forecasting. Values obtained have been used for developing fuzzy rules. Sing (2007) [10] presented a new method in a form of simple computational algorithms. This method is a versatile method of forecasting based on the concept of fuzzy time series. Singh (2008) [3] improved a model based on fuzzy time series having the ability to deal with the situation of high uncertainty having large fluctuations in the consecutive values. Yolcu et al. (2009) [11] proposed a new approach that uses a single-variable constrained optimization to determine the ratio for the length of intervals. This approach was applied to the two well-known time series, which are enrollment data at The University of Alabama and inventory demand data. The obtained results were compared to those of other methods. The proposed method produced more accurate predictions for the future values of the used time series. Gangwar and Kumar (2012) [2] proposed a new model to enhance the accuracy in forecasted values. This method is based on multiple partitioning and higher-order fuzzy time series. Singh and Borah (2013) [12] presented a new model for addressing four main issues in fuzzy time series forecasting. These are defuzzification of fuzzified time series values, handling of fuzzy logical relationship (FLR), determination of weight for each FLR, and determining the effective length of intervals. The determination of the length of intervals is very important for the fuzzification of the time series data set. The length of the intervals was kept the same in most of the fuzzy time series models. There is no specific reason for using fixed range intervals. Huarng (2001) [6] indicates that the effective length of interval always affects the results of forecasting [12]. Wang et al. (2013) [13] studied how to partition the universe of discourse into intervals with unequal length to improve forecasting quality. They calculated the prototypes of data using fuzzy clustering, then formed some subsets according to the prototypes, and proposed an unequal length partitioning method. Ye et al. (2016) [14] proposed a new forecasting method based on multi-order fuzzy time series, technical analysis, and a genetic algorithm. In this algorithm, multi-order fuzzy time series (first-order, second-order, and third-order) are applied and a genetic algorithm is used to find a good domain partition. Yolcu et al. (2016) [15] proposed a novel high-order fuzzy time series approach that considers the membership values, where artificial neural networks are employed to identify the fuzzy relations. In the proposed method, intersection operators are utilized to deal with an excessive number of inputs, and also the fuzzy c-means method is employed for fuzzification. Jiang et al. (2017) [16] constructed a novel high-order fuzzy time series (FTS) model to make time series forecasting. In this study, the optimal lengths of intervals were tuned by applying the harmony search intelligence algorithm. Regularly increasing monotonic quantifiers were employed on fuzzy sets to obtain the weights of ordered weighted aggregation. Singh (2017) [17] introduced a new fuzzy time series (FTS) forecasting model. In this model, for the determination of effective lengths of intervals, the "frequency-based discretization" approach was proposed, which partitions the time series data set into various lengths. Besides the establishment of the fuzzy logical relations (FLRs) and their better representation, an artificial neural network-based architecture was developed. Chen and Phuong (2017) [18] proposed a new fuzzy time series (FTS) forecasting method based on optimal partitions of intervals in the

universe of discourse and optimal weighting vectors of two-factors second-order fuzzy-trend logical relationship groups (TSFTLRGs). This method uses particle swarm optimization (PSO) techniques to obtain the optimal partitions of intervals and the optimal weighting vectors simultaneously. Bas et al. (2018) [19] introduced a new model for determining the fuzzy relationships for high order fuzzy time series forecasting which uses Pi-Sigma neural network. They used a modified particle swarm optimization model o train the Pi-Sigma network. Panigrahi and Behera (2020) [20] addressed two key issues such as modeling fuzzy logical relationships (FLRs) and determination of the effective length of the interval. They used machine learning (ML) techniques for modeling the FLRs and proposed a modified average-based method to estimate the effective length of the interval. Pattanayak et al. (2020) [21] developed a novel method using fuzzy c-means clustering to determine the unequal length of the interval. The membership values were considered while modeling the fuzzy logical relationships using a support vector machine (SVM). The order of the model is determined by analyzing the autocorrelation function and partial autocorrelation function of the time series.

The objective of this study is to solve the problem of determining the length of the intervals by adjusting the new length of the intervals to obtain more accurate forecasting. So, a computational model forecasting based on multiple partitioning is presented in this paper. The proposed method presents simple computational algorithms and is easier for the application. The algorithm of proposed methods has been performed for forecasting the enrollments of the University of Alabama. To display the superiority of this method, the results obtained have been compared with the existent methods. Further, the model suitability in the general forecasting problem has been performed in another real-life dataset. Therefore the proposed method has been applied to the time series data of rice production. This data set is obtained from Pantnagar farm, G.B. Pant University of, Agriculture and Technology, India.

The paper is organized as follows. The fuzzy time series are briefly introduced and related works for fuzzy time series models are presented in section 1. In section 2, an overview of the fuzzy time series has been explained. A new model based on determining the length of the interval is presented for forecasting enrollments in section 3. In section 4, the algorithm of the proposed method was applied to two different data sets, and the mean square error (MSE) and the average forecasting error (AFE) are computed to compare with the existing methods. The conclusions are discussed in section 5.

2. MATERIAL AND METHODS

2.1. Fuzzy Time Series

Song and Chissom (1993) [5] recommended the definitions of fuzzy time series. The various properties and definitions of fuzzy time series forecasting are given stepwise as follows;

1. A fuzzy set is a class of objects with a continuum of a grade of membership. *C* is the Universe of discourse with $C = \{c_1, c_2, c_3, \dots, c_n\}$, where c_i are possible linguistic values of C, a fuzzy set of linguistic variables K_i of C is described by

$$K_i = \frac{\mu_{K_i}(c_1)}{c_1} + \frac{\mu_{K_i}(c_2)}{c_2} + \frac{\mu_{K_i}(c_3)}{c_3} + \cdots + \frac{\mu_{K_i}(c_n)}{c_n}$$

here $\mu_{K_i}$is the membership function of the fuzzy set K_i, $\mu_{K_i}: C = [0,1]$.

If c_j is the member of K_i, $\mu_{K_i}(c_j)$ is the degree of belonging of c_j to K_i.

2. *Y(t)* (t=…,0,1,2,3,…), is a subset of *R*, the universe of discourse on which fuzzy sets $f_i(t)$ (*i*=1,2,3,…) are described. *F(t)* is the collection of f_i, and *F(t)* is described as fuzzy time series on *Y(t).*

3. Assume that there is a fuzzy relationship between *F(t)* and *F(t-1).* If *F(t-1)* only causes *F(t),* $F(t-1) \rightarrow F(t)$ is demonstrated. The fuzzy relational equation expressed as:

F(t)=F(t-1)oR(t, t-1)

where "o" is the max-min composition operator. The relation *R* is called the first-order model of *F(t).* Further, if fuzzy relation *R(t,t-1)* of *F(t)* is independent of time *t,* that means *R*(t_1, t_1-*1)= R*(t_2, t_2-*1)* for different times t_1 and t_2, then *F(t)* is called a time-invariant fuzzy time series

4. Assume that *F(t)* is caused by more fuzzy sets, *F(t-n), F(t-n+1),…, F(t-1).* The fuzzy relationship is demonstrated by

$$K_{i1}, K_{i2}, \dots, K_{in} \rightarrow K_j$$

where $F(t-n) = K_{i1}$, $F(t-n+1), = K_{i2}$, …, $F(t-1) = K_{in}$. This relationship is called the *n*th order fuzzy time series model.

5. Assume that an *F(t-1), F(t-2),*…, and *F(t-m) (m>0)* simultaneously causes *F(t).* The *F(t)* is said to be time-variant fuzzy time series. The fuzzy relational equation expressed as:

F(t)=F(t-1)oR^w*(t,t-1)*

here *w>1* is several years (time) parameter by which the forecast *F(t)* is being affected. A variety of complex calculation methods are existing for the calculations of the relation *R*^{w}*(t, t-1).*

2.2. Proposed Method

In this part, the algorithm suggested by Song and Chissom (1993) [5] was modified. The class width was used to determine interval length and the coefficient of variation was used for time series forecasting. The algorithm of the proposed computational method is presented stepwise.

1. Determine the Universe of discourse, *C* based on the range of time-series data

$$R = E_{max} - E_{min} \quad (1)$$

$$m = 2\sqrt{n} \quad (2)$$

$$h = \frac{R}{m} \quad (3)$$

Intervals are established by continuing to add the class width (*h*) to the minimum data values until the number of classes (*m*) is created.

$$C = [E_{\min}, E_{\min} + h] \quad (4)$$

2. Divide the Universe of discourse into an equal length of intervals: $c_1, c_2, \dots, c_m$. The number of intervals will be according to the number of linguistic variables (fuzzy sets) $K_1, K_2, \dots, K_m$ to be noted.

3. According to the intervals in Step 2 configure linguistic variables K_i and perform the triangular membership rule to each interval in each created fuzzy set.

4. After this time series data is fuzzified, the fuzzy logical relationships are stated. *If* K_i is the fuzzy production of year *n* and K_j is the fuzzify production of year *n+1*, the fuzzy logical relation is demonstrated as $K_i \rightarrow K_j$, where K_i is the current case and K_j is the next case.

5. Algorithm

Used notations are shown as;

$[*K_j]$ is the corresponding interval c_j for which membership in K_j is the supremum

M$[*K_j]$ is the mid-value of the interval c_j having supremum value in K_j

U$[*K_j]$ is the upper bound of the interval $[*K_j]$

L$[*K_j]$ is the lower bound of the interval $[*K_j]$

For $K_i \rightarrow K_j$ (a fuzzy logical relation)

E_i is the actual production of year *n*

E_{i-1} is the actual production of year *n-1*

E_{i-2} is the actual production of year *n-2*

F_j is the crisp forecasted production of the years *n+1*
Algorithm for forecasting production of year *n+1* and onwards
For *t=3…T*

Attained fuzzy logical relation for year *t* to *t+1*

$$K_i \rightarrow K_j$$

$$ED_i = |(E_i - E_{i-1})| \quad (5)$$

$$ED_{ii} = |(E_{i-1} - E_{-2})| \quad (6)$$

$$\overline{ED} = \frac{ED_i + ED_{ii}}{2} \quad (7)$$

$$S_i = (ED_i - \overline{ED}) + (ED_{ii} - \overline{ED}) \quad (8)$$

$$X_i = \mathrm{M}[* K_j] + \frac{S_i * 100}{\overline{ED}} \quad (9)$$

$$F_j = X_i \quad (10)$$

Next *t*

3. RESULTS AND DISCUSSION

The algorithm of the proposed approach mentioned above is applied in the time series data of the records in the University of Alabama. The steps of the algorithm and the results obtained are as follows;

Step 1. Based on the proposed method, the Universe of discourse is divided into equal lengths of intervals. In Table 1, the results obtained are presented. Each interval is computed by using Eq. (1-4) respectively as below;

R=19337-13055=6282

$$m = 2\sqrt{22} \cong 10$$

$$h = \frac{6282}{10} = 628.2 \cong 629$$

$c_1 = [13055, 13684]$, $c_2 = [13684, 14313]$, $c_3 = [14313, 14942]$, $c_4 = [14942, 15571]$,

$c_5 = [15571, 16200]$, $c_6 = [16200, 16829]$, $c_7 = [16829, 17458]$,

$c_8 = [17458,18087]$, $c_9 = [18087, 18716]$, $c_{10} = [18716, 19345]$

Mid-point is stated for each interval and stocked for future consideration.

Table 1. Obtained new intervals, mid-points, and their corresponding elements.

Intervals	Boundaries	Mid-point	Corresponding element
c_1	[13055, 13684]	13369.5	13055, 13563
c_2	[13684, 14313]	13998.5	13867
c_3	[14313, 14942]	14627.5	14696
c_4	[14942, 15571]	15256.5	15145, 15163, 15311,15433, 15460, 15497
c_5	[15571, 16200]	15885.5	15603, 15861, 15984
c_6	[16200, 16829]	16514.5	16388, 16807
c_7	[16829, 17458]	17143.5	16859, 16919
c_8	[17458,18087]	17772.5	
c_9	[18087, 18716]	18401,5	18150
c_{10}	[18716, 19345]	19030.5	18876,18970, 19328, 19337

Step 2. For each of the interval, described linguistic terms

This time-series data set is partitioned ten intervals $(c_1, c_2, \dots, c_{10})$. Therefore, a total of 10 linguistic variables $(K_1, K_2, \dots, K_{10})$ are described. Fuzzy sets demonstrate all these linguistic variables as follows:

$$K_1 = \left\{\frac{1}{c_1} + \frac{0.5}{c_2} + \frac{0}{c_3} + \frac{0}{c_4} + \frac{0}{\square_5} + \frac{0}{c_6} + \frac{0}{c_7} + \frac{0}{c_8} + \frac{0}{c_9} + \frac{0}{c_{10}}\right\}$$

$$K_2 = \left\{\frac{0.5}{c_1} + \frac{1}{c_2} + \frac{0.5}{c_3} + \frac{0}{c_4} + \frac{0}{c_5} + \frac{0}{c_6} + \frac{0}{c_7} + \frac{0}{c_8} + \frac{0}{c_9} + \frac{0}{c_{10}}\right\}$$

$$K_3 = \left\{\frac{0}{c_1} + \frac{0.5}{c_2} + \frac{1}{c_3} + \frac{0.5}{c_4} + \frac{0}{c_5} + \frac{0}{c_6} + \frac{0}{c_7} + \frac{0}{c_8} + \frac{0}{c_9} + \frac{0}{c_{10}}\right\}$$

$$K_4 = \left\{\frac{0}{c_1} + \frac{0}{c_2} + \frac{0.5}{c_3} + \frac{1}{c_4} + \frac{0.5}{c_5} + \frac{0}{c_6} + \frac{0}{c_7} + \frac{0}{c_8} + \frac{0}{c_9} + \frac{0}{c_{10}}\right\}$$

$$K_5 = \left\{\frac{0}{c_1} + \frac{0}{c_2} + \frac{0}{c_3} + \frac{0.5}{c_4} + \frac{1}{c_5} + \frac{0.5}{c_6} + \frac{0}{c_7} + \frac{0}{c_8} + \frac{0}{c_9} + \frac{0}{c_{10}}\right\}$$

$$K_6 = \left\{\frac{0}{c_1} + \frac{0}{c_2} + \frac{0}{c_3} + \frac{0}{c_4} + \frac{0.5}{c_5} + \frac{1}{c_6} + \frac{0.5}{c_7} + \frac{0}{c_8} + \frac{0}{c_9} + \frac{0}{c_{10}}\right\}$$

$$K_7 = \left\{\frac{0}{c_1} + \frac{0}{c_2} + \frac{0}{c_3} + \frac{0}{c_4} + \frac{0}{c_5} + \frac{0.5}{c_6} + \frac{1}{c_7} + \frac{0.5}{c_8} + \frac{0}{c_9} + \frac{0}{c_{10}}\right\}$$

$$K_8 = \left\{\frac{0}{c_1} + \frac{0}{c_2} + \frac{0}{c_3} + \frac{0}{c_4} + \frac{0}{c_5} + \frac{0}{c_6} + \frac{0.5}{c_7} + \frac{1}{c_8} + \frac{0.5}{c_9} + \frac{0}{c_{10}}\right\}$$

$$K_9 = \left\{\frac{0}{c_1} + \frac{0}{c_2} + \frac{0}{c_3} + \frac{0}{c_4} + \frac{0}{c_5} + \frac{0}{c_6} + \frac{0}{c_7} + \frac{0.5}{c_8} + \frac{1}{c_9} + \frac{0.5}{c_{10}}\right\}$$

$$K_{10} = \left\{\frac{0}{c_1} + \frac{0}{c_2} + \frac{0}{c_3} + \frac{0}{c_4} + \frac{0}{c_5} + \frac{0}{c_6} + \frac{0}{c_7} + \frac{0}{c_8} + \frac{0.5}{c_9} + \frac{1}{c_{10}}\right\}$$

The degree of membership of each year's enrollment value belonging to each K_i is procured, where, the maximum degree of membership of a fuzzy set K_i forms at interval c_i $(1 \leq i \leq 10)$.

Step 3. Fuzzify this data set.

If one year's enrollment value belongs to the interval c_i, for that year, the fuzzified enrollment value is considered as K_i. For instance, since the enrollment value of the year 1971 belongs to the interval c_1, it is fuzzified to K_1. Thus, this data set is fuzzified. The values of actual and fuzzified enrollments are given in Table 2.

Table 2. Actual and fuzzified enrollments of University of Alabama

Year	Actual enrollments	Fuzzified enrollments
1971	13055	K_1
1972	13563	K_1
1973	13867	K_2
1974	14696	K_3
1975	15460	K_4
1976	15311	K_4
1977	15603	K_5
1978	15861	K_5
1979	16807	K_6
1980	16919	K_7
1981	16388	K_6
1982	15433	K_4
1983	15497	K_4
1984	15145	K_4
1985	15163	K_4
1986	15984	K_5
1987	16859	K_7
1988	18150	K_9
1989	18970	K_{10}
1990	19328	K_{10}
1991	19337	K_{10}
1992	18876	K_{10}

Step 4.

The calculations have been performed by Eq. (5-10) respectively for the proposed method. The results obtained along with the results of other methods are given in Table 3.

Forecasting for 14696;

$$ED_i = |13867 - 13563|$$

$$ED_{ii} = |13563 - 13055|$$

$$\overline{ED} = \frac{304 + 508}{2}$$

$$S_i = (304 - 406) + (508 - 406)$$

$$X_i = 14627.5 + \frac{144.249 * 100}{406}$$

$$F_j = 14663.029$$

MSE and AFE are used to evaluate the accuracy of fuzzy time series forecasting. For the forecasting method, lower values of MSE or AFE are better. The equations of AFE and MSE are as follows;

$$MSE = \frac{\sum_{i=1}^{n}(Actual\ value_i - Forecasted\ value_i)^2}{n}$$

$$AFE\ (in\ \%) = \frac{sum\ of\ forecasting\ errors}{n}$$

$$Forecasting\ errors\ (in\ \%) = \frac{|Forecasted\ value - Actual\ value|}{Actual\ value} x100$$

The MSE and AFE have been computed to compare the accuracy of the forecasted value obtained by the proposed method with other methods. In Table 3, the values of AFE and MSE calculated are given.

Table 3. Comparative presentations of enrollments forecast by various methods.

Year	Actual enrollment	Method (Cheng et al. 2008) [22]	Method (Wong et al. 2010) [23]	Method (Chen and Tanuwijay, 2011) [24]	Method (Gangwar and Kumar, 2012) [2]	Method (Singh and Borah, 2013) [12]	Proposed Method
1971	13055	-	-	-	-	-	-
1972	13563	14242	-	13512	-	13563	-
1973	13867	14242	13500	13998	13500	13867	-
1974	14696	14242	14500	14658	14500	14696	14663.029
1975	15460	15474.3	15500	15341	15500	15425	15322.030
1976	15311	15474.3	15466	15501	15500	15420	15262.270
1977	15603	15474.3	15392	15501	15500	15420	15980.76
1978	15861	15474.3	15549	15501	15500	15923	15931.357
1979	16807	16146.5	16433	17065	-	16862	16523.242
1980	16919	16988.3	16656	17159	-	17192	17224.31
1981	16388	16988.3	16624	17159	16500	17192	16625.979
1982	15433	16146.5	15556	15341	15500	15425	15348.654
1983	15497	15474.3	15524	15501	15500	15420	15296.851
1984	15145	15474.3	15497	15501	15500	15420	15380.156
1985	15163	15474.3	15305	15501	15500	15627	15354.407
1986	15984	15474.3	15308	15501	-	15627	16013.161
1987	16859	16146.5	16402	17065	-	16862	17278.853
1988	18150	16988.3	18500	17159	18500	17192	18406.002
1989	18970	19144	18534	18832	18500	18923	19057.661
1990	19328	19144	19345	19333	19337	19333	19062.053
1991	19337	19144	19423	19083	19500	19136	19085.964
1992	18876	19144	18752	19083	18704	19136	19164.985
MSE	-	228909.4	88337.2	122085	62976.63	106037.1	**53012.28**
AFE	-	2.3915	1.51894	1.53526	1.269981	**1.19016**	**1.19202**

As shown in Table 3, the MSE value of the proposed model is lower than that of the other models. AFE values of the proposed method and Singh and Borah's (2013) [12] method are very close to each other. According to the values of MSE and AFE, the proposed method provides a forecast of higher accuracy. This indicates the superiority of the proposed method over the others.

The sufficiency of the proposed model is also investigated by performing it into the real-life problem of a dynamic system containing fuzziness like rice production. For this reason, the time-series data of rice production obtained from the huge farm of G.B. Pant University, Pantnagar is used. This data is formed according to productivity in kg per hectare. The algorithm of the proposed model has been applied as above and the results obtained are offered.

R=4554-3219=1335

$$m = 2\sqrt{20} \cong 10$$

$$h = \frac{1335}{10} \cong 134$$

$c_1 = [3219, 3353]$, $c_2 = [3353, 3487]$, $c_3 = [3487, 3621]$, $c_4 = [3621, 3755]$,
$c_5 = [3755, 3889]$, $c_6 = [3889, 4023]$, $c_7 = [4023, 4157]$,
$c_8 = [4157,4291]$, $c_9 = [4291, 4425]$, $c_{10} = [4425, 4559]$

Lengths of the interval were determined according to the proposed approach and mid-points were found for each interval. In Table 4, new intervals obtained, mid-points, and their corresponding elements are given.

Table 4. Obtained new intervals, mid-points and their corresponding elements.

Intervals	Mid-point	Corresponding elements
c_1	3286	3222, 3219
c_2	3420	3372
c_3	3554	3552, 3455, 3592,
c_4	3688	3702, 3670, 3750
c_5	3822	3865, 3851, 3872
c_6	3956	3928
c_7	4090	
c_8	4224	4177, 4170, 4266
c_9	4358	4305
c_{10}	4492	4554, 4439

This data set is split up ten intervals $(c_1, c_2, \dots, c_{10})$ and a total of 10 linguistic variables $(K_1, K_2, \dots, K_{10})$ are assigned. Similarly, the linguistic variables are indicated by fuzzy sets as shown in Step 2 and Step 3.

The degree of membership of each year's enrollment value belonging to each c_i is obtained and this time series data set is fuzzified. The calculations have been carried out by using the algorithm of the proposed method. The actual and fuzzified enrollments values and the results obtained are given in Table 5.

Table 5. Actual and Fuzzified enrollments of rice production

Year	Actual enrollments	Fuzzified enrollments	Proposed model
1981	3552	K_3	-
1982	4177	K_8	-
1983	3372	K_2	-
1984	3455	K_3	3571.801
1985	3702	K_4	3802.984
1986	3670	K_4	3758.281
1987	3865	K_5	3930.97
1988	3592	K_3	3668.688
1989	3222	K_1	3309.570
1990	3750	K_4	3709.334
1991	3851	K_5	3846.882
1992	3231	K_1	3382.004
1993	4170	K_8	4295.844
1994	4554	K_{10}	4520.937
1995	3872	K_5	3881.326
1996	4439	K_{10}	4531.534
1997	4266	K_8	4234.87
1998	3219	K_1	3361.297
1999	4305	K_9	4459.313
2000	3928	K_6	3958.585

MSE and AFE values were calculated to compare the proposed model with other models. The results are given in Table 6.

Table 6. MSE and AFE of rice production forecast

	Proposed Method	**Chen's method (1996) [25]**	**Song and Chissom method (1993) [5]**
MSE	**8561.948**	132162.9	131715.9
AFE	**2.148**	7.934	7.948

In Table 6, it is shown that the suitability of the proposed method is better than Chen's (1996) [25] model and the method of Song and Chissom (1993) [5] by the comparison of MSE and AFE.

4. CONCLUSIONS

In this study, a computation model with high accuracy based on the lengths of the interval is proposed. The algorithms of the proposed model are simple. This model has been used for forecasting the time series data of enrollments of the University of Alabama and has been compared with the existing models. MSE and AFE values were used to compare with the methods. AFE and MSE were used for the measurement of the accuracy of the forecast. According to the values of AFE and MSE obtained by methods, the proposed model outperforms the models proposed by Cheng et al. (2008) [22], Wong et al. (2010) [23], Chen and Tanuwijaya (2011) [24], Gangwar and Kumar (2012) [2], and Singh and Borah (2013) [12] in this dataset. Moreover, the proposed method has also been performed on rice production forecasts. The performance of the proposed method in the forecasting of the rice production is compared with the models suggested by Chen's method (1996) [25] and Song and Chissom

method (1993) [5]. By MSE and AFE, the proposed model provides results of better accuracy than both models. Therefore, the proposed method is a preferable model for fuzzy time series forecasting.

REFERENCES

[1] Hwang, J.R., Chen, S.M. and Lee, C.H. (1998). Handling forecasting problems using fuzzy time series, *Fuzzy sets and systems*, 100(1-3): 217-228.

[2] Gangwar, S.S. and Kumar, S. (2012). Partitions based computational method for high-order fuzzy time series forecasting, *Expert Systems with Applications*, 39(15): 12158-12164.

[3] Singh, S.R. (2008). A computational method of forecasting based on fuzzy time series, *Mathematics and Computers in Simulation*, 79(3): 539-554.

[4] Zadeh, L. A. (1965). Fuzzy sets, *Information and control*, 8(3): 338-353.

[5] Song, Q. and Chissom, B.S. (1993). Forecasting enrollments with fuzzy time series—part I, *Fuzzy sets and systems*, 54(1): 1-9.

[6] Huarng, K. (2001). Heuristic models of fuzzy time series for forecasting, *Fuzzy sets and systems*, 123(3): 369-386.

[7] Huarng, K. (2001). Effective lengths of intervals to improve forecasting in fuzzy time series, *Fuzzy sets and systems,* 123(3): 387-394.

[8] Singh, S.R. (2007). A robust method of forecasting based on fuzzy time series, *Applied Mathematics and Computation*, 188(1): 472-484.

[9] Singh, S.R. (2007). A simple method of forecasting based on fuzzy time series, *Applied mathematics and computation,* 186(1): 330-339.

[10] Singh, S.R. (2007). A simple time variant method for fuzzy time series forecasting, *Cybernetics and Systems: An International Journal*, 38(3): 305-321.

[11] Yolcu, U., Egrioglu, E., Uslu, V. R., Basaran, M. A. and Aladag, C. H. (2009). A new approach for determining the length of intervals for fuzzy time series, *Applied Soft Computing,* 9(2): 647-651.

[12] Singh, P. and Borah, B. (2013). An efficient time series forecasting model based on fuzzy time series, *Engineering Applications of Artificial Intelligence*, 26(10): 2443-2457.

[13] Wang, L., Liu, X. and Pedrycz, W. (2013). Effective intervals determined by information granules to improve forecasting in fuzzy time series, *Expert Systems with Applications*, *40*(14): 5673-5679.

[14] Ye, F., Zhang, L., Zhang, D., Fujita, H. and Gong, Z. (2016). A novel forecasting method based on multi-order fuzzy time series and technical analysis, *Information Sciences*, *367*: 41-57.

[15] Yolcu, O. C., Yolcu, U., Egrioglu, E. and Aladag, C. H. (2016). High order fuzzy time series forecasting method based on an intersection operation, *Applied Mathematical Modelling*, *40*(19-20): 8750-8765.

[16] Jiang, P., Dong, Q., Li, P. and Lian, L. (2017). A novel high-order weighted fuzzy time series model and its application in nonlinear time series prediction, *Applied Soft Computing*, *55*: 44-62.

[17] Singh, P. (2017). High-order fuzzy-neuro-entropy integration-based expert system for time series forecasting, *Neural Computing and Applications*, *28*(12): 3851-3868.

[18] Chen, S. M. and Phuong, B. D. H. (2017). Fuzzy time series forecasting based on optimal partitions of intervals and optimal weighting vectors, *Knowledge-Based Systems*, *118*: 204-216.

[19] Bas, E., Grosan, C., Egrioglu, E. and Yolcu, U. (2018). High order fuzzy time series method based on pi-sigma neural network, *Engineering Applications of Artificial Intelligence*, *72*: 350-356.

[20] Panigrahi, S. and Behera, H. S. (2020). A study on leading machine learning techniques for high order fuzzy time series forecasting, *Engineering Applications of Artificial Intelligence*, *87:* 103245.

[21] Pattanayak, R. M., Panigrahi, S. and Behera, H. S. (2020). High-order fuzzy time series forecasting by using membership values along with Data and Support Vector Machine, *Arabian Journal for Science and Engineering*, *45*(12): 10311-10325.

[22] Cheng, C. H., Wang, J. W. and Cheng, G. W. (2008). Multi-attribute fuzzy time series method based on fuzzy clustering, Expert Systems with Applications, 34: 1235–1242.

[23] Wong, W.K., Bai, E. and Chu, A.W.C. (2010). Adaptive time-variant models for fuzzy-time-series forecasting, *IEEE Transactions on Systems, Man, and Cybernetics, Part B (Cybernetics)*, 40(6): 1531-1542.

[24] Chen, S.M. and Tanuwijaya, K. (2011). Fuzzy forecasting based on high-order fuzzy logical relationships and automatic clustering techniques, *Expert Systems with Applications*, 38(12): 15425-15437.

[25] Chen, S.M. (1996). Forecasting enrollments based on fuzzy time series, *Fuzzy sets and systems*, 81(3): 311-319.

NATURENGS
MTU Journal of Engineering and Natural Sciences
https://dergipark.org.tr/tr/pub/naturengs
DOI: 10.46572/naturengs.872231

Research Article

Numerical Analysis of Geotechnical Seismic Isolation System for High-Rise Buildings

Özgür YILDIZ

Department of Civil Engineering, Faculty of Engineering and Natural Sciences,
Malatya Turgut Özal University, Malatya, Turkey

(**Received**: 01.02.2021; **Accepted**: 04.04.2021)

ABSTRACT: Seismic isolation is a method of protecting buildings from earthquake-induced deformations by using isolators and devices under the superstructure. The purpose of the seismic isolation method is to reduce the earthquake forces transferred from the ground to the structure by placing energy-absorbing elements between the foundation and superstructure. Especially in developing countries, the "Geotechnical Seismic Isolation (GSI)" system has been proposed as an isolation method to reduce earthquake-induced damages on buildings. This study, it is aimed to reduce the effects of earthquakes in a multi-story building with an isolation layer formed by a rubber-sand mixture (RSM). For this purpose, a 10-story reinforced concrete building was numerically modeled. Beneath the foundation of the building model, a seismic energy absorbent RSM layer was placed and its contact with the natural soil was interrupted by using geosynthetic liners. The model was subjected to the 1992 Erzincan (EW) Earthquake motion and its performance has been evaluated in terms of lateral displacements and accelerations. The numerical studies indicated a substantial improvement due to the use of the RSM layer. The accelerations measured by the superstructure decreased up to 48% by employing the isolation layer. The numerical analysis was carried out using the dynamic module of the PLAXIS 2D finite element analysis program.

Keywords: Geotechnical Seismic Isolation, Rubber Soil Mixture, Dynamic Analysis

1. INTRODUCTION

Since common technology is not sufficient to predict the location, magnitude, and time of earthquakes, the design of earthquake-resistant engineering structures has been inevitable for humanity. Especially the earthquakes with large magnitudes we have experienced in the last century and the resulting loss of life and property have made the design of the earthquake-resistant building one of the most important issues of civil engineering. With the methods and approaches developed in this direction, it is aimed to minimize the damages caused by earthquakes in the buildings, to prevent the loss of life and property, and to be able to fulfill the functions of the buildings after the earthquake. In this context, the design of the architectural and structural systems, structural materials to be used, seismicity of the area, and local soil conditions are the most important factors to be considered in earthquake-resistant building design.

Researchers have developed innovative approaches to ensure that structures display the intended level of resistance against earthquakes. In these approaches, seismic isolation elements are generally used above the foundation level, depending on the principle of separating the

Corresponding Author: ozgur.yildiz@ozal.edu.tr
ORCID number of authors: 0000-0002-3684-3750

building from the ground. The basic principle of seismic isolation is to ensure that the ground motion that occurs during an earthquake is transferred to the structure in limited levels and thus the forces that will occur in the structural system are minimized. Isolation elements with low lateral stiffness placed at the level of the foundation enable the structure to oscillate at frequencies lower than the predominant frequency during an earthquake and the superstructure is exposed to lower earthquake forces. The occurrence of higher displacements at the isolation layer compared to the superstructure reduces the relative displacements. With the lengthening of the vibration period of the system, the story accelerations decrease and the structural and non-structural damages are minimized. In an ideal seismic isolation system, the earthquake forces transferred to the building are zero, but it is not possible to achieve this in practice. Successful examples of seismic isolation method in public buildings such as hospitals and transportation facilities were exhibited in our country (Istanbul Sabiha Gökçen International Airport Terminal, 2008; Erzurum Health Campus Buildings, 2012; Marmara University Hospital Buildings, 2013; Başakşehir Çam and Sakura City Hospital, 2020).

Although it has existed as a concept among seismic isolation approaches for a long time, the isolation method suggested by Tsang [1] was first introduced into the literature with the definition of 'Geotechnical Seismic Isolation (GSI)'. This innovative approach was previously proposed by researchers with the idea of laying a synthetic layer under the building foundations and distributing earthquake energy [2, 3]. Similarly, studies were also carried out on reducing horizontal ground movements by using geotextile between soil layers [4]. However, the GSI method became prominent with the modeling of the RSM layer under the foundation of a 10-story building for seismic isolation (Fig. 1) [1]. It is stated that with the use of the RSM layer, not only the horizontal movement is damped, but also the vertical movements are limited. Regarding the content and applicability of the method; it was also underlined that factors such as nonlinear soil behavior, resonance effects of the soil, liquefaction, ground settlement, and environmental effects should be evaluated. In subsequent studies, comprehensive numerical and experimental studies were carried out on the seismic isolation capacity of RSM layers formed with varying rubber contents [1, 5-10].

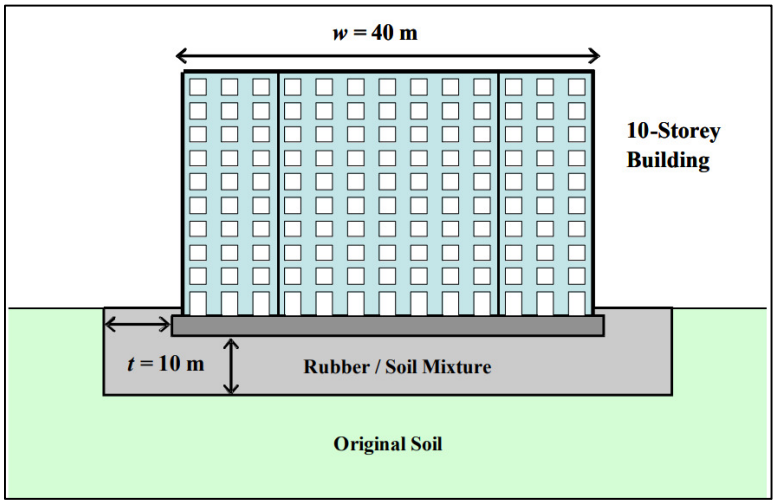

Figure 1. Seismic isolation with rubber-soil mixture [1]

Another example of the GSI method is developing an isolation layer using geosynthetic material with or without an RSM layer. Experimental and numerical studies performed on this method have shown that the seismic performance of low and medium-height buildings improved

significantly with geosynthetic layers created in different configurations [11-13]. The method of improving the earthquake performance of soils with geosynthetics has been used not only under the foundation of superstructures but also for strengthening earth retaining structures [12, 14]. Furthermore, researches were carried out on the use of geosynthetics in sloped soils and conducted numerical studies were conducted [15, 16].

In this study, the seismic performance of a high-rise building isolated by a layer of RSM was investigated. In this context, an RSM isolated 10-story building was numerically modeled. The 1992 Erzincan (EW) earthquake motion with varying amplitudes was applied to the developed model. The performance of the RSM-isolated building was evaluated in terms of accelerations and lateral displacements. The dynamic module of the PLAXIS2D finite element analysis program was used for numerical analysis. The applied earthquake records were obtained from the official website of AFAD. The results are graphically presented as acceleration-time and displacement-time histories.

2. NUMERICAL MODELLING

In this study, a high-rise (10-story) building was modeled using the PLAXIS 2D finite element analysis program and its foundation was isolated with the RSM layer. The width of the building foundation is designed as 12 m, story height 2.85 m and foundation depth 90 cm. The thickness of the RSM layer under the foundation is set at 12 m and is equal to the width of the foundation. Two smooth synthetic liners were used to separate the RSM layer from the natural soil, as suggested by the researcher [4]. The synthetic liners were separated by a space of 1 m. The total lengths of both synthetic liners were set as 60 and 64 m, surrounding the RSM layer under the foundation all around. The generic soil conditions are used as a soil profile. Under the foundation of the building, a clay layer with 15 m thickness and a sand layer with 25 m thickness were designed. The groundwater table is set as deep enough below the foundation level. The schematic view of the numerical model is shown in Figure 2.

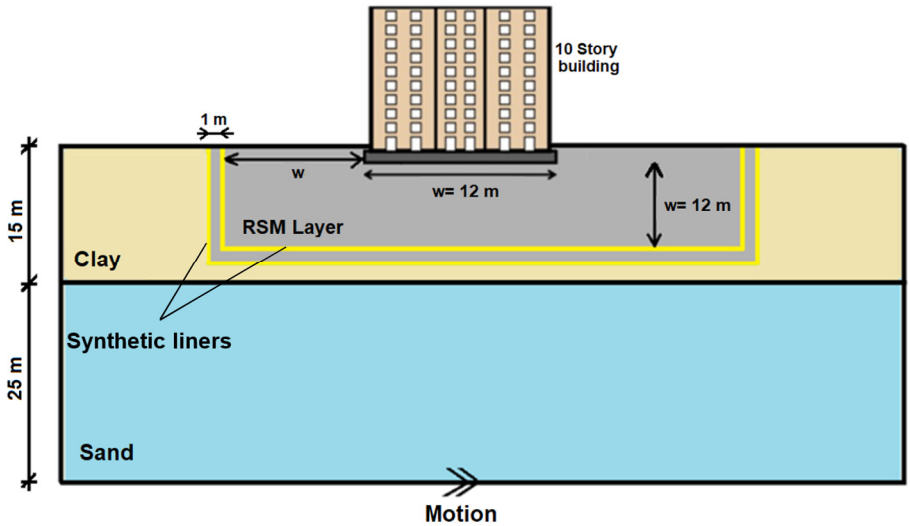

Figure 2. The schematic view of the numerical model

The geometry was simulated using an axisymmetric model in which the building model was positioned along the axis of symmetry. Both the soil and building were modeled with 15-noded elements. Interface elements were placed around the foundation and geosynthetics to model the interaction between separated elements. The boundaries of the model were taken sufficiently

far away (200*50 m) to avoid the direct influence of the boundary conditions. Standard fixities were considered and standard absorbent boundaries were used to avoid spurious reflections. Static load was applied to the building model at the top ceiling level. The strength reduction factor was taken as unity (R_{inter} = 1) for all soil layers. After defining the geometry of the model and assigning the material properties, a two-dimensional mesh was generated to perform the finite element calculations. The mesh generation is performed through 15-noded triangular elements. Since the model includes edges of used geosynthetic liners, the local coarseness factor is set to 1.0 which corresponds to medium size element distributions for all geometry points. Initial effective stresses were generated by the K_o procedure. The meshed view of the RSM isolated building model with two layers of smooth geosynthetic liners is shown in Figure 3.

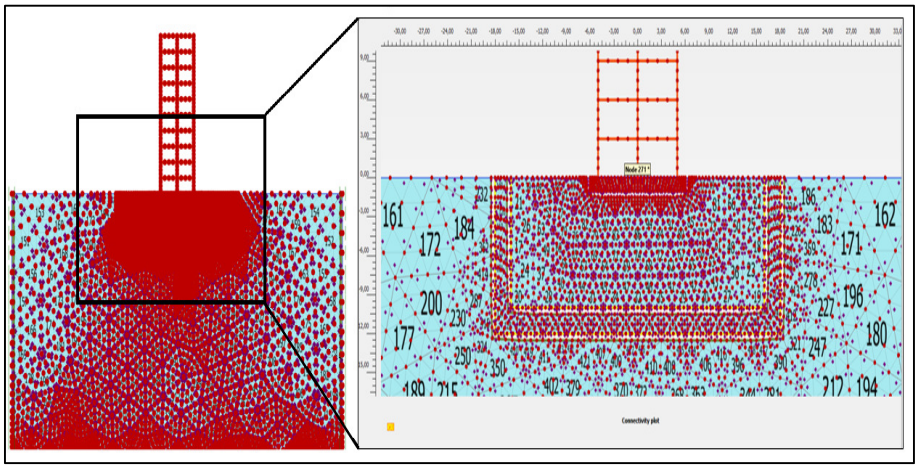

Figure 3. The meshed view of the model with RSM isolation layer

2.1. Material Properties

The RSM layer placed beneath the foundation consists of a mixture of scrap tires and sand materials. The soil material was modeled using the hardening soil model which is an advanced model for the simulation of soil behavior under dynamic loading. The properties and used parameters of the RSM layer, sand, and clay materials are presented in Table 1. Structural elements of the model are selected as plate elements in PLAXIS2D. The parameters of the footing, building and geosynthetic liner are given in Table 2.

Table 1. Material properties

Parameter	Clay	Sand	RSM
E_{50}^{ref}(kPa)	10.000	15.000	6300
E_{oed}^{ref}(kPa)	10.000	15000	6300
E_{ur}^{ref}(kPa)	30.000	45000	20000
c^{ref}(kPa)	5	5	5
ϕ´(°)	26	21	60
Ψ (°)	0	0	35
γ_{sat} (kN/m³)	17,5	17	13.3
γ_{unsat} (kN/m³)	17,5	17	13.3
K_o	0,3	0,4	0.4
ν	0,3	0,2	0.2
e_{init}	0,5	0,5	0.4

E_{50}^{ref}: secant stiffness, E_{oed}^{ref}: oedometer loading stiffness, E_{ur}^{ref}: unloading–reloading stiffness, c_{ref}: effective shear strength, ϕ′: effective friction angle, Ψ: dilatancy angle, γ_{sat}: saturated unit weight, γ_{unsat}: unsaturated unit weight, K_o: pressure coefficients, ν: Poisson's ratio, e_{init}: initial void ratio.

Table 2. Parameters of footing, building and geosynthetic

Parameter	Footing	Building	Geosynthetic
EA (kN/m)	$12E^6$	$9E^6$	$500E^3$
EI (kN/m)	$400E^3$	$67.5E^3$	-

EA: normal stiffness, EI: flexural rigidity

2.2. Dynamic Motion

The 1992 Erzincan (EW) Earthquake (Ms:6.8, PGA: 0.50g) motion record was used for the dynamic analysis. The acceleration-time history of the earthquake motion can be seen in Figure 4. To investigate the effect of the varying amplitudes, the earthquake motion with 1A, 0.5A, and 2A were applied both to non-isolated and isolated building models.

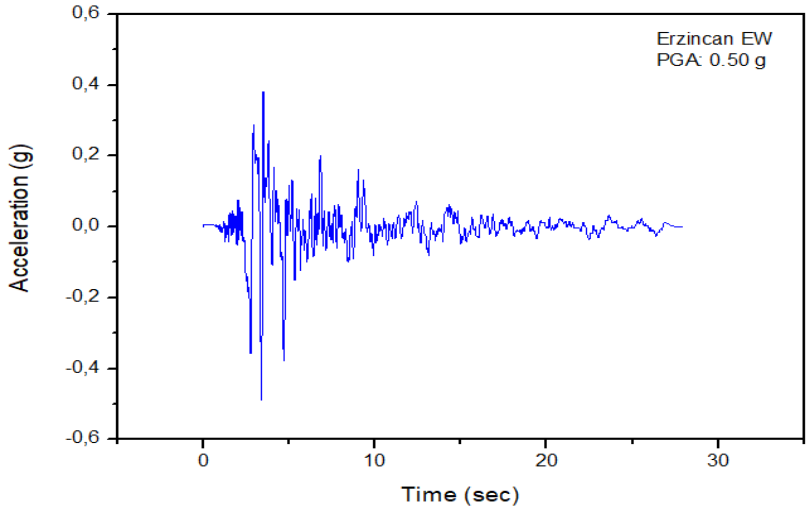

Figure 4. Acceleration time history of 1992 Erzincan EW earthquake motion

3. RESULTS AND DISCUSSION

Numerical results are presented in terms of transmitted accelerations and lateral displacements for a controlling node selected at the mid-top of the building model. Results are given both for non-isolated and isolated cases.

The acceleration-time history of the model subjected to 2A amplitude earthquake motion is shown in Figure 5a. The maximum acceleration value of the non-isolated model is measured as 0.81g at 3.5 sec. The maximum lateral acceleration for the isolated case is measured as 0.42g at 3.8 sec. The reduction of the lateral acceleration with the use of the RSM layer is calculated as 48 %. The maximum lateral displacements are measured as 13 cm and 18 cm for non-isolated and isolated models, respectively (Fig. 5b). The use of the RSM layer leads to deamplification of lateral acceleration whereas it causes a 38% increase in lateral displacement. Soft soils can potentially act as a natural mechanism for passive isolation, especially for near-field earthquakes that are rich in high-frequency wave components. Similarly, the use of the RSM layer, which represents soft soil conditions, leads reduction in accelerations, especially at higher frequencies. The reduction in measured acceleration is also apparent in amplitude spectra of the isolated case (Fig. 6).

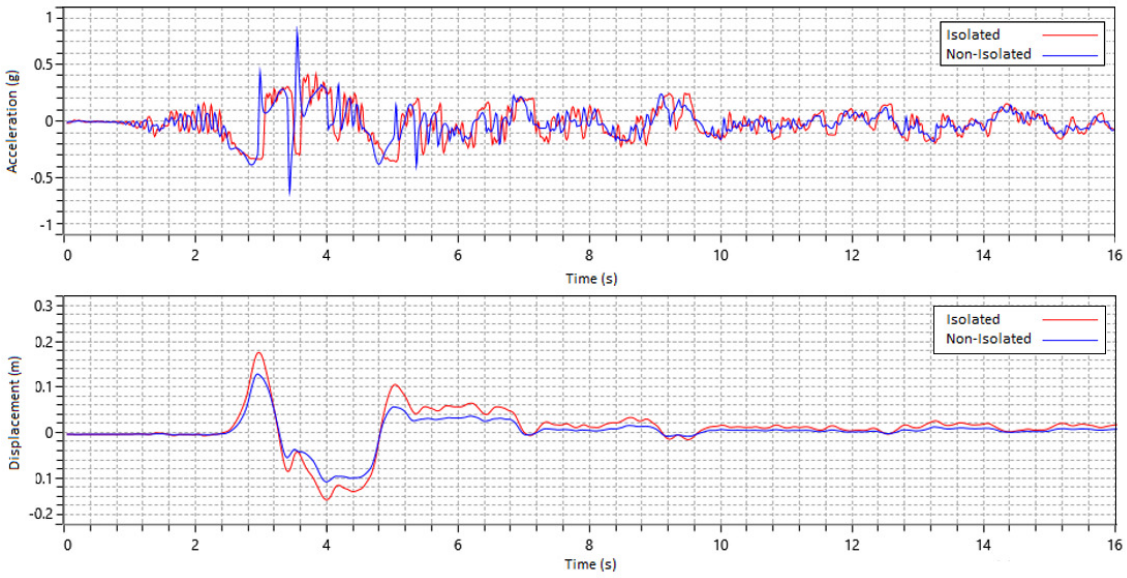

Figure 5. a. Acceleration-time history and **b.** displacement-time history of the models subjected to 2A amplitude of earthquake motion

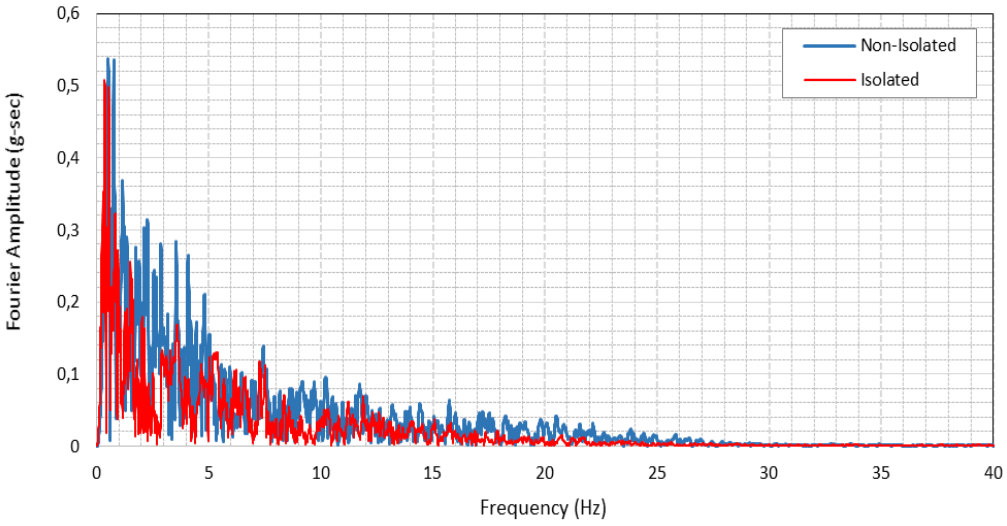

Figure 6. Fourier amplitude spectra of the acceleration time history of the models subjected to 2A amplitude of earthquake motion

The analysis results of the numerical model subjected to 1A amplitude earthquake motion are shown in Figure 7. The maximum acceleration value of the non-isolated model is measured as 0.41g at 3.6 sec. The isolated model reduced the lateral acceleration measured in 4. Second to 0.27 g (Fig.7a). The reduction in acceleration is calculated as 34%. The lateral displacements at the top of the building are measured as 7 cm and 5 cm for isolated and non-isolated models, respectively (Fig.7b). The final lateral distance of the isolated model concerning its original position is about 1 cm which reveals a recentring problem. There is a significant decrease in amplitudes at frequencies greater than 2 Hz. This is attributed to the implementation of a less stiff layer beneath the foundation lengthening the period of shaking (Fig. 8).

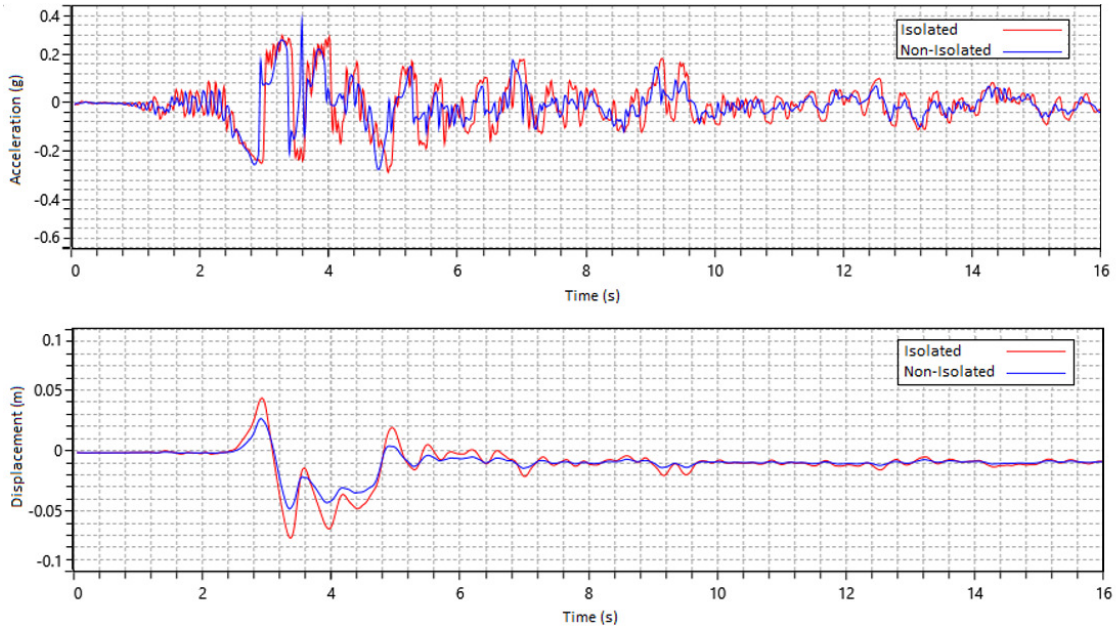

Figure 7. a. Acceleration-time history and **b.** displacement-time history of the models subjected to 1A amplitude of earthquake motion.

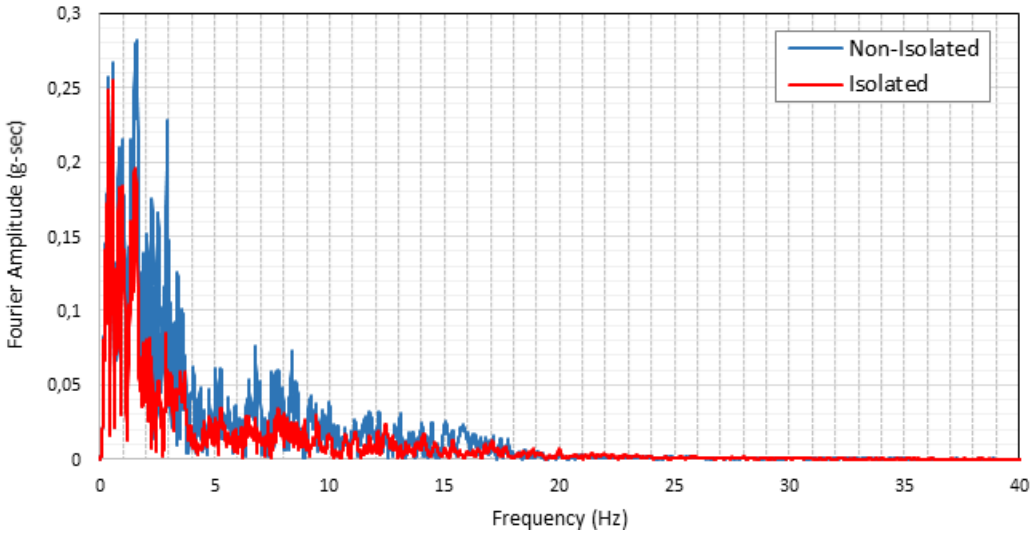

Figure 8. Fourier amplitude spectra of the acceleration time history of the models subjected to 1A amplitude of earthquake motion

The horizontal accelerations measured by isolated and non-isolated models are 0.18 g and 0.22g, at 3.5 and 3.6 seconds, respectively (Fig. 9a). The amount of reduction in lateral displacement is calculated as 18%. The lateral displacement for the non-isolated model is measured as 20 cm. However, as those obtained by models analyzed under higher amplitudes, the lateral displacement measured by the non-isolated model is lower than of isolated model as 12 cm (Fig. 9b). It is observed that the use of an isolation layer decreases the accelerations whereas it leads to an increase in lateral displacements. The amplitude spectra of acceleration for the isolated model are lower than the non-isolated one especially at higher frequencies (Fig.10). The use of the RSM layer under all three amplitudes leads to deamplification of

accelerations. However, it was observed that in cases where the amplitude of the input motion is higher, the deamplification effect becomes more pronounced (Table 3).

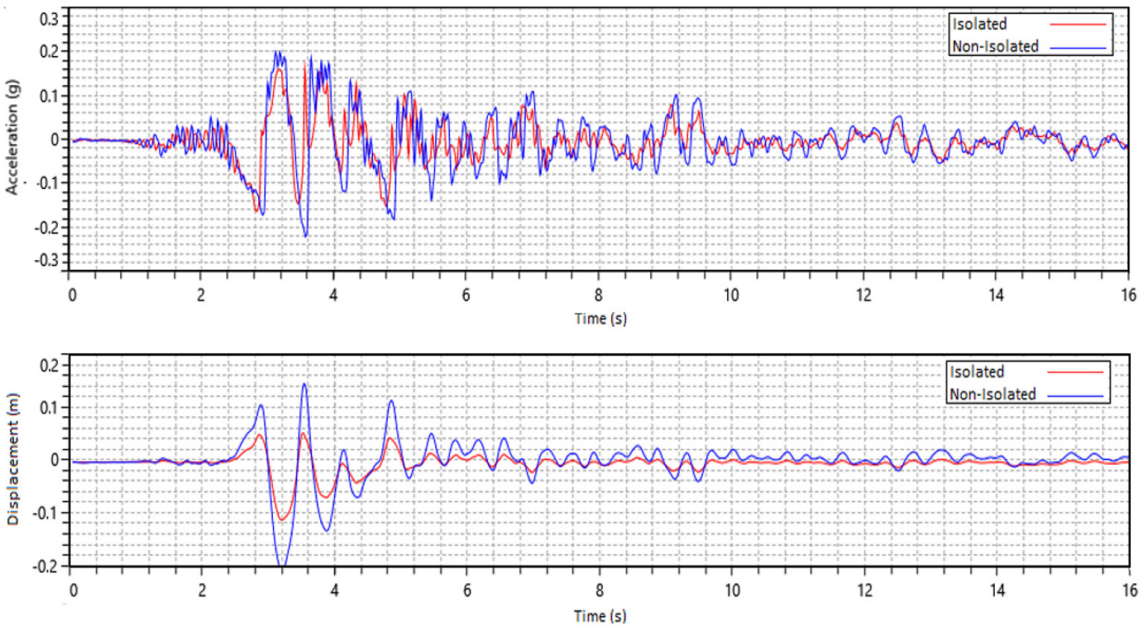

Figure 9. a. Acceleration-time history and **b.** displacement-time history of the models subjected to 0.5A amplitude of earthquake motion.

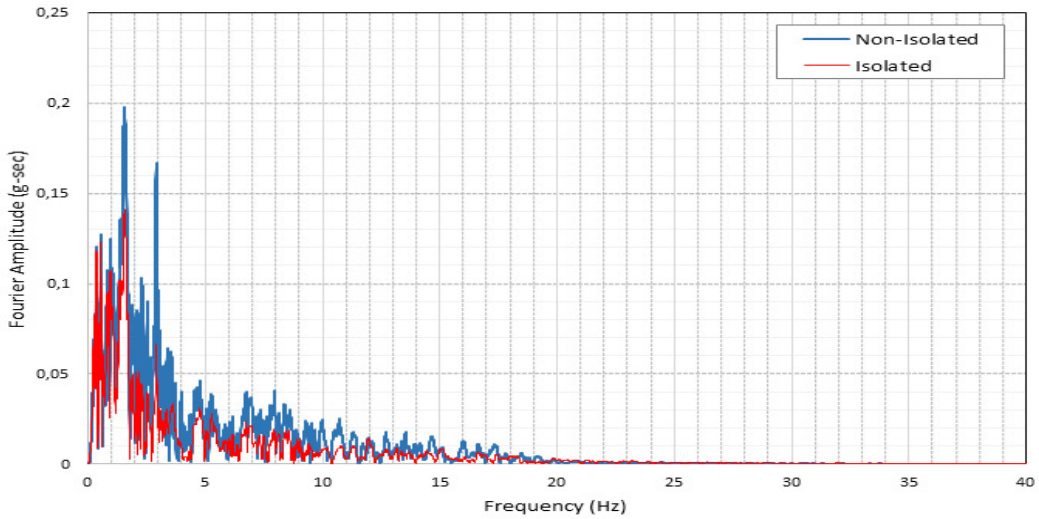

Figure 10. Fourier amplitude spectra of the acceleration time history of the models subjected to 0.5A amplitude of earthquake motion

Table 3. Measured acceleration values and calculated the percentage of reductions.

Model	**Acceleration**		
	2A	**1A**	**0.5A**
Non-Isolated	0.81g	0.41g	0.22g
Isolated	0.42g	0.27g	0.18g
Reduction (%)	48	34	18

5. CONCLUSIONS

In this study, the effectiveness of the Geotechnical Seismic Isolation system was investigated by developed numerical models. In this context, an isolation layer formed by rubber-soil mixture (RSM) was placed under a high-rise building model with two separated smooth synthetic liners. The performance of the model under real earthquake excitation with different amplitudes was examined. Based on the results of numerical analyses the following main conclusions can be drawn:

- The measured acceleration values are reduced between 18 and 48 % with the use of the RSM layer.
- A deamplification is observed in the acceleration values measured at the top of the isolated building model, while an increase in the displacements is observed.
- The recent problem that occurred by isolated models is attributed to the high friction angle of the RSM layer.
- As the amplitude of the applied input motion decreases, the reduction in accelerations measured by the use of the isolation layer decreased.

The GSI method examined in this study is not an alternative to the conventional seismic isolation method. However, it is a promising method since it is a low-cost application and can contribute to environmental problems caused by waste tire stockpiles. Numerical models regarding the use of the GSI method have been developed widely in the literature but it has no known real application. Since the material used in this method has high compressibility, it should be verified to what extent the behavior of the material under heavy structural loads will be compatible with numerical models. Additionally, numerical and low-scale models show that the performance of the proposed method in the laboratory environment under short-term loading conditions is satisfactory. However, the behavior of the RSM layer that will be subjected to high structural loads and environmental influences is still a virgin issue. To clarify these issues with larger-scale model tests is likely to expand the field of the practical application of the GSI method.

REFERENCES

[1] Tsang, H. H. (2008). Seismic Isolation by Rubber–Soil Mixtures for Developing Countries, *Earthquake Engineering and Structural Dynamics*, 283-303.

[2] Kavazanjian, E. J., Hushmand, B., and Martin, G. R. (1991). Frictional Base Isolation Using a Layered Soil-Synthetic Liner System. Proceedings of the Third U.S. Conference on Lifeline Earthquake Engineering (pp. 1139-1151). Los Angeles, California: ASCE Technical Council on Lifeline Earthquake Engineering Monograph No. 4.

[3] Yegian, M. K., and Lahlaf, A. M. (1992). Dynamic Interface Shear Strength Properties of Geomembranes and Geotextiles, *Journal of Geotechnical Engineering*, 760-77.

[4] Yegian, M.K., and Catan, M. (2004). Soil Isolation for Seismic Protection Using a Smooth Synthetic Liner, *Journal of Geotechnical and Geoenvironmental Engineering*, 130 (11): 123-131.

[5] Mavronicola, E., Komodromos, E., and Charmpis, D.C. (2010). Numerical Investigation of Potential Usage of Rubber-Soil Mixtures as a Distributed Seismic Isolation Approach, *Proceedings of the Tenth International Conference on Computational Structures Technology*, 1-12.

[6] Tsang, H., Lo, S. H., Xu, X., and Sheikh, M. Neaz. (2012). Seismic isolation for low-to medium-rise buildings using granulated rubber-soil mixtures: Numerical study, *Earthquake Engineering and Structural Dynamics*, 41(14): 2009-2024.

[7] Xiong, W, and Li, Y (2013). Seismic isolation using granulated tire-soil mixtures for less-developed regions: experimental validation, *Earthquake Engineering & Structural Dynamics*, 42: 2187-2193.

[8] Brunet, S., De La Llera, J. C., and Kausel, E. (2016). Non-linear modeling of seismic isolation systems made of recycled tire-rubber, *Soil Dynamics and Earthquake Engineering*, 85(6): 134–145.

[9] Bandyopadhyay, S., Sengupta, A., and Reddy, G.R. (2015). Performance of Sand and Shredded Rubber Tire Mixture as a Natural Base Isolator for Earthquake Protection, *Earthquake Engineering and Engineering Vibration*, 14(4): 683–693.

[10] Pistolas, G.A., Pitilakis, K., and Anastasiadis, A. (2020). A numerical investigation on the seismic isolation potential of rubber/soil mixtures, *Earthq. Eng. Eng. Vib*., 19: 683–704.

[11] Edinçliler, A., and Toksoy, Y. S. (2017). Geogrid Donatılı Zemin Üzerine İnşaa Edilen Orta Katlı Binaların Sismik Performansına Deprem Karakteristiklerinin Etkisi, *4. Uluslararası Deprem Mühendisliği ve Sismoloji Konferansı*, 11-13 Oct 2017, Eskişehir, Turkey.

[12] Xu, R., and Fatahi, B. (2019). Novel application of geosynthetics to reduce residual drifts of mid-rise buildings after earthquakes, *Soil Dynamics and Earthquake Engineering*, 116: 331-344.

[13] Dhanya, J. S., Boominathan, A., and Banerjee, S. (2019). Performance of geo-base isolation system with geogrid reinforcement, *International Journal of Geomechanics*, 19(7): 1–13.

[14] Basha, B., and Sivakumar Babu, G.L. (2014). Reliability-based load and resistance factor design approach for external seismic stability of reinforced soil walls, *Soil Dynamics and Earthquake Engineering,* 60: 8-21.

[15] Wang, B. H., Chen, G. X., and Hu, Q. X. (2010). Experiment of dynamic shear modulus and damping of Nanjing fine sand, *World Earthquake Engineering,* 26(3): 7–15.

[16] Latha, G.M. and, Varman, A.M.N. (2014). Shaking table studies on geosynthetic reinforced soil slopes, *Int J Geotech Eng.,* 8(3): 299–306.

NATURENGS
MTU Journal of Engineering and Natural Sciences
https://dergipark.org.tr/tr/pub/naturengs
DOI: 10.46572/naturengs.860954

Research Article

Attitudes Towards Vaccines And Intention to Vaccinate Against Covid-19: A Statistical Analysis

Burcu Özcan[1], Edanur Yıldırak[2], Zeynep Aksoy[3*]

[1,2,3] Industrial Engineering, Faculty of Engineering, Kocaeli University, Kocaeli, Turkey.

(**Received:** 15.01.2021; **Accepted:** 09.05.2021)

ABSTRACT: Present study aims to analyze the attitude towards Covid 19 vaccine in Kocaeli province and the factors that may cause this attitude. Data were applied to 248 people via an online survey. The survey consists of three parts: demographic data, data on vaccine attitude and level of knowledge about the vaccine. The association between the idea of being vaccinated and demographic variables were examined with Pearson chi-square analysis and a significant relationship was found only in terms of age and marital status variables. Pearson's correlation analysis was used to determine the relationship between the vaccine attitude scores and the level of knowledge about the vaccine. It was concluded that the relationship between age and marital status with the idea of vaccination was statistically significant. (P<0,01) T-test was used to determine whether it differentiated according to chronic illness and it was determined that it did not. (P>0,05) One-way ANOVA was used for the relationship between fear level against Covid 19 and attitude towards a vaccine and it was observed that there was a significant difference. The effect of seeing social media and television as a source of information on the idea of vaccination was examined using Ordinal Logistics Regression according to the determined reference values and it was seen that there was a significant difference. Also, domestic vaccine positively affects the attitude towards a vaccine.

Keywords: Covid 19, Vaccine attitude, Vaccination misinformation, Statistical analyze.

1. INTRODUCTION

The main purpose of health services is to ensure the continuity of health. Vaccination is one of the most important methods to protect against diseases.

According to the statement made by the Ministry of Health in December 2017, the number of families who refused vaccination exceeded 10,000.

It is very important to examine the fears and concerns of individuals against the vaccine and the factors that may cause this situation and to create a vaccine policy in this direction. Providing accurate information about the vaccine has become an important issue in this process. Otherwise, there will be an increase in epidemic diseases. When the literature is examined, the reasons for not being vaccinated are fear and insecurity against the side effects of vaccines that may occur soon or in the long term. In December 2019, China announced the first cases of coronavirus Disease (COVID-19) due to a new Coronavirus: Severe Acute Respiratory Syndrome-Coronavirus 2 (SARS-CoV 2). The world is currently fighting a serious pandemic,

*Corresponding Author: zeynepaksoy2626@gmail.com
ORCID number of authors: [1] 0000-0003-0820-4238, [2] 0000-0003-1721-2969, [3] 0000-0001-8548-9826.

with more than 61 million people infected with this virus worldwide, cases have been reported from more than 200 countries, and more than 1.43 million people have died by the date of this study [1]. Vaccination is the only viable way to keep this pandemic under control.

In the current covid-19 pandemic, the public's attitude to the vaccine, which is uncertain, is critical for mass immunity. For this reason, in this study, the attitudes and reasons of people living in different occupational groups and regions in Kocaeli, which is among the top five provinces in the country with a high number of cases, will be examined. In the study, a questionnaire including demographic, socio-economic variables, examining the reasons for not being vaccinated, and measuring virus and vaccine information was applied to the participants. The significance of the obtained data and the relationships of independent variables with vaccine attitude will be examined in the findings section.

The literature research conducted is summarized in Table 1, Table 2, Table 3, Table 4 and Table 5.

Table 1. Literature Research Table Summary 1

YEAR	PURPOSE	AUTHOR	INDEPENDENT VARIABLES	TEST STATISTICS	SAMPLE SIZE
2007	Parents' attitude towards vaccines	Benford, Lansley [2]	Economic situation, Ethnicity	One Way ANOVA	2326
2011	Attitudes of people living in Hungary towards HPV vaccine	Marek et al. [3]	Age, gender, region, cost attitude to the HPV vaccine, health information of the participants	Pearson Chi Square Test	298
2012	Attitudes of dentists living in Germany towards seasonal flu vaccine and pandemic flu vaccine	Wicker et al. [4]	Age, gender, acceptance of H1N1 vaccine at the time of 2010-2011	Pearson Chi Square	242
2015	Attitudes of female students in a school in Lebanon towards HPV vaccine	Danny et al. [5]	Demographic information such as smoking, age, sexual experience, education	ANOVA, Paired T Test,	512
2016	In a study conducted in 67 countries, the relationship between religion and vaccine attitude was examined.	Larson et al. [6]	Economic situation, geographical location	Regression Analysis, T test	65.819
2016	The impact of policy changes on the flu vaccine	Slaun white [7]	The social and economic status of the person	T Ttest	202
2017	The attitudes of elderly people living in Singapore towards flu and pneumonia vaccine have been examined	Chow et al. [8]	Age, gender, chronic illnesses, type of housing, income status, ethnicity	T Test, Wilcoxon Test, McNemar Test, Ordinal Logistic Regression	655

Table 2. Literature Research Table Summary 2

YEAR	PURPOSE	AUTHOR	INDEPENDENT VARIABLES	TEST STATISTICS	SAMPLE SIZE
2017	Flu vaccine against the attitude of the parents of allergic rhinitis and asthma patients and doctors living in Turkey	Kaya et al. [9]	Demographic and health variables	Pearson Chi Square Test	189-183
2017	Public attitude towards childhood vaccinations in New Zealand	Lee et al. [10]	Gender, marital status, employment status, age, number of children and annual household income	Multiple Regression Analysis	16.642
2017	Influence of race against vaccination attitude	Quinin et al. [11]	Economic situation, age	T Test	1657
2018	Healthcare professionals' hesitation about vaccination	Succi [12]	Geographical location, ethnicity	Regression Analysis	168
2018	Attitude to hepatitis B vaccine	Liu [13]	Hospital policy, size	ANOVA	929
2019	The effect of superstitions on attitude to the flu vaccine	Lu et al. [14]	Education level, Economic status	Pearson Chi Square Test	668

Table 3. Literature Research Table Summary 3

YEAR	PURPOSE	AUTHOR	INDEPENDENT VARIABLES	TEST STATISTICS	SAMPLE SIZE
2019	Ebola vaccine acceptability in West Africa	Jalloh et al. [15]	Social status, Age, Education	Qualitative and quantitative analysis	316
2019	Attitude towards HPV vaccine in India	Dagarege et al. [16]	Religion, social factors, education	Regression Analysis	1609
2020	Australian residents' attitude towards mumps, measles and rubella vaccines	Toll et al. [17]	Demographic, socioeconomic and health-related variables	Multiple Regression Analysis	4779
2020	The attitude of pregnant women towards flu vaccine in Kenya	Otieno et al. [18]	Education level, age, marital status, income status, religion, region of residence, number of children	Fisher Chi Square Test	507
2020	The attitudes of pregnant women towards pediatric vaccination in Greece	Maltezou et al. [19]	Age, gestational age, education level, current childbearing, prior flu vaccination and vaccination beliefs of women	Logistics Regression	814
2020	Flu vaccine knowledge and attitude of parents of children hospitalized for flu in Australia	Carlson et al. [20]	Child's age, length of stay hospital, by region of residence, gender, pregnancy vaccination	ANOVA	27

Table 4. Literature Research Table Summary 4

YEAR	PURPOSE	AUTHOR	INDEPENDENT VARIABLES	TEST STATISTICS	SAMPLE SIZE
2020	Flu vaccine attitudes of teachers living in Poland.	Ganczak [21]	Gender, residence (city, rural), marital status, socioeconomic status, belief that they will be in the high risk group for influenza	Fisher Chi Square Test	277
2020	The role of the digital platform in vaccination	Franscella et al. [22]	Age, economic situation, religion	ANOVA	919
2020	The effect of doctors on patients who do not want to be vaccinated	Deml et al. [23]	The social life of the person, Education	Regression Analysis	20
2020	Access and acceptance of the vaccine	Spana [24]	Social and behavioral communication, Human factors	Experimental Suggestion Provided	23
2020	Whether HPV is applied by human rights or not	Kruese et al. [25]	Age, gender	Statistical Data Analysis	154
2020	Vaccination attitudes have been examined on social media	Chan et al. [26]	Social features, Age	Correlation Analysis	3005

Table 5. Literature Research Table Summary 5

YEAR	PURPOSE	AUTHOR	INDEPENDENT VARIABLES	TEST STATISTICS	SAMPLE SIZE
2020	Cancer patients' attitudes towards flu vaccine	Okoli et al. [27]	Age, education, gender, smoking, income, residency insurance, cancer type, chronic disease, year of diagnosis, occupation	I^2 test	139-41.346
2020	Parents' attitude towards childhood vaccinations in New Zealand	Lee et al. [28]	Age, race, region and educational status	Actor-Partner Mutual Dependency Model	136
2020	Flu vaccine and covid-19 vaccine attitude of healthcare professionals living in Malta	Grech [29]	Age, gender, health status, vaccine concern, effect, safety	Fisher Chi Square Test	852
2020	Parents' attitude towards covid-19 vaccine in a study conducted in the UK	Bell et al. [30]	Age, gender, household income, employment, marital status of participants, and number and age of children	Paired T Test	1252
2020	Vaccination status of children with IBH and AIH living in Germany	Cagol et al. [31]	Gender, current age, age at diagnosis, treatment and disease	ANOVA, Kruskal Wallis, Wilcoxon, Fisher Chi Square Test	329
2020	The relationship of the public's political opinion with the attitude to the covid-19 vaccine in France	Ward et al. [32]	Gender, age, education, income, Covid 19 diagnosis, political	Logistic Regression	5018
2020	Caregivers' attitude towards vaccination	Goldman et al. [33]	Cultural environment, geographic location	Pearson Chi Square Test	2557

In the study, the attitude of individuals living in Kocaeli province towards the COVID 19 vaccine was examined. The problems to be investigated in the study can be listed as follows.

1. Whether there is a relationship between demographic variables and vaccination idea
2. The relationship between seeing social media and television as a means of obtaining information and the idea of getting vaccinated
3.The effect of the domestic vaccine on attitude
4. Effect of total knowledge score on attitude towards vaccine
5. The relationship between vaccination attitude and education level
6. The relationship between the fear level and the vaccine attitude score
7. Determining the relationship between chronic illness and desire to be vaccinated

2. MATERIAL AND METHODS

2.1. Sample Group

In the study, Kocaeli, which is at the top of the number of cases during the pandemic period, was selected as the population. Self-administered online questionnaire questions were asked to 248 participants in multiple districts, different income levels and professions. Participation in the survey took place between 30 November and 3 December. The descriptive statistics of the demographic characteristics of the participants are shown in Table 6.

Table 6. The descriptive statistics of the demographic characteristics of the participants

Gender	**Frequency**	**Percent Frequency**
Woman	133	53.6
Male	115	46.4
Total	248	100
Marital status	**Frequency**	**Percent Frequency**
The married	144	58.1
Single	104	41.9
Total	248	100
Education Status	**Frequency**	**Percent Frequency**
Primary School-Secondary School	78	31.5
High school	60	24.2
University	89	35.9
Postgraduate	21	8.5
Total	248	100
Age	**Frequency**	**Percent Frequency**
18-28 Age	82	33.2
29-39 Age	33	13.4
40-50 Age	21	8.5
50-60 Age	37	15.0
60+	74	30.0
Total	247	100

2.2. Data Collection Tool and Method

In the study, the data was provided through a questionnaire that can be answered online. In the questionnaire answered by 248 participants, demographic questions such as age, gender, marital status, educational status, information obtained (TV, social media, experts, scientific

publications), presence of chronic illness consisting of yes-no answers, previous disease status, vaccination training (1-Strongly disagree, 2-Disagree, 3-Indecisive, 4-Agree, 5-Strongly Agree), questions such as income loss status, confidence of the participant against the vaccine, belief in its protection, idea of vaccination, information about the vaccine the effect of vaccine trust on the vaccine trust, the effect of the vaccine on the vaccine trust, the effect of the vaccine's institution on the vaccine attitude, the effect of the vaccination fee on the vaccination decision, the effect of the expert advice on the vaccination attitude, the effect of the vaccine's success rate on the vaccination decision, the effect of the vaccine storage conditions on the vaccination decision There are questions measuring fear, and true-false questions to measure vaccine knowledge.

Pearson chi-square analysis was conducted to examine the relationship between demographic variables and vaccination attitude, which we determined as the dependent variable. First, the hypothesis test is established, the established hypothesis is shown.

2.3. Analysis of Data on Attitude Against Vaccine

To analyze the sample group, the reliability of the data was tested first. (Tabachnick & Fidell, 2013), the skewness and kurtosis values between -1.5 and +1.5 show that they are normally distributed. A normality test was performed and kurtosis and skewness values were found to be between these values for 22 different variables, and normal distribution was appropriate. According to Özdamar (2015), Cronbach's Alpha value is between 0.70 and 0.90 shows that the scale has high reliability, it takes a value between 0.60 and 0.70, and the scale has sufficient reliability. 22 different factors of vaccination attitude, Cronbach alpha value. It was found to be 0.830**.**

3. RESULTS AND DISCUSSION

3.1. Chi-Square Analysis of the Relationship Between Demographic Variables and Vaccination Idea

Pearson chi-square analysis was conducted to examine the relationship between demographic variables and vaccination attitude, which we determined as the dependent variable. First, the hypothesis test is established, the established hypothesis is shown.

Table 7. Age-Vaccination Thought Observed and Expected Value

		Vaccination Thought							
Age		**I don't think**		**I am intensive**		**I think**		**Total**	**Sig.**
		N	**Post-Hoc**	**N**	**Post-Hoc**	**N**	**Post-Hoc**		
18-40 Age	Count	42	42a	41	41a	32	32 a	115	
40 + Age	Count	15	15b	38	38 a	79	79 b	132	
Total		57		79		111		247	0.000

The age independent variable is evaluated in terms of vaccination attitude. To prevent 20% of the data being under five, the age variable considered in five groups (18-28, 29-39, 40-50, 50-

60, 60+) is combined into two groups. Likewise, the idea of vaccination stated in the 5-point Likert scale is combined into three evaluations. As can be seen in Table 7, it is seen that the participants in the 18-40 age group mostly answered "I do not think", and the participants over the age of 40 answered "I think" more.

Looking at the Pearson chi-square result, it is seen that the p value is less than 0.05. Therefore, H_0 is rejected. It is commented that there is a statistically significant relationship between age and the idea of being vaccinated.

A comparison of the columns is made. In Table 7, it is seen that there is a significant difference between the columns expressed with different letters. It is seen that there is a difference between the ages of 18-40 and over 40 in terms of thinking about vaccination, and there is no difference between the two age groups in terms of indecision towards vaccination.

Table 8. Expected and Observed Values of the Vaccination Thought by Gender

		Vaccine Thought				
Gender		**I don't think**	**I am indecisive**	**I think**	**Total**	**Sig**
Female	Count	34	41	58	133	0.583
Male	Count	23	38	54	115	
Total		57	79	112	248	

Considering the idea of getting vaccinated according to the gender independent variable, it is seen that female participants responded with "I think" more, and male participants responded more "I think".

Table 9. Expected and Observed Values of Vaccination Thought According to Education

		Vaccination Thought				
Education		**I don't think**	**I am indecisive**	**I think**	**Total**	**Sig.**
Primary/ Secondary School	Count	14	22	42	78	0.151
High School	Count	12	18	30	60	
University	Count	31	39	40	110	
Total		57	79	112	248	

When the idea of vaccination is evaluated according to the education independent variable, to prevent 20% of the expected value falling below 5 in four groups (primary school, secondary school, high school, university (associate degree, undergraduate), graduate (master, doctorate) The graduate group was merged with the university. As can be seen from the table, primary-secondary school graduates responded more "I think." Participants who were high school graduates and university graduates responded more like "I think".

Considering the result of the Pearson chi-square analysis, it can be said that there is no significant relationship between the educational status variable and the idea of being vaccinated because the p value is above 0.05 and the H_0 a hypothesis is accepted.

Table 10. Pearson's Chi-Square Analysis Result of the Vaccination Thought According to Marital Status

		Vaccination Thought				
Marital Status		**I don't think**	**I am indecisive**	**I think**	**Total**	**Sig.**
Married	Count	23	37	84	144	0.000
Single	Count	34	42	28	104	
Total		57	79	112	248	

When the marital status independent variable and the idea of being vaccinated are evaluated together, it is seen that married participants responded more like "I think" and single participants responded more "I think".

Pearson's chi-square analysis result is examined. It can be said that the p value is less than 0.05, that is, the H_0 the hypothesis will be rejected, and there is a significant relationship between marital status and the idea of being vaccinated.

3.2. Examining the Relationship Between Gender and Knowledge Level with T Test

The sub-problems of the study were examined and whether the data obtained from two independent variables were meaningful with each other or not.T test was applied and the confidence interval was stated as 95%. It has been investigated whether gender is related to the level of knowledge of Covid 19. A total scoring was made in the information about the information.

Table 11. T Test Result for the Relationship Between Gender and Knowledge Level

Gender	**N**	**X**	**SS**	**Sig.**
Female	133	0.819	0.184	0.207*
Male	115	0.787	0.214	

*p<0.05

There was no significant relationship between gender and level of knowledge.

3.3. Examination of the Relationship Between Chronic Disease and Thinking of Being a Covid Vaccine Using T Test

It has been investigated whether those with chronic diseases are related to the desire to get the Covid 19 vaccine.

Table 12. The T-Test Result of the Relationship Between Chronic Disease and Thinking About Covid Vaccine

Chronic Disease	**N**	**X**	**SS**	**P value**
Yes there is	147	3.490	1.631	0.578*
No not	101	3.376	1.541	

*p<0.05

People with chronic diseases are more likely to be vaccinated than those who do not. However, there is no significant relationship between considering vaccination and chronic illness. People with chronic illnesses are expected to have a much higher request for vaccination than those who do not it may be thought to do.

3.4. The Relationship Between Fear Level and Attitude Score Against Vaccine

While the H_0 hypothesis argues that there is no difference between the fear level and the idea of being vaccinated, the H_1 hypothesis shows that there is a difference between them.

It is seen that there is a significant difference between the fear level of individuals and their attitude towards vaccination. To determine the direction of the difference, Turkey Test was conducted and it was observed that all groups differed significantly over each other. The vast majority of participants are extremely afraid of Covid 19.

Table 13. Result of the Relationship Between Fear Level and Attitude Score Against Vaccine

	Fear-Level	**N**	**X**	**SS**	**F**	**P Value**	**Significant Difference**
Attitude Score	I have no fear	32	2.819	0.884	25.799	0.0006	I have no fear-Moderate-I am extremely afraid
	Moderately scared	62	3.411	0.607			
	I'm too afraid	154	3.764	0.693			

3.5. The Relationship Between Vaccine Domestic Status and WHO Support and Attitude Score Against Vaccine

There is a significant relationship between the vaccine being indigenous and being supported by WHO and the attitude towards the vaccine.

Table 14. Result of the Relationship Between Local Vaccine and WHO Support and Attitude Score Against Vaccine

	Local Vaccine-WHO Support	**N**	**X**	**SS**	**F**	**P Value**	**Significant Difference**
Attitude Score	I strongly disagree	23	3.571	1.006	3.597	0.007	Absolutely I agree- I strongly disagree
	I do not agree	35	3.109	0.904			
	I am indecisive	86	3.635	0.623			
	I agree	51	3.641	0.566			
	Absolutely I agree	53	3.627	0.857			

$P<0.05$

In determining the direction of the difference, Turkey Test was used and 0.531 negative significance was found between Absolutely agree or not.

3.6. Information and Comments on the Relationship Between Attitude towards Vaccine and Level of Knowledge

Table 15. The Correlation of the Relationship Between Attitude and Knowledge Level

		Attitude Score	**Total Knowledge Score**	**R**
Attitude Score	Correlation Significance	1	0.002	0.197
	N		248	
Total Knowledge Score	Correlation Significance	0.002	1	
	N	248		

The relationship between the participants' attitude scores towards the vaccine (Mean = 3.554, SD = 0.768) and the total knowledge score (Mean = 8.290, SD = 2.279) was measured by Pearson correlation. A low level, a positive significant relationship was found between these variables. (R (246) =, 197, p <0.01)

3.7. Investigation of the Effect of Using TV and Social Media to Access Information with Ordinal Logistic Regression on the Thought of Vaccination

In this analysis, the use of TV and social media, which are independent variables, is evaluated categorically. The idea of vaccination, which is the dependent variable, is expressed with a sequential increasing scale. Therefore, Ordinal Logistic Regression use was deemed appropriate. The research aims to measure the effect of people who use TV and Social Media resources to obtain information on the idea of vaccination. This measurement was based on the odds (OR) ratio. Odds, the probability of observing any event; is the ratio of the probability of not being observed [34]. SPPS does not provide Odds output for the data analyzed in version 22. For this reason, the output table is transferred to Microsoft Excel and Exp(β_k) It was calculated according to the formula. Ordered Logistics Analysis also contains some assumptions.

When the analysis is done in SPSS package program, the results are as follows:

Table 16. Frequencies of Data

		N	Cumulative percent (%)
Are you considering getting the Covid 19 vaccine?	" NO"	57	23.0
	"i am indecisive"	79	31.9
	" YES"	112	45.2
TV	0	72	29.0
	1.0	176	71.0
Social Media	0	67	27.0
	1.0	181	73.0
Valid		248	100.0
Missing		0	
Total		248	

Table 17.Significance and Chi-Square Value of the Model

Model	-2 Log Likelihood	Chi Square Value	Df	Sig.
Intercept Only	49.746			
Final	32.504	17.241	2	0.000

For this analysis, it can be said that there is a significant difference between the variables in which the H_0 a hypothesis is rejected since the p value is lower than 0.05 in the general result.

Table 18. The goodness of Fit Assumption for the Model

	Chi Square Value	Df	Sig.
Pearson	0.471	4	0.976
Deviance	0.476	4	0.976

When the Pearson p value for the goodness of fit test was examined, it was seen that it was considerably higher than 0.05. So the H_0 the hypothesis is accepted. The data are suitable for the model.

Table 19. Parallelism Test for the Model

Model	-2 Log Likelihood	Chi Square Value	Df	Sig
Null Hypothesis	32.504			
General	32.062	0.442	2	0.802

A parallel test is examined. It is concluded that the p value is greater than 0.05, that is, the assumption that the H_0 a hypothesis is accepted.

Table 20. The Result of Ordinal Logistic Regression Analysis

		Estimate	Std. Error	Wald	Df	Sig	OR
Threshold	[I do not think to be vaccinated= 1.0]	-1.397	0.187	55.68	1	0.000	0.25
	[I am indecisive= 3.0]	0.088	0.161	0.298	1	0.085	1.1
Location	[TV=,0]	-1.025	0.270	14.445	1	0.000	0.36
	[TV=1.0]	0[a]	.	.	0	.	
	[Social Media=,0]	0.625	0.281	4.936	1	0.026	1.87
	[Social Media=1.0]	0[a]	.	.	0	.	

Considering the test result, the state of thinking about getting vaccinated is the dependent variable selected as a reference, while the reference in the independent variables is the state of thinking about television as a means of obtaining information and the state of thinking about social media as an information tool. If the result is to be interpreted, the idea of being in contact with those who do not think of TV as a means of obtaining information is 0.36 times higher than those who think. ($p<0.05$,%95 CI, 0.21-0.60) Those who do not think of social media as a means of obtaining information have 1.87, or approximately two times higher, than those who think about getting vaccinated ($p<0.05$, %95 CI, 1.07-3.24).

4. CONCLUSIONS

An online questionnaire was applied to 248 participants in Kocaeli province. The relationships between the participants' attitudes towards the Covid 19 Vaccine, their thoughts on getting vaccinated and their knowledge level about Covid 19 were investigated.

43.3% of the respondents are university graduates, with 53.6% female, 46.4% male, 35.9% undergraduate and 8.5% graduate.

Skewness and kurtosis values between -1.5 and +1.5 indicate normal distribution to determine whether the data set conforms to the normal distribution. Cronbach's alpha value was found to be 0.830.

T test was used for the effect of chronic discomfort on vaccination idea and there was no significant difference. The reason for this may be that those with chronic discomfort of Covid 19 fear the side effects of the vaccine. has been seen.

Pearson's chi-square analysis was conducted to examine the relationship between demographic variables and the idea of vaccination, which we determined as the dependent variable. It was concluded that the relationship between age and marital status was statistically significant. No relationship was found between education and gender and the idea of being vaccinated.

ANOVA was made for the relationship between the vaccine being indigenous and supported by WHO and the attitude and it was seen that there was a significant difference.

The difference was determined by the Turkey Test and there is a negative significance between strongly disagree and agree.

The fact that the vaccine is local is cultivated positively.

The effect of using TV and social media on the idea of vaccination was investigated to reach information with ordinal logistic regression.

Considering the test result, the state of thinking about getting vaccinated is the dependent variable selected as a reference, while the reference in the independent variables is the state of thinking about television as a means of obtaining information and the state of thinking of social media as an information tool. As a result, it has been observed that there is a significant difference between those who think of TV as a means of obtaining information and those who do not. Likewise, it was found that there is a significant difference between those who think of social media as a means of obtaining information and those who do not.

REFERENCES

[1] World Health Organization: WHO, "Covid 19 World Statistics" Access: 15 December.2020, https://covid19.who.int/

[2] Bedford, H ve Lansley, M. (2007). More vaccines for children? Parents' views, *Vaccine*, 7818-7823.

[3] Marek, E., Dergez, T., Kricskovics, A., Kovacs, K., Nagy, G., Gocze, K., Kiss, I., Ember, I. and Gocze, P. (2011). Difficulties in the prevention of cervical cancer: Adults' attitudes towards HPV vaccination 3 years after introducing the vaccine in Hungary, *Vaccine*, 29(32): 5122-5129.

[4] Wicker,S.,Rabenau,H.,Betz,W., Lauer,H.C.,(2012). Attitudes Of Dental Healthcare Workers Towards The İnfluenza Vaccination, *International Journal of Hygiene and Environmental Health*, 215(4):482-486.

[5] Dany,M.,Chidiac,A.,Nassar,A., (2015). Human papillomavirus vaccination: Assessing knowledge, attitudes, and intentions of college female students in Lebanon, a developing country, *Vaccine*, 33(8): 1001-1007.

[6] Larson,H,Figueriedo,A.,Xiahong,Z,Schuls,W.,Verger,P,Johnston,L,Jones,N.(2016). The State of Vaccine Confidence 2016: Global Insights Through a 67-Country Survey, *EBioMedicine*, 295-301.

[7] Slaunwhite,J,Smith,S.,Halpferin,B.,Longley,J,Halpferin,S(2016).The Role Of Healthcare Provider Attitudes İn İncreasing Willingness To Accept Seasonal İnfluenza Vaccine Policy Changes, *Vaccine*, 5704-5707.

[8] Ho,H.,Chan,Y.Y,Ibrahim, M.A.,Wagle,A.,Wong,C.,Chow,A.,(2017). A Formative Research-Guided Educational İntervention To İmprove The Knowledge And Attitudes Of Seniors Towards İnfluenza And Pneumococcal Vaccinations, *Vaccine*, 35(47): 6367-6374.

[9] Kaya,A,Altınel,N.,Karakaya,G.,Çetinkaya,F.,(2017),.Knowledge And Attitudes Among Patients With Asthma And Parents And Physicians Towards İnfluenza Vaccination, *Allergoligia et Immunopathologia*, 45(3): 240-243.

[10] Lee, C., Overall, N., Sibley, C., (2020).Maternal And Paternal Confidence İn Vaccine Safety: Whose Attitudes Are Predictive Of Children's Vaccination?, *Vaccine*, 38(45): 7057-7062.

[11] Quinin,C,Jamioson.,A,Freimuth,V.,An,J.,Hancock,G.,Musa,D.(2017). Exploring racial influences on flu vaccine attitudes and behavior: Results of a national survey of White and African American adults, *Vaccine,* 1167-1174.

[12] Succi,R.(2018). Vaccine refusal – what we need to knowRecusa vacinal – o que é preciso saber, *Jornal De Pediatria*, 574-581.

[13] Liu,Y,Ma,C.,Jia,H,Xu,H.,Zou, Y, Zhang, Z, Hao, L. (2018). Knowledge, Attitudes, And Practices Regarding Hepatitis B Vaccination Among Hospital-Based Doctors And Nurses İn China: Results Of A Multi-Site Survey, *Vaccine*, 2307-2313.

[14] Lu,j,Luo,M.,Yee,A,Sheldenkar,A.,Lau,J,Liwin,M (2019). Do Superstitious Beliefs Affect İnfluenza Vaccine Uptake Through Shaping Health Beliefs?, *Vaccine*, 1046-1052.

[15] Jalloh,M,Jalloh,M.,Albert,A,Wolff,B.,Callis,A,Ramakrishman,A,..,Nordenstedt,H (2019). Perceptions And Acceptability Of An Experimental Ebola Vaccine Among Health Care Workers, Frontline Staff, And The General Public During The 2014–2015 Ebola Outbreak İn Sierra Leone., *Vaccine*, 1495-1502.

[16] Dagarege,A,Krupp,K.,Fennie,K,Srinivas,V.,Li,T,Stephens,D,Madhivanan,P (2019). An Integrative Behavior Theory Derived Model To Assess Factors Affecting HPV Vaccine Acceptance Using Structural Equation Modeling., *Vaccine*, 945-955

[17] Toll, M., Li, A.,(2020) Vaccine Sentiments And Under-Vaccination: Attitudes And Behaviour Around Measles, Mumps, And Rubella Vaccine (MMR) in An Australian Cohort. *Vaccine Journal*.

[18] Otieno, N., Nyawanda, B., Otiato, F., Adero, M., Wairimu, W., Atito, R., Wilson, A., Casanova, I., Malik, F., Verani, J., Widdowson, M., Omer, S., Chaves, S.,(2020). Knowledge And Attitudes Towards Influenza And Influenza Vaccination Among Pregnant Women in Kenya. , *Vaccine*, 38(43): 6832-6838.

[19] Maltezou,H.,Theadora,M.,Lydras,T.,Fotiou,A.,Nino,E.,Theodoridou,M.,Rodolakis,A. (2020). Knowledge, Attitudes And Practices About Vaccine-Preventable Diseases And Vaccinations Of Children Among Pregnant Women In Greece., *Vaccine*, 38(48): 7654-7658.

[20] Carlson, S.J., Scanlan, C., Marshall, H., Blyth, C., Macartney, K., Leask, J. (2019).Attitudes About And Access To Influenza Vaccination Experienced By Parents Of Children Hospitalised For Influenza in Australia., *Vaccine*, 37(40): 5994-6001.

[21] Ganczack, M., Kalinowski, P., Dabrowska, M., Biesiada, D., Dubiel, P., Topczewska, K., Biesiada, A., Mazurek, D., Korzen., M. (2020).School Life And İnfluenza İmmunization: A Cross-Sectional Study On Vaccination Coverage And Influencing Determinants Among Polish Teachers*., Vaccine*, 35(34): 5548-5555.

[22] Francella,B,Alacreu,A.,Balzarini,F,Sigronelli,C.,Lopalko,İ,Odene,A(2020). Effectiveness Of Email-Based Reminders to Increase Vaccine Uptake: A Systematic Review., *Vaccine,* 433-443.

[23] Spana,M,Brunson,E.,Long,R,Ruth,A.,Ravi,S,Trotochaund,M,..,White,A.(2020). The Public's Role in COVID-19 Vaccination: Human-Centered Recommendations to Enhance Pandemic Vaccine Awareness, Access, And Acceptance in The United States. *Vaccine*

[24] Chan,M,Jamieson,K.,Albarcin,D.(2020). Prospective Associations Of Regional Social Media Messages With Attitudes And Actual Vaccination: A Big Data And Survey Study Of The Influenza Vaccine in The United States, *Vaccine*, 6236-6247.

[25] Kruse,M,Bednarczyk.,R,Evans,D.(2020). A Human Rights Approach To Understanding Provider Knowledge And Attitudes Toward The Human Papillomavirus Vaccine in São Paulo, Brazil., *Papillomavirus Research*, 100-197.

[26] Chan,M,Jamieson,K.,Albarcin,D.(2020).Prospective Associations Of Regional Social Media Messages With Attitudes And Actual Vaccination: A Big Data And Survey Study Of The Influenza Vaccine in The United States, *Vaccine*, 6236-6247.

[27] Okoli,C.,Lam,O.,Abdulwahed,T.,Neilson,C.,Mahmud,S.,Setta,A.,(2020). Seasonal Influenza Vaccination Among Cancer Patients: A Systematic Review And Meta-Analysis Of The Determinants. , *Current Problems in Cancer*

[28] Lee, C., Overall, N., Sibley, C., (2020).Maternal And Paternal Confidence in Vaccine Safety: Whose Attitudes Are Predictive Of Children's Vaccination?., *Vaccine,* 38(45): 7057-7062.

[29] Grech, V., Gaucci, C.,(2020).Vaccine Hesitancy in The University Of Malta Faculties Of Health Sciences, Dentistry And Medicine Vis-À-Vis Influenza And Novel COVID-19 Vaccination., *Early Human Development*

[30] Bell, S., Clarke, R., Jack, S., Walker, J., Paterson, P.,(2020).Parents' And Guardians' Views On The Acceptability Of A Future COVID-19 Vaccine: A Multi-Methods Study in England., *Vaccine,* 38(49): 7789-7798.

[31] Cagol, L. ,Seitel, T. ,Ehrenberg, S., Frivolt, K., Krahlı, A., Lainka, E., Gerner, P., Lenhartz, H., Vermehren, J., Radke, M., Koletzko, S., Debatin, K., Mertens, T., Pozovszky, C. (2020).Vaccination Rate And Immunity Of Children And Adolescents With Inflammatory Bowel Disease Or Autoimmune Hepatitis in Germany.,*Vaccine*, 38(7): 1810-1817.

[32] Ward,J.,Alleaume,C..,Watel,P.P,(2020).The French Public's Attitudes To A Future COVID-19 Vaccine: The Politicization Of A Public Health Issue*., Social Science & Medicine*, 265.

[33] Goldman, M., Seiler, B., Eileen, K., Shimizu (2020). Caregivers' Willingness to Accept Expedited Vaccine Research During the COVID-19 Pandemic: A Cross-Sectional Survey., *Clinical Therapeutics*, 2124-2133.

[34] Şenel, S., Alatlı, B. (2014) Lojistik Regresyon Analizinin Kullanıldığı Makaleler Üzerine Bir İnceleme, *Eğitimde ve Psikolojide Ölçme ve Değerlendirme Dergisi,*5(1): 35-52.

NATURENGS
MTU Journal of Engineering and Natural Sciences
https://dergipark.org.tr/tr/pub/naturengs
DOI: 10.46572/naturengs.858208

Research Article

The Usage of Mg - Metal Chlorides in Hydrogen Generation

Begüm Esra AYTAŞ[1*], Sevim YOLCULAR KARAOĞLU[2]

[1]Materials Science and Engineering Department, Graduate School of Applied and Natural Science Ege University, İzmir, Turkey.
[2]Chemical Engineering Department, Engineering Faculty, Ege University, İzmir, Turkey.

(**Received:** 11.01.2021; **Accepted:** 09.05.2021)

ABSTRACT: The reaction of metals with water is one of the hydrogen generation methods. Mg stands out as a viable alternative when compared to other metals for producing hydrogen. However, the emergence of $Mg(OH)_2$, which interrupts hydrogen production in its reaction with water, has led to the search for new methods to improve the hydrogen production process. For this reason, in our study, chloride salts ($CoCl_2$ and $AlCl_3$) have been used to improve hydrogen generation. The composites have been prepared with the addition of different chlorides ($AlCl_3$ and $CoCl_2$) into Mg with ball milling. $AlCl_3$ and $CoCl_2$ have been used separately and together while forming Mg-metal composite powder. Powder mixtures have been grounded by a planetary ball mill at different times (2 and 4 hours). Deformations, which are thought to contribute positively to the reaction, have been obtained on the metal surface with ball milling. The microscopic images of the powder mixtures have been analyzed by SEM. In addition, distilled water, acetic acid and citric acid have been used in our study to observe the effects of hydrogen production. When distilled water has been used with powder mixtures in the hydrogen generation experiments, a minimal amount of hydrogen gas output has been observed. It has been observed that the use of acetic acid or citric acid solutions significantly enhances the amount of hydrogen formed. 4 hours milled Mg- 10wt% $CoCl_2$ composite has the best hydrolysis properties for all experiments with its 138 ml of hydrogen generation at 30°C in 30 ml, 2 M citric acid solution.

Keywords: Mg, Hydrogen production, Mg- metal chloride composites, Ball milling.

1. INTRODUCTION

Environmental pollution that occurs while producing and consuming energy is an important issue. The negative effects of these issues threaten our future. The energy demand is rising with the increasing population, technology, and standard of living in the world [1]. For the time being, this energy demand is mostly provided by fossil fuels [2]. However, the use of conventional fossil fuels causes vigorously pollution of the environment [3]. So, the decline of the non-renewable energy reserves has accelerated the search for alternative and renewable energy sources [4].

Hydrogen has attracted great attention in recent years due to its high energy carrier potential and environmentally friendly end product [5]. Hydrogen is a carrier of energy. The chemical energy releases from two hydrogen bonds as a result of combustion and only water forms as a by-product. The energy content of hydrogen (120 MJ/ kg) is quite high compared to gasoline (44 MJ/ kg) [6]. Today, the use of hydrogen as a fuel is rising day by day. The vehicles that may be operated with hydrogen fuel cells are almost three times more efficient than gasoline-

*Corresponding Author: begume.aytas@gmail.com
ORCID number of authors: [1]0000-0003-3528-208X, [2]0000-0003-0954-6889

powered engines [7]. It is expected that hydrogen fuel cells will be used widely in the future and therefore environmental pollution will be lowered.

Hydrogen can be produced by different methods such as steam reforming of hydrocarbons, electrolysis of water, gasification of heavy oil, coal or biomass [8]. However, the manufacturing of hydrogen by fossil fuels is ineffectual and unsustainable applications which cause releasing of pollutants and harmful gases such as NO_x, SO_x, etc. and also increase CO_2 emissions [9]. The significant point is the use of clean and inexpensive energy sources while obtaining hydrogen [10]. For this purpose, many scientific types of research focus on hydrogen generation by using metals [4, 11], metal hydrides [12] and their alloys [13].

Most of the laboratory studies have been used active metals such as Mg [5, 8], Al [4], Li [14, 15], borohydrides such as $NaBH_4$ [16] and metal hydrides such as $LiAlH_4$ [17], etc. In particular, Al and Mg were preferred in most of the studies because of their high activity and low toxicity [4, 5, 8, 18].

Hydrogen can be obtained as a result of the following reaction between solid magnesium with water:

$$Mg(s) + 2H_2O(l) \rightarrow Mg(OH)_2 + H_2(g)$$

Mg based systems provide high H_2 yield in the presence of water and activator. H_2 conversion from aqueous solutions is based on the cathodic/anodic reaction of H^+ or H_2 molecules in H_2O and a highly interactive material [10,19]:

Cathodic reactions:

$$2H_2O + 2e- \rightarrow H_2 + 2OH-$$

and/or

$$2H^+ + 2e- \rightarrow H_2$$

Anodic reactions:

$$Mg \rightarrow Mg^{2+} + 2e-$$

It was observed that the reaction rate increased in a highly corrosive environment. In various scientific studies, it has been stated that acids [8, 10, 20], saline solutions [8, 14, 19, 21] and seawater [18] are used by the researchers to improve the hydrogen yield.

Organic acids such as citric acid ($C_6H_8O_7$, molar mass: 192.124 g/mole) and acetic acid (CH_3COOH, molar mass: 60.052 g/mole) have been reported as accelerate the rate of hydrogen production [22]. The following equation shows the hydrolysis reaction with using acetic acid and citric acid:

$$2Mg(s) + 2H_2O(l) + 2CH_3COOH(l) \rightarrow Mg(OH)_2(aq) + Mg(CH_3COO)_2(aq) + 2H_2(g)$$

$$2Mg(s) + 2H_2O(l) + C_6H_8O_7(s) \rightarrow Mg(OH)_2(aq) + C_6H_8MgO_7(aq) + H_2(g)$$

Acetic acid and citric acid have been preferred because they are easily accessible, promote hydrogen production, do not produce toxic end products, do not harm to the health and environment while using in the experiments [20]. End of the reactions between Mg and acetic acid solution forms $Mg(CH_3COO)_2$ (magnesium acetate) which can be used food additive in industrial processes [23]. The reaction between Mg and citric acid solution results in the $C_6H_8MgO_7$ (magnesium citrate) salt [24]. This substance is used as an additive in the pharmaceutical and food industry.

Mg [11], MgH_2 [12], Mg_2Si [13], various Magnesium Borohydrides such as $Mg(BH_4)_2.2NH_3$ [17], $Mg(BH_4)_2$ [5], Mg nanopowder [25] and waste Mg shavings [8] are used as the source of hydrogen production with Mg.

Researchers have submitted some physical and chemical procedures for improving hydrogen generation such as ball milling [14, 21, 26-28], using carbon materials [29], usage of catalyst [30], arc plasma method [25], two-step water splitting method [31], etc.

However, the most effective methods for generating hydrogen are ball milling which has been performed on various metals such as Mg and Al and their hydrides and composites for hydrogen generation by hydrolysis [8, 26].

In our study, for optimizing the hydrogen generation, the effects of the ball milling method, the use of the metal chlorides ($CoCl_2$ and $AlCl_3$) which forms composite with Mg at various grinding times (2 and 4 hours), the content of the solutions in which the experiments took place were investigated. The initial experiments were carried out at 60°C using 30 ml of distilled water, 0.24 g of powder and a magnetic stirrer. To observe the effect of the acid solutions on the $Mg(OH)_2$ layer which disrupted the reaction, experiments were also carried out with stirring, using 30 ml of 1 M and 2 M acetic acid and citric acid solutions and using 0.12 g of composite powders at 30°C. The effects of the acid solution type and variating milling time on hydrogen production have been investigated. Characterization of composite materials was carried out by SEM (Carl Zeiss 300VP) analysis. The results were compared with each other.

2. MATERIALS AND METHOD

2.1. Materials

Mg was purchased from Merck with 99% purity. The components, $AlCl_3$ (99.99% Merck), $CoCl_2$ (98%, Merck) have been milled with Mg. Distilled water has been used for hydrolysis experiments, preparing solutions and diluting acetic acid. In the first experiments, distilled water has been used for hydrolysis. Acetic acid (100% purity, Merck) and citric acid monohydrate (8.7% water include was purchased from Weifang Ensign Industry Co.) have been used for creating an acidic medium.

2.2. Method

2.2.1. Preparation of powder mixtures

The effect of using different metal chlorides on hydrogen production has been observed in the experiments. In addition, the effect of changing the weight percentages of chlorides in Mg composite and changing the milling times have been investigated. The metal chlorides used in the preparation of the composites, the weight percentages of the chlorides in the composites and the milling times have been represented in Table 1.

Table 1. The contents and the milling times of Mg-metal composites.

Mg amount in the composite (wt%)	Metal chloride amount in the composite (wt%)	The metal chloride content of the composite	Milling time (h)
90	10	$CoCl_2$	2
95	5	$CoCl_2$	2
90	5 + 5	$CoCl_2$ + $AlCl_3$	2
95	2.5 + 2.5	$CoCl_2$ + $AlCl_3$	2
90	10	$CoCl_2$	4
95	5	$CoCl_2$	4
90	5 + 5	$CoCl_2$ + $AlCl_3$	4
95	2.5 + 2.5	$CoCl_2$ + $AlCl_3$	4

2.2.2. Preparing composites by ball milling

The composites have been used to compare the results using different grinding durations and amounts of salts on hydrogen production. Stainless steel vials and balls have been used in the milling process. The balls were about 200 grams and the powder-to-ball mass ratio was 1:20. The maximum milling time was 4 hours. Longer grinding times have not been preferred for energy and time-saving. For the milling process, ECO planetary ball miller (200 rpm, 25 Hertz) has been used.

2.2.3. Performing the experiments

For the experiments, a three-necked (250 ml), round bottom glass reactor has been used. The reactor has been placed into a magnetic stirrer heater (Figure 1). The connection of the reactor and a glass measuring cylinder (250 ml) that was suspended by inverting in a half-full beaker, has been made using a 400 mm long 8 mm inner diameter pipe. Hydrogen formed in the reactor, which passed through the pipe and cooled with water at room temperature, has been collected in the measuring cylinder. Hydrogen production has been recorded with the help of the measuring cylinder. The water displacement procedure has been used for measuring the amount of produced hydrogen.

The experiments have been carried out in distilled water, 1 M and 2 M citric acid and acetic acid solutions, respectively. Each test has been repeated at least twice, and the margin error has been accepted as $<\pm 5\%$ in the experiments. Each hydrogen generation experiment has been observed for one hour.

Figure 1. Experimental setup

3. RESULTS AND DISCUSSION

It is well known that the reaction between Mg and water causes hydrogen generation [26]:

$Mg(s) + 2H_2O(l) \rightarrow Mg(OH)_2 + H_2(g)$

In our study gas output has not been observed when distilled water and other solutions have been used with non-milling Mg to obtain hydrogen. The biggest handicap of this reaction is that the formed hydroxide layer discontinues the reaction. To eliminate this formed hydroxide layer, different weights of metal chlorides have been used together with Mg. The ball milling method has been preferred to create Mg- metal chloride composites. The formed Mg-metal chloride composites have been reacted with distilled water, and acidic (acetic acid and citric acid) solutions to observe hydrogen production. The effects of the ball milling in the production of hydrogen, the use of metal chlorides and the interaction of Mg-metal chloride composite materials with different solutions have been studied also in the Master's Thesis [27].

It is widely recognized that the repeated grinding process in ball-milling changes microstructure, distribution of the components and formation. It is submitted that combining these defects may support also metal corrosion. The effects of the ball-milling process on powder mixtures have been observed with the help of SEM images (Carl Zeiss 300VP). The original material was Mg powder (Figure 2) which had a relatively smooth surface, which after milling, became irregular and exhibited breakdown in the powder surface. In the literature studies, it is seen that the milling of Mg with solid salts is very effective for improving the hydrolysis reactivities. The salt additive is generally reported to act as a process control agent in the milling process which increases the specific surface area of Mg powder [11, 14, 19, 29].

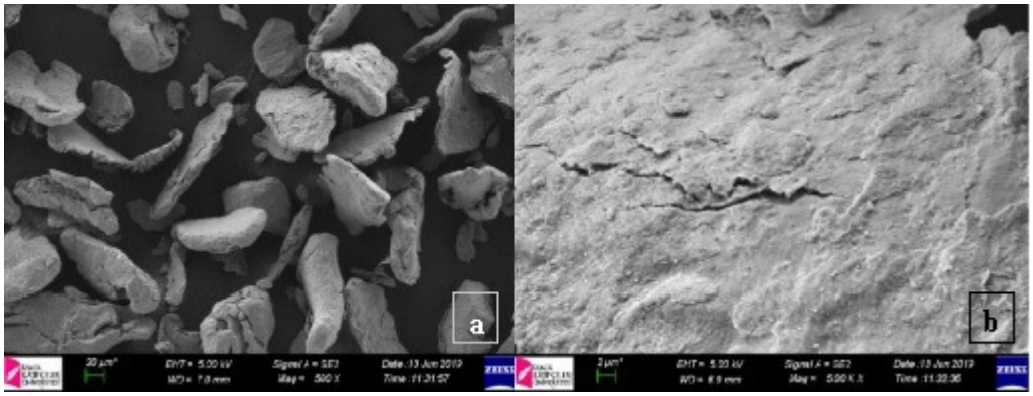

Figure 2. SEM images of Mg powder without milling a) and b) with different magnifications.

The ball-milling time is a very important parameter that affects hydrogen generation. Various changes have been observed with increasing milling time in the composite material subjected to milling. One of the most important of these changes is the slow reduction of the powder mixture which causes an increase in the surface area. It has been considered that 2 hours of milling caused a noticeable increase in the surface area of the powder (Figure 3).

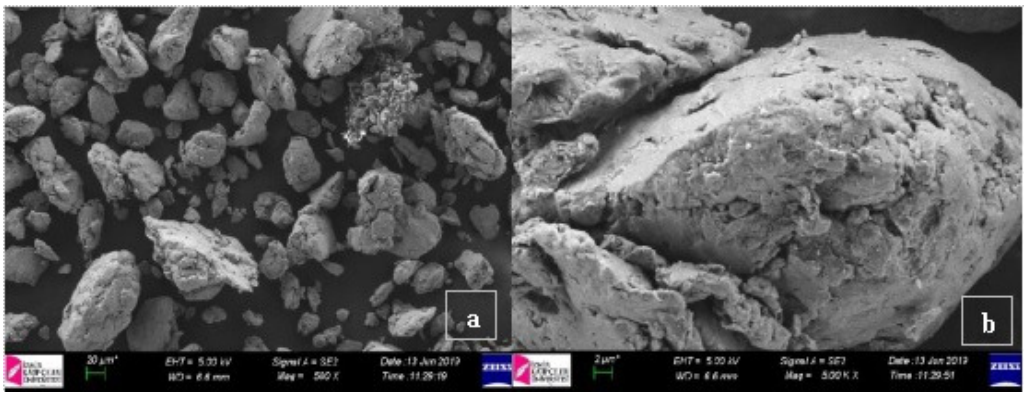

Figure 3. SEM images of 10wt% $CoCl_2$ – 90wt% Mg composite with 2h milling time, a) and b) with different magnifications

Another change is that the milling process causes deformations on the surface of the material, thereby increasing the formation of fresh surfaces. Increased surface deformation can be observed in 4 hours milled 10wt% $CoCl_2$- 90wt% Mg composite (Figure 4), compared to 2 hours milled same powder and unmilled Mg powder.

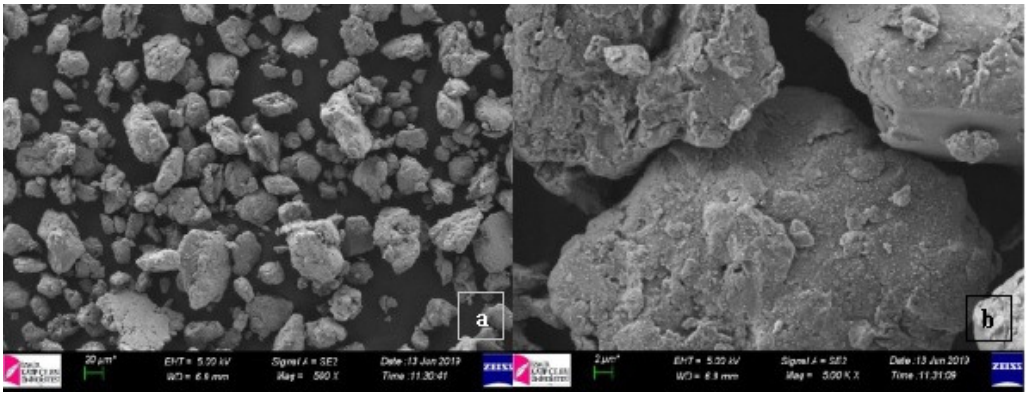

Figure 4. SEM images of 10wt% $CoCl_2$ – 90wt% Mg composite with 4h milling time, a) and b) with different magnifications

It can also be concluded that metal chloride salts are held onto the surface of Mg powder during milling (Figure 5). Prolonged milling of Mg-containing powders may result in cold welding and agglomeration of the particles, as opposed to reducing the particle size [21, 26]. For this reason and to save energy, milling times 2 and 4 hours have been selected, longer milling times have not been preferred.

The weight percentage of metal chloride in Mg-metal chloride composite is the other important parameter. Although the cold welding predominated on ductile Mg, the addition of chlorides such as $CoCl_2$, and $AlCl_3$ have favored the fracturing of Mg during the milling process (Figure 5). It may be concluded that adding chloride to the composite and increasing the weight percentage of chloride in the composite may effectively improve the hydrolysis kinetics.

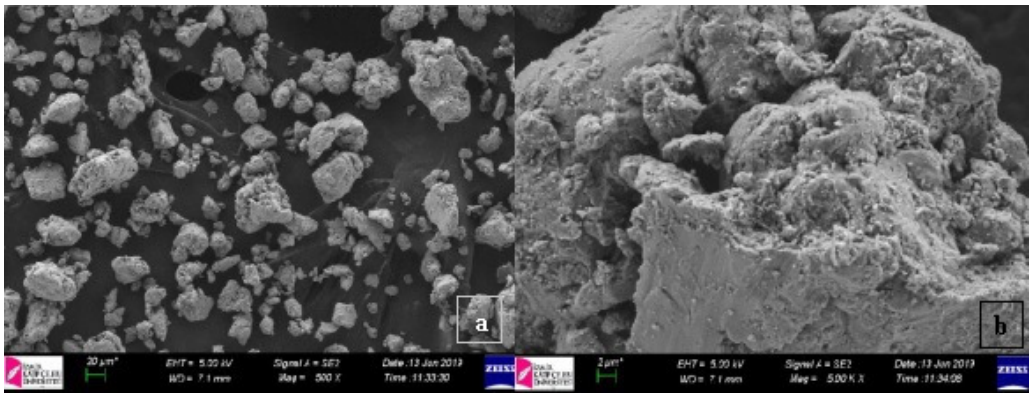

Figure 5. SEM images of 5wt% $CoCl_2$ – 5wt% $AlCl_3$ – 90wt% Mg composite with 4h milling time, a) and b) with different magnifications

$AlCl_3$ is often used for the preparation of aluminum hydroxide and may react with water as the following [14]:

$$AlCl_3(s) + 2H_2O(l) \rightarrow Al(OH)_3 + 3HCl(aq)$$

223.85 kJ/mol heat releases during $AlCl_3$ dissolution. Liu et al. (2012) stated that the H^+ ions from the generated HCl may dissolve $Mg(OH)_2$ layer formed from the reaction, thus increasing the fresh Mg surfaces revealed. So, the large amount of releasing heat and the generating HCl from $AlCl_3$ dissolution may improve the hydrolysis reaction [14].

In the study of Liu et al.(2013), 3 mol% $AlCl_3$ has been added to the Mg powder and the mixture has been milled for 6 hours. 50 mg powder and 10 ml distilled water has been used. The best result in that study has been recorded as approximately 455.9 ml. min/(g Mg). In our study, different milling times and percentage amounts have been used in the experimental study.

Also, a replacement reaction may occur during the ball milling process between Mg and metal chlorides. After the replacement reaction, the hydrolysis properties of Mg-metal chloride composites may be improved with the electronegativity of the metal element in the chlorides which possibly created a more effectual micro galvanic cell with Mg [11, 26].

Sun et al. (2014) have mentioned that the replacement reaction between Mg and $CoCl_2$ may occur during the milling process [11]:

$$Mg + CoCl_2 \rightarrow MgCl_2 + Co$$

Increasing the $CoCl_2$ content of the powder mixture may pioneer a remarkable improvement in hydrogen generation.

In the study of Sun et al.(2014), the different weight percentage of $CoCl_2$ (2, 4, 6, 8, 10 wt %) has been added to the Mg powder and the mixture has been milled for 1 hour. 1 g powder has been used. Powder: Water ratio has been informed as 1:40. The best result in the study has been recorded as 558.6 ml. min/(g Mg). It may be noted that the results are given in terms of Hydrogen Generation Rate (ml. min/(g Mg)). In our study, the results have been given in terms of the amount of Hydrogen Generation (ml). Different amounts of powder and the milling times have been used in our experimental studies.

There are many studies in the literature on hydrogen production using Mg-chloride powders. Creating Mg-chloride composites with the ball milling method has made quite noticeable contributions to hydrogen production. In their work, Liu et al. have contributed to the literature by using $CoCl_2$, and Sun et al. with using $AlCl_3$. In our study, the effect of using chlorides separately on hydrogen generation has been given. In addition, we have used also the combination of $CoCl_2$ and $AlCl_3$ salts to observe their effects on hydrogen production in our study. In addition, the reactions of Mg-chloride composites with organic acids and hydrogen recovery have been detailed.

The highest hydrogen formation in 30 ml distilled water at 60°C using the Mg composite containing 5wt% $CoCl_2$ + 5wt% $AlCl_3$ (4 hours milled) has been recorded as 78 ml. The use of these two metal chlorides in the Mg composite may have a synergistic effect. Another remarkable result with 4 hours milled Mg + 10wt% $CoCl_2$ has been recorded as 68 ml of hydrogen gas. Increasing the milling time from 2 hours to 4 hours has been supported by the increase in the amount of hydrogen obtained. Besides, it has been observed that composite powders containing 5wt% $CoCl_2$ alone and 2.5wt% $CoCl_2$ + 2.5wt% $AlCl_3$ with 2 hours milling time were not as effective as the powders containing 10wt% chlorides for all milling times (Figure 6).

Since chloride ions have a catalytic effect, it may have removed the fresh hydroxide layer formed from the surface of Mg. They may also have a preventive effect on the formation of the new hydroxide layer. In this case, more water molecules may reach the surface, so more hydrogen may be obtained.

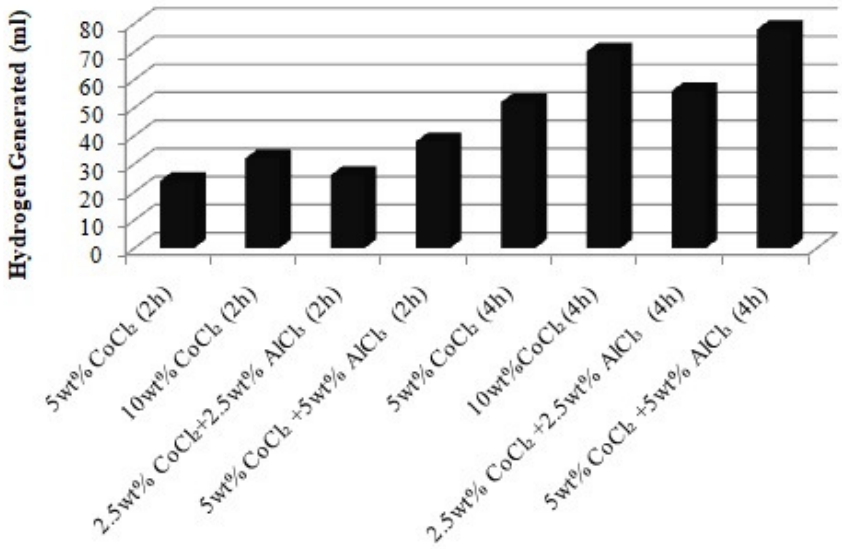

Figure 6. Hydrogen generation with 0.24 g of powder and 30 ml distilled water at 60ºC.

Acidic solutions have been also used to observe the influence on the hydrogen generation process in this study. Acetic acid and citric acid have been used for creating the acidic medium. To produce H_2, the transition of H^+ ions into the medium should be procured. Therefore, the hydrolysis reaction with using Mg interrupts quickly and requires an activator. Acids such as metals and chlorides can also be preferred as activators [20]. The use of two different acid solutions (acetic and citric acid) has been acted as an activator in the hydrolysis medium. When 30 ml, 1 M acid solutions (acetic and citric acid) have been used at even 30ºC, it has been observed that using acid solutions enhanced the hydrogen generation tremendously.

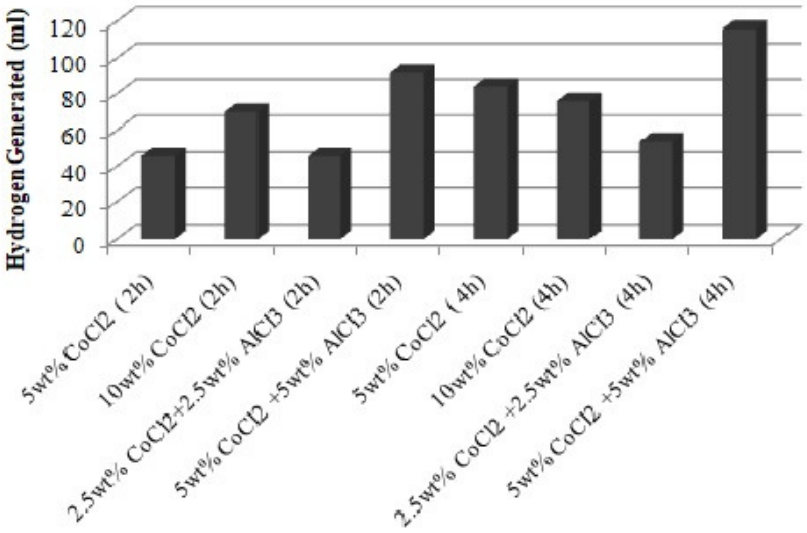

Figure 7. Hydrogen generation with 0.12 g of powders and 30 ml, 1 M acetic acid solution.

The increase in weight percent of $CoCl_2$ in the Mg-metal chloride composite may cause a significant improvement in the generation of hydrogen. Also, it may be seen that the combination of $AlCl_3$ and $CoCl_2$ in Mg-metal chloride composites enhances the hydrolysis properties. Adjusting the total chloride to 10wt% may improve hydrogen production as may be seen from the results. 4 hours milled 0.12 g of Mg- 5wt% $CoCl_2$- 5wt% $AlCl_3$ composite has the best hydrolysis properties with its 116 ml of hydrogen generation for 1 M acetic acid solution (Figure 7).

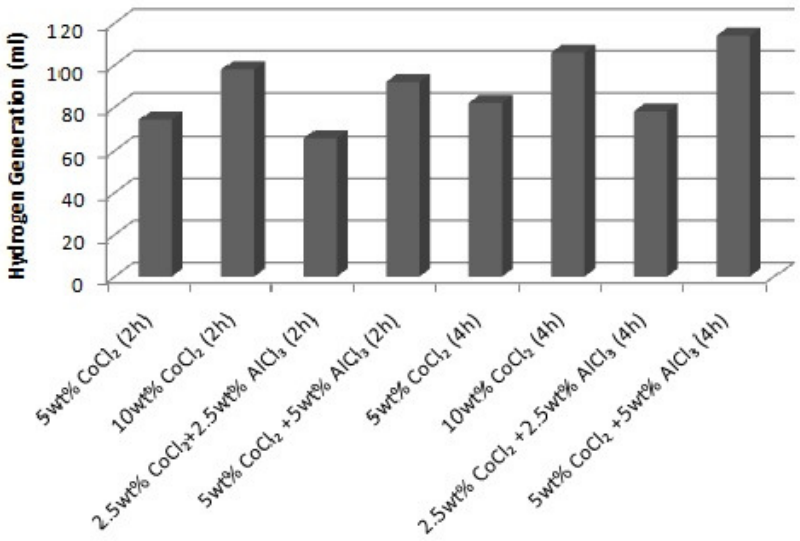

Figure 8. Hydrogen generation with 0.12 g of powder and 30 ml, 1 M citric acid solution.

The presence of an acid in the solution may be supported the continuation of the hydrolysis reaction. Acid concentration has an important role in the hydrogen production process when used with Mg-metal chloride composite. It has been noted that when using $CoCl_2$ in samples containing 5wt% metal chloride, the maximum hydrogen gas has been released as 82 ml. It may be possible to conclude that the use of 10wt% metal chloride significantly improves the hydrolysis properties. The positive effect of using 5wt% $CoCl_2$ and 5wt% $AlCl_3$ together has been reflected in the results. The hydrogen production of this composite structure with a milling time of 4 hours has been enrolled as 114 ml (Figure 8).

The organic acids compared to distilled water may be promising candidates for their contribution to the hydrogen production process. When the concentrations of acetic acid and citric acid solutions have been adjusted to 2 M and the experiments have been repeated to understand the effect of acid concentration on hydrogen production, the obtained results were quite remarkable. Whenever the results of the experiments using 2 M acetic acid solution have been examined, the effect of Mg-metal chloride composite containing the combination of 5wt% $CoCl_2$ and 5wt% $AlCl_3$ on hydrogen generation can become preeminent. Hydrogen generation has been achieved more than 100 ml in both milling times for this combination (Figure 9).

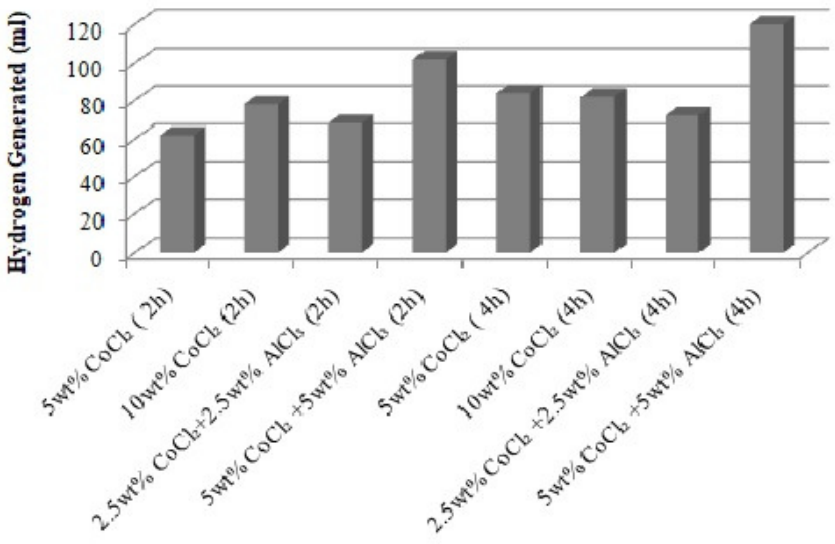

Figure 9. Hydrogen generation with 0.12 g of powder and 30 ml, 2 M acetic acid solution.

As can be seen in Figure 10, the best result obtained with a citric acid concentration of 2 M and Mg-metal chloride composite containing 10wt% $CoCl_2$ has been recorded as 138 ml. When the same experiments have been carried out in 1 M citric acid solution, 106 ml of hydrogen evolution has been observed (Figure 8). Another remarkable result has been noted as 134 ml hydrogen production during experiments involving the 5wt% $CoCl_2$ and 5wt% $AlCl_3$ duo with 4 hours milling time. It may be also supported by these results that the increase in milling time increases hydrogen production. When the composite containing 10wt% $CoCl_2$ with a milling time of 4 hours has been used, 12 ml more hydrogen has been obtained than the same composite with 2 hours milling time. Whenever the results have been compared, it has been seen that doubling the organic acid concentration has been contributed to the increase in the amount of hydrogen obtained.

It may be understood that samples containing only 5wt% metal chloride in total have not been efficient in hydrogen production processes. But they may be supportive data to create comparisons. It may be noted that citric acid solution takes a more active role. The increase in weight percentages of metal chlorides in Mg-metal chloride composites and the use of $CoCl_2$ and $AlCl_3$ together provided remarkable results in terms of the efficiency of the process.

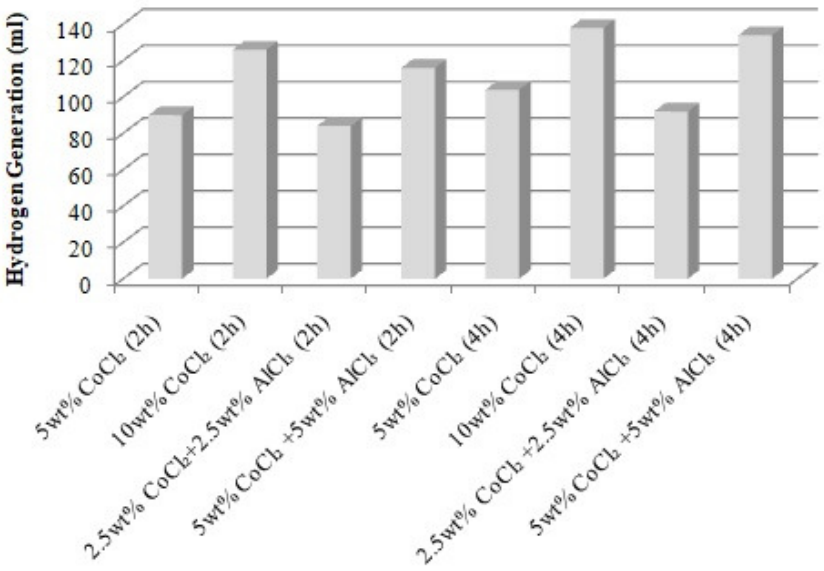

Figure 10. Hydrogen generation with 0.12 g of powder and 30 ml, 2 M citric acid solution.

4. CONCLUSIONS

To use Mg more effectively in H_2 production, surface properties should be improved. For this purpose, in our study, the preparation of Mg-metal chloride composite has been carried out by ball milling. To make the hydrolysis medium more conductive, acetic acid and citric acid solutions (1 and 2 M) have been used and the effect on hydrogen gas production has been investigated. It may be appropriate to use environmentally friendly acetic acid and citric acid as a catalyst with Mg-metal composites in the hydrogen generation reaction. In addition, the use of acetic acid and citric acid may further reduce the cost of hydrogen production. The results showed that $CoCl_2$ and $AlCl_3$ addition increased the reactivity and hydrogen generation amounts. Also, the use of $CoCl_2$ and $AlCl_3$ together improved the hydrogen generation rates and performances. Mg–metal chlorides are very promising for hydrogen production applications.

REFERENCES

[1] Zhang, J. (2008). Hydrogen production by biomass gasification in supercritical water, *Energeia*, 19: 1-5.

[2] Kaneko, H., Miura, T., Ishihara, H., Taku, S., Yokoyama, T., Nakajima, H., Tamaura, Y. (2007). Reactive ceramics of CeO_2-MO_x (M=Mn, Fe, Ni, Cu) for H_2 generation by two-step water splitting using concentrated solar thermal energy, *Energy*, 32: 656-663.

[3] Fan, M.Q., Liu, S.S., Zhang, Y., Sun, L.X., Xu, F. (2010). Superior hydrogen storage properties of MgH_2-10 wt% TiC composite, *Energy*, 35: 3417-3421.

[4] Yolcular, S., Karaoglu, S. (2017). Activation of Al powder with NaCl-assisted milling for hydrogen generation, *Energy Sources, Part A: Recovery, Utilization and Environmental Effects*, 39(18): 1919-1927.

[5] Wang, M., Ouyang, L., Zeng, M., Liu, J., Peng, C., Shao, H., Zhu, M. (2019). Magnesium borohydride hydrolysis with kinetics controlled by ammoniate formation, *International Journal of Hydrogen Energy*, 44: 7392-7401.

[6] Lalaurette, E., Thammannagowda, S., Mohagheghi, A., Maness, P.C. ve Logan, B.E. (2009). Hydrogen production from cellulose in a two-stage process combining fermentation and electrohydrogenesis, *International Journal of Hydrogen Energy*, 34: 6201-6210.

[7] Barbir, F., Ulgiati, S. (2008). *Sustainable Energy Production and Consumption*, Springer, Dordrecht, Holland, 372.

[8] Yu, S.H., Uan, J.Y., Hsu, T.L. (2012). Effects of concentrations of NaCl and organic acid on generation of hydrogen from magnesium metal scrap, *International Journal of Hydrogen Energy*, 37: 3033-3340.

[9] Youssef, E.A., Nakhla, G. ve Charpentier, P.A. (2011). Oleic acid gasification over supported metal catalysts in supercritical water: hydrogen production and product distribution, *International Journal of Hydrogen Energy*, 36: 4830-4842.

[10] Uan, J.Y., Yu, S.H., Lin, M.C., Chen, L.F., Lin, H.I. (2009). Evolution of hydrogen from magnesium alloy scraps in citric acid-added seawater without catalyst, *International Journal of Hydrogen Energy*, 34: 6137-6142.

[11] Sun, Q., Zou, M., Guo, X., Yang, R., Huang, H., Huang, P., He, X. (2014). A study of hydrogen generation by reaction of an activated Mg–$CoCl_2$ (magnesium–cobalt chloride) composite with pure water for portable applications, *Energy*, 79: 310-314.

[12] Ouyang, L., Ma, M., Huang, M., Duan, R., Wang, H., Sun, L., Zhu, M. (2015). Enhanced Hydrogen Generation Properties of MgH_2-Based Hydrides by Breaking the Magnesium Hydroxide Passivation Layer, *Energies*, 8: 4232-4257.

[13] Tan, Z.H., Ouyang, L.Z., Huang, J.M., Liu, J.W., Wang, H., Shao, H.Y., Zhu, M. (2019). Hydrogen generation via hydrolysis of Mg_2Si, *Journal of Alloys and Compounds*, 770: 108-115.

[14] Liu, Y., Wang, X., Dong, Z., Liu, H., Li, S., Ge, H., Yan, M. (2013). Hydrogen generation from the hydrolysis of Mg powder ball-milled with $AlCl_3$, *Energy*, 53: 147-152.

[15] Weng, B., Wu, Z., Li, Z., Yang, H. (2012). Hydrogen generation from hydrolysis of NH_3BH_3/MH (M = Li, Na) binary hydrides, *International Journal of Hydrogen Energy*, 37: 5152-5160.

[16] Singh, P.K., Das, T. (2017). Generation of hydrogen from $NaBH_4$ solution using metal-boride (CoB, FeB, NiB) catalysts, *International Journal of Hydrogen Energy*, 42: 29360-29369.

[17] Leng, H., Xu, J., Jiang, J., Xiao, H., Li, Q., Chou, K.C. (2015). Improved dehydrogenation properties of $Mg(BH_4)_2 \cdot 2NH_3$ combined with $LiAlH_4$, *International Journal of Hydrogen Energy*, 40: 8362-8367.

[18] Figen, A.K., Coskuner, B. (2015). Hydrogen production by the hydrolysis of milled waste magnesium scraps in nickel chloride solutions and nickel chloride added in Marmara Sea and Aegean Sea Water, *International Journal of Hydrogen Energy,* 40(46): 16169-16177.

[19] Figen, A.K., Coskuner, B., Piskin, S. (2015). Hydrogen generation from waste Mg based material in various saline solutions ($NiCl_2$, $CoCl_2$, $CuCl_2$, $FeCl_3$, $MnCl_2$), *International Journal of Hydrogen Energy*, 40: 7483-7489.

[20] Oz, C., Filiz, B.C., Figen, A.K. (2017). The effect of vinegar- acetic acid solution on the hydrogen generation performance of mechanochemically modified magnesium (Mg) granules*, Energy*, 127: 328-334.

[21] Grosjean, M.H., Roué, L. (2006a), Hydrolysis of Mg-salt and MgH_2-salt mixtures prepared by ball milling for hydrogen production, *Journal of Alloys and Compounds*, 416: 296-302.

[22] Ho, Y.S. (2013). *Hydrogen Generation from Magnesium Hydride By Using Organic Acid*, MSc Thesis, University of Wisconsin, Milwaukee.

[23] PubChem, "Magnesium Acetate", https://pubchem.ncbi.nlm.nih.gov/compound/8896, (Date of Access: 08.01.2021).

[24] Pubchem, "Magnesium Citrate", https://pubchem.ncbi.nlm.nih.gov/compound/6099959 (Date of Access: 08.12.2021).

[25] Uda, M., Okuyama, H., Suzuki, T.S., Sakka, Y. (2012). Hydrogen generation from water using Mg nanopowder produced by arc plasma method, *Science and Technology of Advanced Materials*, 13: 1-7.

[26] Grosjean, M.H., Zidoune, M., Roué, L., Huot, J.Y. (2006b). Hydrogen production via hydrolysis reaction from ball-milled Mg-based materials, *International Journal of Hydrogen Energy*, 31: 109-119.

[27] Aytaş, B.E. (2019). *The use of Mg-metal chloride composites in hydrogen production*, MSc Thesis, Ege University Graduate School of Applied and Natural Science, İzmir.

[28] Wang, S, Sun, L.X., Xu, F., Jiao, C.L., Zhang, J., Zhou, H.Y., Huang, F.L. (2012). Hydrolysis reaction of ball-milled Mg-metal chlorides composite for hydrogen generation for fuel cells, *International Journal of Hydrogen Energy*, 37: 6771-6775.

[29] Tian, M., Shang, C. (2019). Mg-based composites for enhanced hydrogen storage performance, *International Journal of Hydrogen Energy*, 44: 338-342.

[30] Cho, C., Wang, K., Uan, J. (2005). Evaluation of a new hydrogen generating system: Ni-rich magnesium alloy catalyzed by platinum wire in sodium chloride solution, *Materials Transactions*, 46: 2704-2708.

[31] Zhao, Z.W., Chen, X.Y., Hao, M.M. (2011). Hydrogen generation by splitting with Al-Ca alloy, *Energy*, 36: 2782-2787.

NATURENGS
MTU Journal of Engineering and Natural Sciences
https://dergipark.org.tr/tr/pub/naturengs
DOI: 10.46572/naturengs.883706

Review Article

Microfluidic Technology and Biomedical Field

Zülfü TÜYLEK

Electronics and Automation Department, Yesilyurt Vocational School, Malatya Turgut Ozal University, Malatya, Turkey.

(**Received:** 20.02.2021; **Accepted:** 21.05.2021)

ABSTRACT: It is seen that the development of microfluidic laboratories working passively on chips has increased over the years. The field of microfluidics includes the use of microstructured devices, which typically have micrometer sizes and allow precise processing of low volumes. Nano fields are the main fields of nanotechnology, which includes science fields such as earth science, organic chemistry, molecular biology, semiconductor physics, micromachinery where the control of the atomic and molecular unit will take place. New techniques are needed to meet existing for the development phase. Micro and nano-volume multi-stage systems through micrometer-sized channels and microfluidics, which are applied science branches, have drawn significant attention in engineering. The circulation of fluids through micrometer-sized channels examines factors that can affect the behavior of fluids, such as surface tension, the utilization of energy, and fluid resistance in the system. Microfluidic devices and systems have a variety of functions to replace routine biomedical analysis and diagnostics. It emphasizes a higher level of system integration with advanced automation, control and High-Efficiency processing potential while consuming small amounts of sample and reagent in less time. Thanks to miniaturization, better diagnostic speed, cost-effectiveness, ergonomics and sensitivity are achieved.
This work presents a detailed literature survey on the field of microfluidic technology, including system components. There are two main objectives of the review study: First, to provide the mechanisms, applications and recent developments on microfluidic techniques and Second, to suggest current research topics and possible future research in the biomedical field in microfluidic technology.

Keywords: Microfluidic, Microtechnology, Miniaturized, Sensors, SARS-CoV-2.

1. INTRODUCTION

It is very important to use small volumes of fluids in high volume scanning, diagnostic and research applications. Microfluidics is a way of processing small volume liquids between microlitres and picolitres. Existing literature reports various aspects of these devices including fluid transfer, system characteristics, detection techniques, and bioanalytical applications. Low production costs, cost-effective disposable chips and allowing mass production are reasons for a preference [1]. In the Hagen-Poiseuille studies in the 1840s, it is seen that they did the study related to the chemical structure of the polidimetilsiloksan (PDMS) material used in microfluidics. Dow Corning founded Midland in 1943 to work on silicones and is its first manufacturer. In the 1950s, thanks to advances in semiconductor technology, the design of miniature systems and components began. In 1958 Jack Kilby started working with the first microchannels [2]. In a study by Stephen Terry in the mid-1970s at Stanford University, a miniature gas chromatograph in the form of a wafer was produced by superimposing silicon sheets. Gas chromatography creates the first working example to be called a laboratory on a

Corresponding Author: zulfu.tuylek@ozal.edu.tr
ORCID number of authors: 0000-0002-9086-1327

chip (lab on a chip) that creates a miniature thermal conductivity detector as capillary path inputs and outputs through the sample injection system. In 1993, a glass chip was developed to perform capillary electrophoresis of amino acids in a matter of seconds. With help of this work, it is possible to create a miniature laboratory on a chip that can be used for complex analysis.

Nowadays, researchers have conducted studies to develop fast passive labs on chips to meet the demands of the biomedical field. Recent developments indicate that passive microfluidic techniques including mechanisms and applications considerably increase. Microfluidics is used for various laboratory experiments such as drug testing and discovery, filtration and particle separation, cell separation and counting, cell culture, 3D printing, stoichiometry, and flow synthesis [3].

2. FUNCTIONALITY IN MICROFLUIDIC DEVICES

Microfluidic techniques, related mechanisms and applications are being developed day by day. It will be possible to list the microfluidic components used today under the following headings.

2.1. Cell Manipulation

Two cells in a genetically identical group are different from each other. Cell heterogeneity plays an important role in the accurate interpretation of diagnostic and therapeutic consequences of diseases. Therefore, various cell manipulation techniques have been developed for specific purposes and applications in microfluidics. Cell manipulation techniques in microfluidics could be categorized as externally applied forces for optical, magnetic, electrical, mechanical, and other manipulations [4]. The use of immobile microfluidics without the external force among cell manipulation techniques has attracted great interest. Recently, microfluidic systems used are suitable for simple and highly efficient cell separation and analysis [5]. Silicone is the first choice among microfluidic system manufacturing when considering advantages such as its readiness, chemical compatibility and thermostability. Ease of manufacture, design flexibility, semiconductor properties, and the possibility of surface modifications are sufficient reasons why silicon has been the dominant material for microfluidic platforms for decades [6].

2.2 Cell, Tissue and Organ Culture Platforms

The emerging technology of microfluidic cell culture systems has the potential to make a significant impact on cell biology research. Many cells in our body do not participate in the circulation, instead, they depend on an environment called an extracellular matrix to survive. For example, proteins called integrin receive specific signals as a result of the physical attachment of cells to the matrix and focal adhesion sites and transmit them to the skeletal machine inside the cell. Therefore, skeletal proteins for many cells, including integrin, exist in the 3-dimensional physical microenvironment [7]. A complex three-dimensional extracellular (in vivo) matrix causes radical changes in cell morphology and function. Miniature culture systems (in vivo) have improved tissue functions compared to existing in vivo studies. This allows the complex mechanisms underlying tissue growth, regeneration and disease to be studied more accurately than existing in vitro models, without the inherent difficulties of in vivo studies [8]. Luo et al. studied the numerical simulation of oxygen and glucose transport to improve the functionality of biomedical microfluidic devices. They designed an integrated microfluidic device for the culture of individual coral polyps, including a uniform flow medium, rapid mass transfer, and precise temperature control [9]. The microfluidic device provided a reliable analytical approach for model and mechanism studies of coral bleaching and reef

conservation. Williams et al. addressed one of the problems with microfluidic cell culture platforms and found that the confinement of unwanted air bubbles in the gate often caused cell damage or device delamination [10].

2.3. Sensors

The foundations of the microfluidic industry were laid in the early 1990s and gained momentum with the development of microtechnology. It is a multidisciplinary structure combining the fields of physics, chemistry, biology, engineering, nanotechnology, medicine and biotechnology. By creating micro-channels in a material, it enables biological fluids, even biological particles such as cells and organisms, to be prepared for analysis at a certain speed. Horiuchi et al. It is seen that he developed an immunoassay chip consisting of vertically integrated capillary tubes to create negative pressure and pump the liquid towards it [11]. The Lab on a Chip (LOC) concept is a system that combines fluid mechanics, physics and nanotechnology in which large laboratory tests are reduced to a single stage. On-chip sensors integrated with microfluidic devices have great potential in the On-chip laboratory or independent systems for various biological and biomedical applications [12]. The flow of the surface tension in the liquid through the microchannels is triggered due to the change in liquid volumes. Passive microfluidics with the electrochemical sensor in the microchannel is suitable for LOC flow injection. Basic principles of nano and microfluidic chips are detection of RNA / DNA from target organisms or antigen and toxin substances specific to target organisms [13]. This detection takes place through biosensors. Biosensors are a transducer device that detects the presence of substances by binding the substances to be analyzed and interacts with the sensor and can signal this interaction. The use of nanomaterials in the design of biological sensors; enables the process to be carried out in a short time, to be portable and to be processed at low cost. Therefore, nanotechnology tools provide a broader perspective on new vaccine design strategies. For example, a nano-based formulation for SARS-CoV-2 therapeutics is being developed as a delivery tool, along with a new nano vaccine metastasis platform and nano drugs useful for the treatment of SARS-CoV-2 infections. Scientists are now working to quickly identify and develop appropriate nano-vaccines and treatment options, including new nano-based technologies [14].

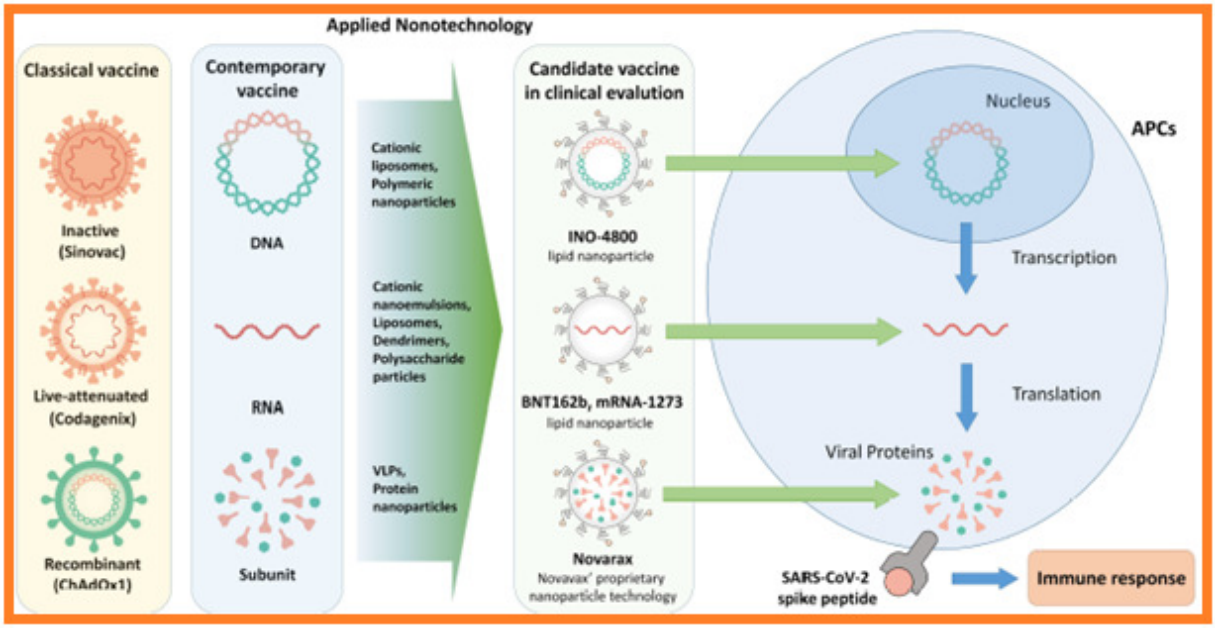

Figure 1. Classical vaccine, Moderna vaccine and nanotechnology applied vaccine against SARS-CoV-2

In studies, nanoparticles similar to immunogenic viruses have been developed and produced with nanoparticle vaccine technology (Figure 1) [15]. Also developed by Inovio Pharmaceuticals, Inc., Plymouth Meeting, PA, USA, INO-4800 is a candidate DNA vaccine among nucleic acid vaccines (Figure 1). Similar to RNA vaccines, INO-4800 is a nucleic acid vaccine that can induce an immune response by being translated into proteins within human cells [16]. An RNA vaccine candidate against SARS-CoV-2 is now known as mRNA-1273 (Moderna, Cambridge, MA, USA) (Figure 1). This vaccine contains a synthetic mRNA strand so that the binding site for ACE2 can be translated into a pre-modified SARS-CoV-2 S protein [17]. BNT162b1, under development by Pfizer, New York, NY, USA, is an optimized mRNA vaccine with the codon encoding the SARS-CoV-2 RBD (Figure 1) [18].

2.4. Micro Pumping

The micropump has a pump inlet and an outlet. It can continuously create a vacuum or negative pressure at the inlet. At the outlet, large outlet pressure is created. It is a small-sized device whose working medium is liquid. In these microfluidic devices, silicone-based elastomeric materials based on the lithography technique called PDMS are used. PDMS is also a non-toxic, gas-permeable molecule to cells and excellent optically compatible. Microfluidic cell culture devices have pumps and valves that allow small volumes of liquid to be transferred [19]. In 1979, the first magnetic MEMS microvalve was developed. The function of the microvalve used in microfluidic systems is to change the flow direction at the desired time to control and regulate the liquid flow. In microfluidic systems, microvalves are the most important component of integrated LOC devices. These high-performance microvalves can perform sequential loading and washing operations accurately and quickly [20]. This feature is in high demand in the on-chip biomedical lab or point-of-care devices. It is a compact, robust, self-powered micropump that does not need a complex external system. However, in today's microfluidic technologies there is a need to develop a micro-valve that can change fluid flow quickly, without leakage, and with less dead volume [21]. Magnetic micro-valves used today can often be hybrid integrated with permanent magnets to increase magnetic forces with less power consumption. Electromagnetic micro-valve representation is given in Figure 2.

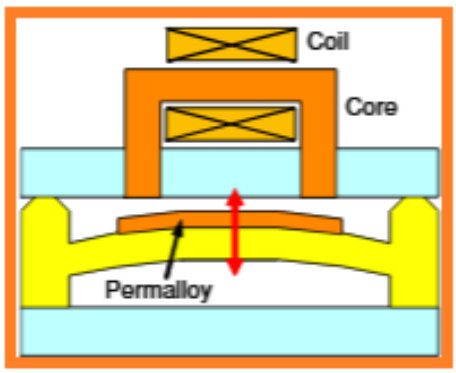

Figure 2. Micro valve and amplifier unit [22]

Various pumping methods such as finger-operated pumping, capillary pumping, gravity-based pumping and pre-degassed pumping have been developed to get rid of complex structures. Today, a vacuum-assisted pumping method using the gas permeability or solubility of PDMS is highly suitable for many biomedical microfluidic systems due to its simple application [23]. Wang et al. They have developed a compact, syringe-assisted, vacuum-powered micro-pump

module that can be easily attached to the outlet of any existing microfluidic device and provides greater flexibility in many biomedical applications. They whether integrated and analyzed a polymeric microfluidic device into a portable mechanical micro-pumping system that uses liquid-sensitive polymer particles as an actuator without an external power supply. Xu et al. They are reported that the flow of water from the semipermeable membrane to the osmotic reagent reservoir facilitates the fluid flow in the channel by the osmosis process when a semipermeable membrane is sandwiched between the inner osmotic reagent reservoir and the external water reservoir [24]. Updates to osmotic driven passive pumping techniques in micro fluids are summarized in Table 1.

Table 1. Passive pumping techniques [25-26]

Passive Pumping Techniques in Microfluidics			
Materials Used	**Flow Rate**	**Advantages**	**Disadvantages**
PDMS cubic chambers	0.15 µl h^{-1}	It provides the concentration gradient for more than a week	Low flow rate
PDMS and natural rubber	17 µl min^{-1}	It can be placed directly on a microdevice	Reactivation of pump requires water
PDMS chamber	0.33 µl min^{-1}	Low flow rate is used for constant refreshing of culture medium	Regular refreshing of osmotic reagent

3. MICROFLUIDIC SYSTEMS

The first microfluidic devices were generally made of silicone and glass. Researchers used silicon and glass with the technology of that time. However, these products have some drawbacks. Silicone is expensive and cannot be combined in optical microscopy due to its opacity. Also, both silicone and glass have low gas permeability. Next, the researchers examine organic polymers as the most viable option to develop an alternative that can be optically transparent, easy to process, flexible and inexpensive compared to its predecessors. Later, PDMS was developed microfluidic systems in the 1990s. With this development, it is preferred as the most used material in microfluidics and is widely used today. Compared to traditional materials used in other micro electrics, one of the main advantages of PDMS is its compatibility with cells and the ease of culturing simple organisms. In the late 1990s, it was observed that microfluidic devices were created for cell biology applications such as cell and protein separation modeling, cell-based biosensors, culture and research [27]. Towards the 2000s, it is seen that researchers started to work on microfluidic devices that can be used as tissue and organ models for drug discovery and development. In these studies, they developed the (organs-on-a-chip) by examining pathophysiology and biological processes. Since the 2000s, many tissue models of gut, liver, brain, heart, eye, skin, lung, muscle, blood vessels and tumor have been studied on a chip [28]. In 2010, a biometric device was developed to simulate the lung alveolar-capillary interface in structural, functional and mechanical aspects. Thanks to this work, a functional micro-environment was created and integration of different tissues into a single chip was achieved. The developed device has human alveolar epithelial cells on one side and human pulmonary endothelial cells on the opposite or underside. Thus, it consists of two PDMS microchannels separated by a porous PDMS membrane forming epithelial and endothelial compartments. It mimics human breathing by injecting air into the sidewall or walls of the alveoli and then vacuuming it [29]. It appears that an organ chip study was conducted in the human intestine in 2018. One of the most important features of the human intestine is digestion and absorption. It is also where the gut microbiome and microbes live in common. In this study, drug absorption was attempted in an organ chip made with an intestinal model.

Intestinal samples were placed in the upper part of the developed microfluidic portion, and a porous membrane separating it from the bottom was placed to check whether the administered drugs were absorbed. Precise control of the volume and manipulation of liquids is essential for many scientific fields, including chemistry, analytical biochemistry, biotechnology, and engineering. Microfluidics has become an important tool for designing environments with precise control of the conditions under study [30]. Microfluidics often includes devices and methods for controlling and manipulating liquids at a submillimeter scale. This technology has been presented as a popular candidate to replace traditional experimental approaches, especially in the biomedical field. The most popular and common approach for manufacturing microfluidic devices involves the use of "soft lithography" of poly-dimethylsiloxane (PDMS). This method has greatly contributed to the development of microfluidic technology. The use of these materials makes it easy to mold structures with micrometric resolution using a simple casting mold [31]. Different methods have been developed for the manipulation of both liquids and particles in microfluidics using electrical, magnetic, optical, capillary and mechanical forces [32]. It is seen that microfluidic devices are created by various integration of fluids, electronics, optics and biosensors. The main purpose is to meet the need for pathological analysis while the fluid is in motion. Microfluidic systems have proven useful in finding methods to diagnose fatal and chronic diseases at an early stage. A very-large-scale integration (VLSI) system is the process of creating integrated circuits by combining thousands of transistors on a single chip. With modern technologies, the number of transistors that can be installed per unit area has increased to billions, and this term has begun to give way to the term ULSI (Largest Scale Integration). Due to the emergence of advanced technologies such as MEMS, NEMS, it has become possible to integrate multiple interdisciplinary modules into a single-chip device. The interdisciplinary interaction of this technology can be schematized as shown in Figure 3.

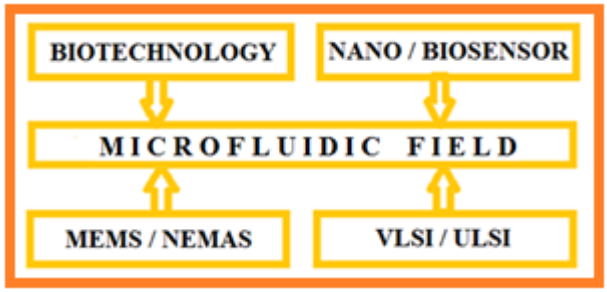

Figure 3. Interdisciplinary interaction in microfluidic technology

PDMS offers features such as low cost, optical transparency, flexibility, gas permeability, ease of use and high accuracy repeatability of models. The combination systems were created to allow both miniaturization and parallel matching of processes in compact devices, saving reagents and costs. Thanks to the easy production and flexibility of these devices, various functional microfluidic elements such as sensors, mixers, separators, distributors, pumps, valves have been produced. However, some concerns have arisen regarding the use of PDMS for biomedical research. It was found that leakage of non-crosslinked oligomers from PDMs can be toxic to cells. Due to its hydrophobic properties and permeability, it has been observed that hydrophobic small molecules are absorbed by PDMS. In addition, water vapor permeability can cause rapid evaporation, which can adversely affect experiments, mainly without static flow. However, the disadvantages associated with PDMS can be mitigated and additional device preparation may be required [33]. Recently, alternative materials to PDMS, namely thermoplastics (polystyrene - PS, cyclic olefin copolymer - COC, polymethyl methacrylate - PMMA and polycarbonate - PC), paper, Wax and textile products have been investigated.

Mukhopadhyay et al. They appear to suggest a microchannel bend in polymethylmethacrylate (PMMA) of different widths. The effects of channel aspect ratio and different separation angles were examined in terms of fluid flow. Mukhopadhyay et al. It suggests a microchannel bend in polymethylmethacrylate (PMMA) of different widths. The effects of channel aspect ratio and different separation angles in terms of fluid flow were investigated [34].
In connection with microfluidic technology, microfluid applications assume full integration of various microfluidic components and procedures in a single chip for miniaturizing chemical and biological processes [35]. Organ on a Chip refers to complex microengineering systems that aim to mimic the physiological basic properties of certain human organs, human tissues and interactions. There are several steps involved in the processing of the microfluidic device. Microfluidic processing begins with the collection of the physiological sample and then the specific analyte/biomarker is extracted from that sample. The transducer will act on the analyte electrically, electromechanically, optically or mechanically, depending on the biomedical application. The next step involves counting, classifying and raising the transducer output by the application. Finally, the amplified sample is processed using microelectronic methods. The latest trend shows that research in this area is increasing [36]. Many projects and research groups have been established in many countries of the world. The main purpose of these groups is to use micro/nanostructures; To develop new micro and nano technologies for microfluidics and to demonstrate new microfluidic applications in biomedical and life sciences.

4. MICROFLUIDIC TECHNOLOGY APPLICATION

The demand for microfluidic devices in many areas is due to the various technological advantages of fluid technology such as portability, automatic sample handling and reconfigurability. Real-time PCR detection chips for bacteria detection are some of the applications of microfluidic technology in the biomedical field, such as DNA chip, gene chip, cellular analysis chip, flow cytometry (for HIV) [37]. Wooseok et al. It appears that they focus on the properties of microfluidic chips to be used to meet the requirements of point-of-care diagnostic systems and increase their efficiency [38]. Since the functional modules and operating principles required in microfluidic systems are generally dependent on target analytes, applications of POCT systems (Point-of-care tests) are categorized by analyte types such as cells, proteins, metabolites and nucleic acids. POCT systems (point of care tests) are capable of detecting certain biomarkers from these analytes. These different biomarkers require different tests, diagnostic principles, and operating systems. Thus, in each category, the configuration of modules, detection methods, and advantages and disadvantages of microfluidic-based POCT diagnostic systems are reviewed. Cardoso et al. worked for the development of disposable and fully integrated microfluidic devices for microfluidic and clinical applications in biological fluids and monitoring of concurrent parameters [39]. This chip is produced by integrating biosensors, optical filters and electronic circuits on a single flow technique to promote pumping and mixing of microfluidics in microchannels. Mathematical models are required to complete the design of the channel. Therefore, Makhijani et al. developed a numerical model to simulate liquid filling due to the presence of surface tension at the liquid-air interface and demonstrated the application of disposable biochips for clinical diagnosis. It was mainly used for analysis and optimization to achieve the desired flow [40]. It appears that a transducer based on a piezoelectric material such as β-PVDF (polyvinylidene fluoride prepared in phase) is used to create this acoustic flow. This polymer is processed to be functionally graded to maintain heating and control the motion of fluids along with the input signal applied to the converter. To facilitate portability with less mixing time and to achieve high sensitivity and reliability in microfluidic systems, it is recommended to use a white light source and spectrophotometry as a sensing technique that can be made possible by combining

highly selective optical interference filters. Katla Sai et al. discussed the impact of inorganic nanomaterials on biofunctionalization, synthesis and clinical translation assessment for biomedical applications of microfluidic devices [41]. Microfluidic methods result in less energy consumption, rapid synthesis of quantum dots, and inorganic nanomaterials such as metals, nanocomposites and metal oxides. This also demonstrates the need for LOC devices for faster completion of clinical translations by conducting superior in vitro studies. There are three main types of biochips: lab-on-chip (LOCs), DNA chips, and protein chips. LOCs use a combination of one or more lab functions in a single integrated chip [42]. Due to recent advances in computational simulations, it is now possible to synthesize nanomedicine applications based on inorganic nanomaterials into a single structure using microfluidic technology useful for therapeutic applications. Recent advances in microfluidic technology and design strategies lead to the development of useful universal sample-result microfluidic devices to effectively detect pathogens with high specificity and sensitivity [43]. There are goals to be designed to have many advantages, such as main focus, point-of-care diagnosis, processing of small volume samples, fast detection time, miniaturization, and portability. In addition, emphasis is placed on the development of accessory-free and fully integrated standalone microchips. These advances will help reduce mortality and control the spread of life-threatening diseases such as Tuberculosis (TB), HIV and the like. Wen et al. gave an overview of microparticles produced by droplet microfluidics in their compilation studies [44]. In addition, recent developments in the biomedical fields are discussed. In subsequent developments, the droplet formation mechanism was designed and devices used to create various droplets were described. Methods for preparing template microparticles from these droplets are summarized and the unique and complex structures provided by microfluidic techniques are highlighted. Next, the biomedical applications of these microparticles are explained with a focus on recent advances in their use as drug delivery devices and cell-loaded matrices. Other applications are also briefly described, including biosensors and artificial cells. Finally, the current challenges of these microparticles could potentially are discussed and concluded with perspectives and possible implications. Auerswald et al. Their studies reveal the need for the development of microfluidic devices necessary for the multiplex detection of various antibiotic families in raw milk [45]. It has been reported that four antibiotic families are overused in the dairy diet, leading to stronger bacterial resistance. This will pose a serious problem and threaten effective antibacterial therapy in humans. An automatic, easy-to-use, fast and cost-effective multiplex detection system has been developed to detect these antibiotic families. The design principle of the microreactor including microfluidic mixing reactor and ordinary micro reactor types is introduced [46]. Next, the latest advances in microreactor applications are reviewed (reaction kinetics, enzymatic bio reactions, biosynthesis and medical testing with the micro-mix reactor and rtPCR, ELISA immune reaction and nucleic acid hybridization with ordinary microreactor strains). Finally, on-chip detection methods such as common and low-cost methods (laser-induced fluorescence, ultraviolet (UV) absorption, and electrochemical method) are summarized. Kalaitzakis et al. It is seen that he explains the proteomic profiling techniques integrated with knowledge management methodologies and analysis platforms [47]. Its main purpose is to identify clinically relevant analytes and biomarkers for early-stage detection of pancreatic cancer. Ultrasonic and physical detection of pancreatic cancer becomes complex and burdensome as the pancreas is deep in the abdominal cavity. Approximately 95% of such cases are diagnosed in the last stages; For example, stage III or IV causes a high mortality rate. The Loccandia project is primarily concerned with the diagnosis of early-stage cancer of the pancreas. This can be done through a microfluidic development, namely the validation of the plasma protein integrated with the application of profiling with the help of a new nanotechnology-based platform and a complete proteomic analysis chain. The success of this project is based on the seamless combination of bio, nano and data processing and knowledge management

methodologies. Ziober et al. describe the emergence of microfluidic devices for biomarker-based identification and early diagnosis of oral cancer [48]. It is seen that head and neck cancers constitute approximately 40% of oral cavity cancers. Oral cavity cancer includes squamous cell carcinoma that occurs on the lips, mouth, tongue, gums, buccal mucosa, hard and soft palate, and floor. OSCC (Oral squamous cell carcinoma) is deadly cancer and results in high mortality, morbidity, and deformity. Traditional diagnostic and screening methods for OSCC are not cost-effective and highly accurate and require lengthy and detailed procedures by advanced equipment, modern laboratories, and qualified personnel. To overcome these problems, a miniature, accurate, automatic, integrated and inexpensive microfluidic chip is required. Screening patients for OSCC will be considered as this microfluidic saliva input sample, and then processed by minimally trained personnel, thus providing timely results. Identification of oral cancer and its precursor (starting chemicals used in the synthesis of a chemical substance) will be possible with the cells in the chip, the membrane-associated cell proteins expressed alone in the membranes of dysplastic and cancer cells and have unique gene transcription profiles. Dutse et al. studied the need for microfluidic-based chips that can be used as complementary tools to control the effects of pathogenic agents to prevent environmental damage [49]. These systems are easy to use, fast, precise, reliable enough and portable. Therefore, it offers many advantages over traditional methods that are expensive, tedious and time-consuming. The main application of microfluidic systems in pathogen detection includes DNA-based methods based on electrochemical techniques. Fluid mechanics of systems are discussed at the nanoscale. The main limitation is that the use of mechanical pumps required for liquid transfer requires attention and reduces performance. Three examples are presented to illustrate the potential of microfluidics in the medical field. First, when it comes to patients monitoring blood lithium, a pre-filled, disposable chip-based on capillary electrophoresis is discussed [50]. Orally, lithium is often used to treat patients suffering from bipolar disorder. Therefore, a glass chip based on vacuum pre-filled with capillary electrophoresis and buffer solution was produced. Vacuum refers to any area where the pressure is less than atmospheric pressure (negative pressure). Vacuum-operated devices utilize the ability of an MFD to absorb the sample through negative pressure without any extra on/off the microfluidic unit. However, in osmosis-induced Mfds, the osmotic reagent had to be refreshed at regular intervals, which limited their application [51]. LOC applications, such as pumping the fluid flow with the platforms reported by the valve, and separating and detecting the different chemical species applied in a microfluidic format, require a review of the modes of operation on different chips. Finally, microfluidic cell culture has been developed expressing the use of surface tension in passive pumping based on the physical and micro-related concept environment where differential pressure is generated due to different volumes at the inlet and outlet port to aid fluid flow [52]. The same chip has the potential to detect magnesium and calcium in cow blood to detect milk fever. It is seen that the sodium in the urine can also be measured with this chip platform, which is very useful for kidney patients. In the second example, a simple chip is presented that is used to count sperm cells in sperm to determine male fertility. Finally, improved in vitro models used for drug development are presented. As an example of the organ on-chip, the blood-brain barrier on the chip has been noticed to create a versatile platform for the screening of drugs and has the potential to greatly alter and reduce animal testing [53]. The need for simple, fast and timely diagnosis and elimination of global alarming diseases such as malaria has led to the emergence of microfluidic PCR diagnostic methods. Taylor et al. His work has identified a microfluidic technology that has the potential to overcome the costly, complex and challenges of traditional molecular diagnostics, especially in developing countries [54]. RT-PCR testing is a widely used and highly specific messenger RNA detection and quantification technique that can detect the presence of SARS-CoV-2 in a biological sample. Real-time RT-PCR testing uses fluorescent dyes to allow scientists to see results almost

instantly [55]. Ai et al. reported that they have 97% high sensitivity for detecting COVID-19 by CT in adults when used as the reference RT-PCR. This study also demonstrated how the timeline of Negative-Positive chest CT scans compares with the corresponding RT-PCR test timelines [56]. Although the RT-PCR test plays a very important role in accurately detecting SARS-CoV-2 on a case-by-case basis, it also has inherent problems that limit its usefulness. Current barriers to the widespread use of RT-PCR testing include the lack of test kits and a long processing time before results are obtained [57]. Microfluidic devices, the structure is given in Figure 4, allow the analysis of various samples such as blood, saliva or cell tissues to provide a fast and accurate diagnosis.

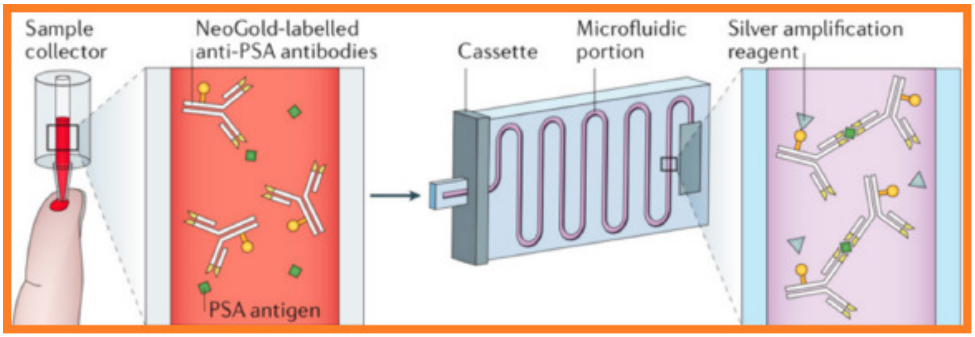

Figure 4. An example of a microfluidic diagnostic device [58]

Microfluidic platforms are created for microbial extraction and combined with a variety of analytical methods that detect pathogenic microorganisms [59]. For example, a microfluidic chip can catch pathogens in the air. Thus, the laminar flow is transformed into the curved airflow in the device, increasing the possibility of contact with the bacteria in the airflow with the duct wall. Microfluidic platforms can collect hundreds of bacteria in a few microliters of aqueous media, which is sufficient for direct immunoassay or nucleic acid analysis. This technique cannot work on its own, but it facilitates sampling and downstream bioanalysis [60].

5. CONCLUSIONS

Microfluidics is widely used in different fields such as biomedical, engineering and chemistry. Depending on the nature of the application, a person can only design and prototype a microfluidic device. The described micromixer, microvalve and micro motor are considered good candidates for use in existing microfluidic devices. According to studies conducted or to be conducted, microfluidic chip technology has a wide range of applications in the biomedical field. Its microfluidic devices are suitable for point-of-care diagnosis as they provide fast and timely diagnostic results. For many other applications, platforms have been created to design microfluidic devices.

The complex design of microfluidic chips, the stable binding and integration of different functional organ chips, and the modification and development of different culture conditions in various cell cultures require further optimization and experimentation. The problems of molecular absorption, mass transfer and bubble formation within the equipment require immediate solutions. Good operational stability and repeatability are essential for the introduction of the method. In addition, costly and complex preparation and operation processes are also issues to consider. If more convenient, user-friendly and inexpensive devices can be developed, the microfluidic chip promises to play a greater role in pharmaceutical analysis.

REFERENCES

[1] Saggiomo, V. and Velders, A. H. (2015). Simple 3D printed scaffold-removal method for the fabrication of intricate microfluidic devices. Adv. Sci. 2, 1-5.

[2] Whitesides, G. (2006). The origins and the future of microfluidics. Nature 442, 368-373.

[3] Sackmann, E., Fulton, A. and Beebe, D. (2014). The present and future role of microfluidics in biomedical research. Nature 507, 181-189.

[4] Luo, T., Fan, L., Zhu, R., Sun, D. (2019). Microfluidic Single-Cell Manipulation and Analysis: Methods and Applications. Micromachines 10(2): 104.

[5] Suwannaphan, T., Srituravanich, W., Sailasuta, A., Piyaviriyakul, P., Bhanpattanakul, S., Jeamsaksiri, W., Sripumkhai, W., Pimpin, A. (2019). Investigation of Leukocyte Viability and Damage in Spiral Microchannel and Contraction-Expansion Array. Micromachines. 10(11): 772.

[6] Nielsen, J. B., Hanson, R. L., Almughamsi, H. M., Pang, C., Fish, T. R., Woolley, A. T. (2020). Microfluidics: Innovations in Materials and Their Fabrication and Functionalization. Anal. Chem. 92, 150-168.

[7] Young, E. W., Beebe, D. J. (2010). Fundamentals of microfluidic cell culture in controlled microenvironments. Chemical Society Reviews, 39(3): 1036-1048.

[8] Baydoun, M., Treizeibré, A., Follet, J., Vanneste, S. B., Creusy, C., Dercourt, L., Delaire, B., Mouray, A., Viscogliosi, E., Certad, G., Senez, V. (2020). Micromachines. 11(2): 150.

[9] Luo, Y., Zhao, J., He, C., Lu, Z., Lu, X. (2020). Miniaturized Platform for Individual Coral Polyps Culture and Monitoring. Micromachines. 11(2): 127.

[10] Williams, M. J., Lee, N. K., Mylott, J.A., Mazzola, N., Ahmed, A., Abhyankar, V. V. (2019). A Low-Cost, Rapidly Integrated Debubbler (RID) Module for Microfluidic Cell Culture Applications. Micromachines. 10(6): 360.

[11] Horiuchi, T., Miura, T., Iwasaki, Y., Seyama, M., Inoue, S., Takahashi, J. İ., Haga, T., Tamechika, E. (2012). Passive Fluidic Chip Composed of Integrated Vertical Capillary Tubes Developed for On-Site SPR Immunoassay Analysis Targeting Real Samples. Sensors. 12(6): 7095-7108.

[12] Fu, J., Wu, L., Qiao, Y., Tu, J., Lu, Z. (2020). Microfluidic Systems Applied in Solid-State Nanopore Sensors. Micromachines. 11(3): 332.

[13] Chokkalingam, V., Tel, J., Wimmers, F., Liu, X., Semenov, S., Thiele, J., Figdor, C. G. and Huck, W. T. (2013). Probing cellular heterogeneity in cytokine-secreting immune cells using droplet-based microfluidics, Lab Chip, 13, 4740-4744.

[14] Sahu, K. K., Lal, A., Mishra, A. K. (2020). Latest updates on COVID-2019: a changing paradigm shift. J Med Virol. 92(6):533-535. doi:10.1002/jmv.25760

[15] Coleman, C. M., Liu, Y. V., Mu, H. Y., et al. (2014). Purified coronavirus spike protein nanoparticles induce coronavirus neutralizing antibodies in mice. Vaccine. 32(26): 3169-3174.

[16] Sheahan, T. P., Sims, A. C., Leist, S. R., et al. (2020). Comparative therapeutic efficacy of remdesivir and combination lopinavir, ritonavir, and interferon beta against MERS-CoV. Nat Commun. 11(1). doi:10.1038/s41467-019-13940-6

[17] Tu, Y. F., Chien, C. S., Yarmishyn, A. A., et al. (2020). A review of SARS-CoV- 2 and the ongoing clinical trials. Int J Mol Sci. 21(7): 2657. doi:10.3390/ijms210726572

[18] Mulligan, M. J., Lyke, K. E., Kitchin, N., et al. (2020). Phase 1/2 study of COVID-19 RNA vaccine BNT162b1 in adults. Nature. 586(7830):589-593. doi:10.1038/s41586-020-2639-4

[19] Huh, D., Hamilton, G. A., and Ingber, D. E. (2011). From 3D cell culture to organs-on-chips. Trends in cell biology, 21(12): 745-754.

[20] Wang, A., Koh, D., Schneider, P., Breloff, E., Oh, K. W. (2019). A Compact, Syringe-Assisted, Vacuum-Driven Micropumping Device. Micromachines. 10(8): 543.

[21] Fu, C., Rummler, Z., Schomburg, W. (2003). Magnetically driven micro ball valves fabricated by multilayer adhesive film bonding," J Micromech Microengineering, vol. 13, pp 96-102.

[22] Goettsche, T., Kohnle, J., Willmann, M., Ernst, H., Spieth, S.,Tischler, R., Messner, S., Zengerle, R., Sandmaier, H., (2005). Novel approaches to particle tolerant valves for use in drug delivery systems Sensors Actuators 118, 70-7.

[23] Xu, Z. R., Yang, C. G., Liu, C. H., Zhou, Z., Fang, J. and Wang, J. H. (2010). An osmotic micro-pump integrated on a microfluidic chip for perfusion cell culture, Talanta, 80(3): 1088-1093.

[24] Park, J. Y., Kim, S. K., Woo, D. H., Lee, E. J., Kim, J. H. and Lee, S. H. (2009). Differentiation of Neural Progenitor Cells in a Microfluidic Chip-Generated Cytokine Gradient, Stem Cells, 27(11): 2646-2654.

[25] Paguirigan, A. L., and Beebe, D. J. (2009). From the cellular perspective: exploring differences in the cellular baseline in macroscale and microfluidic cultures, Integr. Biol. 1(2): 182-195.

[26] Folch, A. and Toner, M. (2008). Cellular micro models on biocompatible materials, Biotechnology Programs, skin. 14(3): 388-392.

[27] Huh, D., Matthews, B. D., Mammoto, A., Montoya-Zavala, M., Hsin, H. Y. and Ingber, D. E. (2010). Reconstruction of lung function at the organ level on a chip, Science, 328(5986): 1662-1668.

[28] Bae, B., Kim, N., Kee, H., Kim, S., Lee, Y., Lee, S., Park, K. (2002). Feasibility test of an electromagnetically driven valve actuator for glaucoma treatment, J Microelectromech Syst, vol. 11, pp. 344-354.

[29] Esch, E. W., Bahinski, A. and Huh, D. (2015). Organs on chips at the borders of drug discovery, Nature Reviews Drug Discovery, skin. 14(4): 248-260.

[30] Hou, X., Zhang, Y. S., Trujillo-de Santiago, G., Alvarez, M. M., Ribas, J., Jonas, S. J. and Khademhosseini, A. (2017). Interplay between materials and microfluidics. Nature Reviews Materials, 2(5): 1-15.

[31] Bhattacharjee, N., Urrios, A., Kang, S., and Folch, A. (2016). The upcoming 3D-printing revolution in microfluidics. Lab on a Chip, 16(10): 1720-1742.

[32] Trantidou, T., Elani, Y., Parsons, E., and Ces, O. (2017). Hydrophilic surface modification of PDMS for droplet microfluidics using a simple, quick, and robust method via PVA deposition. Microsystems & nanoengineering, 3(1): 1-9.

[33] Pan, L. J., Tu, J. W., Ma, H. T., Yang, Y. J., Tian, Z. Q., Pang, D. W., Zhang, Z.L. (2018). Controllable synthesis of nanocrystals in droplet reactors. Lab. Chip. 18, 41-56.

[34] Mukhopadhyay, S., Roy, S. S., Mathur, A., Tweedie, M. and McLaughlin, J. A. (2010). Experimental study on capillary flow through polymer microchannel bends for microfluidic applications, Micromech. Microeng. 20(5): 055018.

[35] Samiei, E., Tabrizian, M., & Hoorfar, M. (2016). A review of digital microfluidics as portable platforms for lab-on a-chip applications. Lab on a Chip. 16(13): 2376-2396.

[36] Li, W., Zhang, L., Ge, X., Xu, B., Zhang, W., Qu, L and Weitz, D. A. (2018). Microfluidic fabrication of microparticles for biomedical applications. Chemical Society Reviews, 47(15): 5646-5683.

[37] Mac Connell, A. B., Price, A. K. and Paegel, B. M. (2017). An integrated microfluidic processor for DNA-encoded combinatorial library functional screening. ACS combinatorial science, 19(3): 181-192.

[38] Wooseok, J., Han, J., Choi, J-W. and Ahn, C. H. (2015). Pointof-care testing (POCT) diagnostic systems using microfluidic lab-on-achip technologies, Microelectronic Engineering Journal, 132, 46-57.

[39] Cardoso, V. F., Catarino, S. O., Lanceros-Mendez, S., & Minas, G. (2011). Lab-on-a-chip using acoustic streaming for mixing and pumping fluids. In 1st Portuguese Biomedical Engineering Meeting (1-4). IEEE.

[40] Makhijani, V. B., Reich, A. J., Puntambekar, A., Hong, C. and Ahn, C. (2001). Advances in passively driven microfluidics and lab-on-chip devices: a comprehensive literature review and patent analysis, Tech Connect Briefs, 1, 266-269.

[41] Krishna, K. S., Yuehao, L. i., Shuning, L. i. and Challa, S., Kumar, S. R. (2013). Labon-a-chip synthesis of inorganic nanomaterials and quantum dots for biomedical applications, Advanced Drug Delivery Reviews Journal, 65(11): 1470-1495.

[42] Volpatti, L. R. and Yetisen, A. K. (2014). Commercialization of microfluidic devices, Trends Biotechnol., 32(7): 347-350.

[43] Luo, G., Du, L., Wang, Y., and Wang, K. (2019). Recent developments in microfluidic device-based preparation, functionalization, and manipulation of nano-and micro-materials. Particuology, 45, 1-19.

[44] Li, W., Zhang, L., Ge, X., Xu, B., Zhang, W., Qu, L. and Weitz, D. A. (2018). Microfluidic fabrication of microparticles for biomedical applications. Chemical Society Reviews, 47(15): 5646-5683.

[45] Auerswald, J., Berchtold, S., Diserens, J. M., Gijs, M. A., Jin, Y. H., Knapp, H. F. and Voirin, G. (2009). Lab-on-a-chip for Analysis and Diagnostics: Application to Multiplexed Detection of Antibiotics in Milk. In Nanosystems design and technology (117-142). Springer, Boston, MA.

[46] Shi, H., Nie, K., Dong, B., Long, M., Xu, H. and Liu, Z. (2019). Recent progress of microfluidic reactors for biomedical applications. Chemical Engineering Journal, 361, 635-650.

[47] Kalaitzakis, M., Kritsotakis, V., Grangeat, P., Paulus, C., Gerfault, L., Perez, M., Reina, C., Potamias, G., Tsiknakis, M., Kafetzopoulos, D. and Binz, P. A. (2008). Proteomic based identification of cancer biomarkers: The LOCCANDIA integrated platform, Proceedings of 8th IEEE International Conference on BioInformatics and BioEngineering, Athens, 1-7.

[48] Ziober, B. L., Mauk, M. G., Falls, E. M., Chen, Z., Ziober A.F. and Haim H. B. (2008). Lab-on-a-chip for oral cancer screening and diagnosis, Head & Neck Journal. 30(1): 111-121.

[49] Sabo, W. D., and Nor, A. Y. (2011). Microfluidics-based lab-on-chip systems in DNA-based biosensing: An overview, Sensors Journal, 11(6): 5754-5768.

[50] Aryasomayajula, A., Bayat, P., Rezai, P. and Selvaganapathy, P. R. (2017). Microfluidic Devices and Their Applications. In Springer Handbook of Nanotechnology (487-536). Springer, Berlin, Heidelberg.

[51] Xu, Z. R., Yang, C. G., Liu, C. H., Zhou, Z., Fang, J. and Wang, J. H. (2010). An osmotic micro-pump integrated on a microfluidic chip for perfusion cell culture, Talanta, 80(3): 1088-1093.

[52] Young, E. W. and Beebe, D. J. (2010). Fundamentals of microfluidic cell culture in controlled microenvironments, Chem. Soc. Rev., 39, 1036-1048.

[53] Bruijns, B., Van Asten, A., Tiggelaar, R., and Gardeniers, H. (2016). Microfluidic devices for forensic DNA analysis: A review. Biosensors, 6(3): 41.

[54] Taylor, B. J., Howell, A., Martin, K. A., Manage, D. P., Gordy, W., Campbell, S. D., & Atrazhev, A. (2014). A lab-on-chip for malaria diagnosis and surveillance. Malaria Journal, 13(1): 179.

[55] Long, C., Xu, H., Shen Q, et al. (2020). Diagnosis of the coronavirus disease (COVID-19): rRT-PCR or CT? Eur J Radiol.126:108961

[56] Ai, T., Yang, Z., Hou, H, et al. (2020). Correlation of chest CT and RT-PCR testing in coronavirus disease 2019 (COVID-19) in China: a report of 1014 cases. Radiology, 296(2): 41-45.

[57] Website. Chinese clinical guidance for COVID-19 pneumonia diagnosis and treatment, (2021). https://www.acc.org/latest-in-cardiology/articles/2020/03/17/11/22/chinese-clinical-guidance-for-covid-19-pneumonia-diagnosis-and-treatment

[58] Mejía-Salazar, J. R., Rodrigues Cruz, K., Materón Vásques, E. M., Novais de Oliveira Jr, O. (2020). Microfluidic Point-of-Care Devices: New Trends and Future Prospects for eHealth Diagnostics. Sensors, 20, 1951.

[59] Zhang, D., Bi, H., Liu, B., Qiao, L. (2018). Detection of Pathogenic Microorganisms by Microfluidics Based Analytical Methods. Anal. Chem. 90, 5512–5520.

[60] Narimani, R., Azizi, M., Esmaeili, M., Rasta, S. H., Khosroshahi, H. T. (2020). An optimal method for measuring biomarkers: Colorimetric optical image processing for determination of creatinine concentration using silver nanoparticles. 3 Biotech. 10, 416.

NATURENGS
MTU Journal of Engineering and Natural Sciences
https://dergipark.org.tr/tr/pub/naturengs
DOI: 10.46572/naturengs.895283

Research Article

Non-linear and Equivalent Linear Site Response Analysis of Istanbul Soils

Özgür YILDIZ

Department of Civil Engineering, Faculty of Engineering and Natural Sciences,
Malatya Turgut Özal University, Malatya, Turkey

(**Received**: 11.03.2021; **Accepted**: 21.05.2021)

ABSTRACT: The effect of local soil characteristics on the propagation of earthquake waves has been commonly studied by researchers. However, the validity of the results obtained by these studies is limited only to the relevant soil conditions. The main purpose of this study is to examine the effect of soil conditions on the propagation of seismic waves in Istanbul. In this regard, soil information belonging to different districts of Istanbul has been compiled. The site response analysis was simulated using a time-domain non-linear response analysis based on the effective stress method and frequency-domain equivalent linear analysis based on the total stress method. A widely used one-dimensional response analysis program DEEPSOIL was used to estimate the soil response of the sites. Modeled soil profiles were subjected to 1999 Kocaeli earthquake motion and the results of the analysis are presented as spectral acceleration, PGA and lateral displacements. The results obtained from both of the analyses were evaluated comparatively in terms of the effect of soil properties on the propagation of the seismic waves. The effect of the analysis method based on different approaches on the results is examined. Substantial findings have been revealed regarding how the propagation of the earthquake waves is affected by local soil conditions. The liquefaction potential of soil profiles was also evaluated using the data of the soil properties of the investigation area.

Keywords: Site response, Equivalent linear analysis, Non-linear analysis, Deepsoil, Earthquake.

1. INTRODUCTION

The Mw 7.4 earthquake that occurred in Kocaeli/Gölcük on August 17th 1999, was felt throughout the Marmara region and in a wide area from Ankara to Izmir. Due to the destruction, the loss of life, and the injuries it caused, considerable socio-economic consequences have occurred. Considering the ongoing seismic activities and the earthquake history of the region, it is thought that a possible high-magnitude earthquake that will affect Istanbul may cause significant losses. Although it is approximately 150 km away from the epicenter of the earthquake, the destruction that occurred after the 1999 Kocaeli earthquake in Avcılar district is attributed to the effect of site conditions on earthquake waves as much as the low constructional quality of the building stock. This brought to mind the term of 'site effect' used in literature after the 1985 Michoacan earthquake caused significant destruction in Mexico City, despite being 435 km away from the epicenter. The only reason for this is the increase in the displacement of the buildings as a result of the coincidence of the natural vibration periods of the buildings with the dominant periods of the earthquake waves formed on the soft soil surface. Likewise, no building damage occurred in Bursa city center, 135 kilometers away from the epicenter of the 28th March 1970 Gediz Earthquake (M= 7.1) but the collapse of the atelier buildings of a factory in the Bursa plain is explained by the enlargement of the seismic wave amplitudes due to layered soft soils [1].

Corresponding Author: ozgur.yildiz@ozal.edu.tr
ORCID number of authors: 0000-0002-3684-3750

The effect of the earthquake at a location depends on many factors such as the magnitude of the earthquake, the distance from the epicenter, duration of ground motion, the geological environment the wave propagated through, the frequency content and the soil conditions in the region. Within all these parameters, the site effect has become an important concern of geotechnical earthquake engineering. It leads to changes in the characteristics of the motion due to the propagation of seismic waves in soil deposits and as a result, has a great impact on the response of structures during earthquake events [2]. In cases the soil profile is single-layered, it is less complex to examine the local soil effect on the propagation of seismic waves compared to stratified soil environments. However, in cases where the soil profile is stratified, relative density, stiffness, thickness, shear wave velocity, damping ratio, and other physical properties of the soil layers and certainly the intensity of the propagating earthquake waves have become important parameters that primarily affect soil behavior. In addition to the effect of soil conditions on seismic waves, soil layers exposed to strong ground motion lose their strength and behave as a viscous liquid that cannot be ignored (such as liquefiable soils). This is known as 'liquefaction' in the literature and is not itself an event that causes structural damage. However, the excessive displacements and settlements due to liquefaction cause foundation failures resulting in great damages.

The effects of soil conditions on the propagation of earthquake waves are measured using site response analysis. These analyzes are performed in two categories; i. linear and equivalent linear analysis in the frequency domain and ii. linear and non-linear analysis in the time domain [2]. In the first studies in this field, the behavior of the soil under dynamic loading was investigated by frequency-domain equivalent linear analysis [3,4]. Later, a software program, SHAKE, was developed by researchers to analyze the seismic site response [5]. A number of modifications have been applied to this program to better reflect the soil behavior [4]. Empirical equations have been developed to analyze the effect of soil properties on propagating seismic waves [6]. Subsequently, both the design response spectra [7] and the effect of different parameters on site response analysis were examined by the researchers [8, 9]. Also, successful analyses were performed on locations having high liquefaction potential in Turkey [10, 11].

The main purpose of this study is to perform a one-dimensional site response analysis of soils from different districts of Istanbul by using two different methods: i. the equivalent linear method based on total stress modeling in the frequency domain, ii. the non-linear method based on effective stress modeling in the time domain. It is aimed to investigate the effect of soil formations in Istanbul, where rock formations such as limestone or sandstone (i.e. greywacke) with different degrees of weathering are mostly existed, on earthquake waves. In accordance with this purpose, locations with different soil characteristics in the Anatolian and European sides of Istanbul have been selected. Soil profiles of the selected cases were modeled using DEEPSOIL 1D site response analysis program. The non-linear (NLA) and equivalent linear (ELA) analyses were performed with developed soil models. By evaluating the results obtained by both approaches comparatively, substantial findings have been drawn regarding the effects of the local site conditions on the propagation of seismic waves. Evaluations were made on the liquefaction potential of both investigation areas according to commonly used criteria.

2. GEOLOGICAL STRUCTURE

Paleozoic formations with a thickness of 2000 meters are found in Istanbul and its surroundings. The upper parts of these formations are made up of Carboniferous aged sandstone (greywacke), siltstone, and claystone, which are called as Trakya formation. On the Paleozoic sequence, there

are Eocene white-colored, hard fractured limestones with intercalations of marl and carbonated sandstone. The younger sediments with Neogene age exist on top of Eocene units. From the bottom to the top, there are extremely consolidated clay (Gürpınar Formation, Tdg), gravely silty sand (Çukurçeşme Formation), organic clay (Güngören Formation), marl and limestone (Bakırköy Formation) and gravely sandy clay layers (Samandıra Formation). Due to confusion in the field applications and geological maps, the Gürpınar, Çukurçeşme and Güngören formations were collectively named as 'Avcılar Formation' and mapped as a single unit (Figure 1) [12].

The geological structure of Istanbul and its surroundings, whose general stratigraphy is summarized above, consists of formations with lithologies that can frequently change from bottom to top with the erosion of the region. Arkoz and quartzites, which are the oldest units in the visible base, have a very hard rock appearance and sometimes completely sand content. The greywackes known as the Trakya formation, which are encountered in a wider area of Istanbul, are mostly weathered on the surface and cracked up to 15 to 20 meters in thickness at lower depths, and weathered, bluish-gray colored, less weathered units at the bottom. Gürpınar, Çukurçeşme, Güngören, and Bakırköy formations are existing on top of the Eocene limestones, which are located on the graywacke units of the Trakya formation. At the top of these formations, there are gravelly, sandy, silty, clayey alluvial units (Figure 2).

3. RESPONSE ANALYSIS

1D site response analysis is used to investigate the effect of local soil conditions on the propagation of seismic waves. Throughout these analyzes, different approaches are used by researchers. These analyzes are applied by using linear, equivalent linear, and non-linear methods. Among these methods, the linear analysis method is performed in the frequency and time domain, the equivalent linear analysis method in the frequency domain, and the non-linear analysis method in the time domain. Linear and equivalent linear analyses are based on the independence of the damping and shear modulus from shear strain, while non-linear analysis is strain-dependent. The soil response with generated excess pore water pressure in time domain analysis is completely different from frequency domain analysis which is a total stress analysis. The excess pore water pressure generated in the site due to a seismic motion have a significant effect on soil behavior by leading to degradation in stiffness. Therefore the soil response obtained using the equivalent linear method does not fully capture the soil behavior. However, as a simple and less number of input variables requiring method, it is suggested to perform equivalent linear analysis in parallel to non-linear analysis especially for soft and having high liquefaction potential soils. In this study, the effects of local soil conditions on wave propagation were comparatively investigated using non-linear and equivalent linear analysis methods. The liquefaction potential of the soil profiles is also examined by using soil properties.

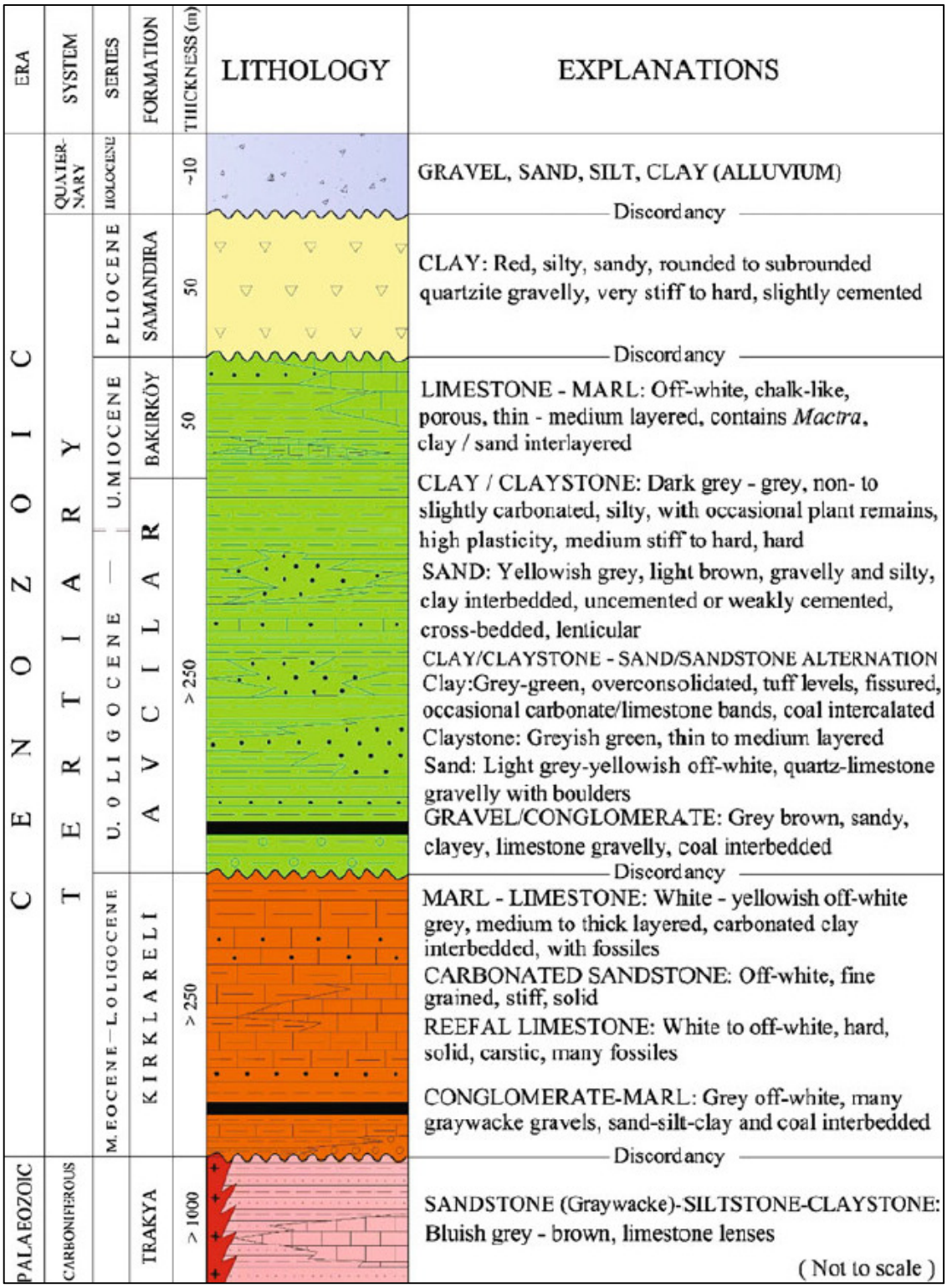

Figure 1. Revised stratigraphy of Istanbul [12]

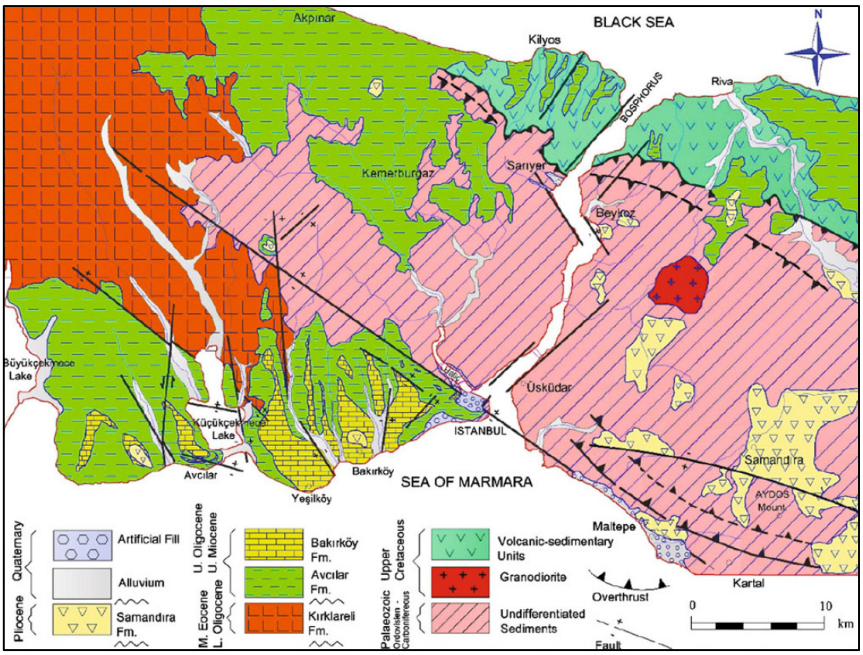

Figure 2. General geological map of Istanbul and its surrounding area [12]

4. MATERIALS AND METHODS

The borehole logs obtained by private soil investigation company a total of 4 boreholes, 2 on the Anatolian side (Şile and Pendik district) and 2 on the European side (Avcılar and Beylikdüzü district) were numerically modeled. The first case from the Anatolian side of Istanbul belongs to the field investigation of single-span bridge construction in the Şile district. The second borehole log has taken from a field study of the construction of an educational institution in Avcılar district. The following borehole log is belonging to the site investigation of a transportation facility in Pendik district. The last case is belonging to a site investigation study of a transfer hub in the Büyükçekmece district. The details of the selected boreholes are summarized in Table 1. The soil profile of the first case consists of alluvial deposits upon clay, sand and carbonated limestone layers. The soil profile of the second case mainly consists of clay layers named Çekmece Formation (Tç). The third case consists of gravelly-sandy clay layers overlying arkosic sandstone which is known as Sultanbeyli Formation (Ts). The last case consists of clayey-gravelly sand layers overlying stiff clay layers which is a typical example of Avcılar formation. Each of the selected cases consists of soil profiles that can have effects on seismic wave propagation. In this context, they will be representative cases for areas with similar soil properties in terms of their effects on the propagation of seismic waves. The soil profiles of the determined locations were modeled using DEEPSOIL site response analysis program which is an widely used an equivalent linear and non-linear one-dimensional (1D) seismic site response analysis software. The analyses were conducted in two categories namely; i. non-linear time-domain (NL-TD) and ii. equivalent-linear frequency domain (EL-FD) site response analysis. The general quadratic/hyperbolic model (GQH) which defines the shape of the backbone curve for stress-strain relation proposed by Groholski [13] was used in the analysis. Non-masing hysteresis models are used to reduce the size of loops and achieve similar behavior of the soil as in laboratory conditions. The soil profile was divided into different numbers of sub-layers with a thickness not exceeding 2 m and following lower and upper depths given in Table 2. Thus, the maximum frequency of the soil layers was provided to be greater than 30 Hz. The empirical modulus reduction and damping curves proposed by Darendeli [14]

were used in response analysis to represent soil behavior. The MRDF fitting procedure was applied to modulus reduction and damping curves. The shear wave velocity of the soil layers was calculated using the following empirical correlation;

$$V_s = 51.5\ N\ 0.516 \quad (1)$$

where N is the blow number of SPT test [15]. The lithology and soil properties of the selected cases are given in Table 2. Simulations were carried out by using Kozlu station records of the 1999 Kocaeli Earthquake. The acceleration time history of the motion employed in the numerical analysis is shown in Figure 3.

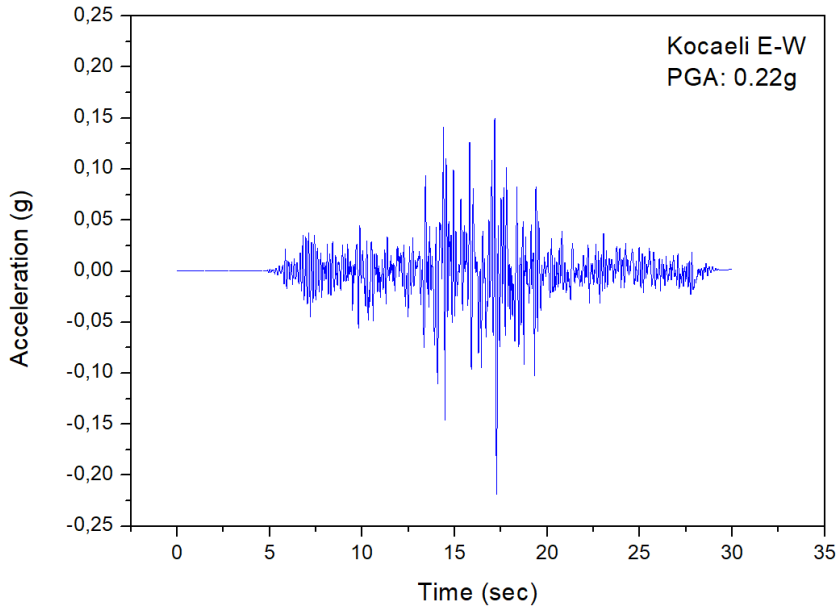

Figure 3. The acceleration time history of the 1999 Kocaeli EW earthquake

Table 1. The location and depth details of the boreholes

Case	Borehole	District	Coordinates		Final Depth (m)	GWT (m)
			x	y		
Case I	BHI	Şile	486667	4555680	42	2
Case II	BHII	Avcılar	392662	4540042	25	19.60
Case III	BHIII	Pendik	443169	4529686	30	14.60
Case IV	BHIV	B.çekmece	384294	4544018	40	16

Table 2. The lithology and soil properties of selected cases

Borehole	Depth (m)	Lithology	c kPa)	ϕ (°)	γ (kN/m^3)	PI (%)	SPT-N_{avg}	V_s (m/sec)
BHI	0-1.5	Artificial fill	0	25	17	-	-	100
	1.5-9	Medium clay	46	8	18	20.6-38.2	10	169
	9-37.5	Medium sand	0	30	18	-	13	193
	37.5-42	Limestone	150	38	24	-	R	390
BHII	0-1.5	Sandy stiff clay	0	22	17	-	20	235
	1.5-7.5	Very stiff clay	10	24	18	8-30	32	308
	7.5-25	Very stiff-hard clay	18	27	19	32-34	60	426
BHIII	0-15.35	Artificial fill	0	24	17	-	-	100
	15.35-20	Gravelly sandy clay	0	27	19	-	12	178
	20-50	Gravelly sandy clay	10	29	19	15	45	367
BHIV	0-1.5	Fill, angular gravel, sand, clay	0	24	17	-	35-R	323
	1.5-8	Clayey gravelly sand	0	33	19	-	50	388
	8-21	Very stiff-hard clay	30	28	20	27-36	55	407

5. RESULTS AND DISCUSSION

5.1. Non-linear Analysis

Under the applied seismic motion, the general soil profile responses are evaluated by means of Peak Ground Acceleration (PGA) and acceleration response spectra with 5% damping. The NLA site response analysis under the 1999 Kocaeli Earthquake was performed and the variations of site response spectra for the selected boreholes are given in Figure 4. The upper layers of BHI and BHIII borehole logs having lower shear wave velocities displayed an amplification effect on applied earthquake motion. However, the lower layers with higher SPT-N values and shear wave velocities deamplified the applied motion. The soil layers represented by BHII and BHIV borehole logs deamplified the applied motion. It was observed that relatively soft and loose artificial fill layers of soil profiles displayed an amplification effect, while deamplification effect in varying degrees was observed by stiff clay or dense sand layers. Even it is classified as a fill layer, the top layer of the BHIV borehole log having relatively higher SPT-N and shear values displayed better performance than a typical uncontrolled filling layer. The variation of PGA and displacement values with the depth of soil profiles for NLA can be seen in Figure 5. PGA values are measured with reference to the top of the related soil layer. The PGA of the applied ground motion is 0.22g. The upper layers of BHI and BHIII borehole logs amplified the PGA up to 0.32g and 0.27g, respectively. Considering the PGA 0.22g input motion, the increase in acceleration is calculated as 45% and 23%, respectively. The lower layers of those profiles and all layers of BHII and BHIV borehole logs displayed deamplification of seismic waves. The maximum deamplification is observed as 78% by the lowest layer of BHIV which mainly consists of very stiff hard clay layers. The highest lateral displacement was calculated by BHII as 14 mm so that it is almost constant along with the depth of profile.

5.2 Equivalent Linear Analysis

The variation of acceleration response spectra with 5% damping for ELA is represented in Figure 6. The highest acceleration values are obtained by top layers of BHI, BHIII and BHIV as 1.3g, 1.4g and 0.8g, respectively. These results of the ELA analysis indicate a considerable change in the characteristics of seismic incident waves by amplifying them at surface layers.

However, lower layers of those boreholes consisting of very stiff clay layers deamplified the applied motion. The soil layers of the BHII borehole log consists of stiff clay layers that deamplified the acceleration of the input motion down to 0.4g. The variation of PGA and displacement values with the depth of soil profiles for ELA can be seen in Figure 7. Remembering the PGA of the input motion is 0.22g, the PGA values calculated at surface layers of the soil profiles of BHI, BHII and BHIV borehole logs are lower than of the applied input motion. The deamplification observed by BHII borehole log is attributed to the stiff clay layers. The displacements calculated by BHII and BHIV borehole logs are observed to have the highest values at the surface as 22 mm and 20 mm, respectively. In contrast to the measured acceleration values, it was observed that the maximum displacement values obtained along the depth of the soil profiles were varied within a limited range for each of the investigated boreholes.

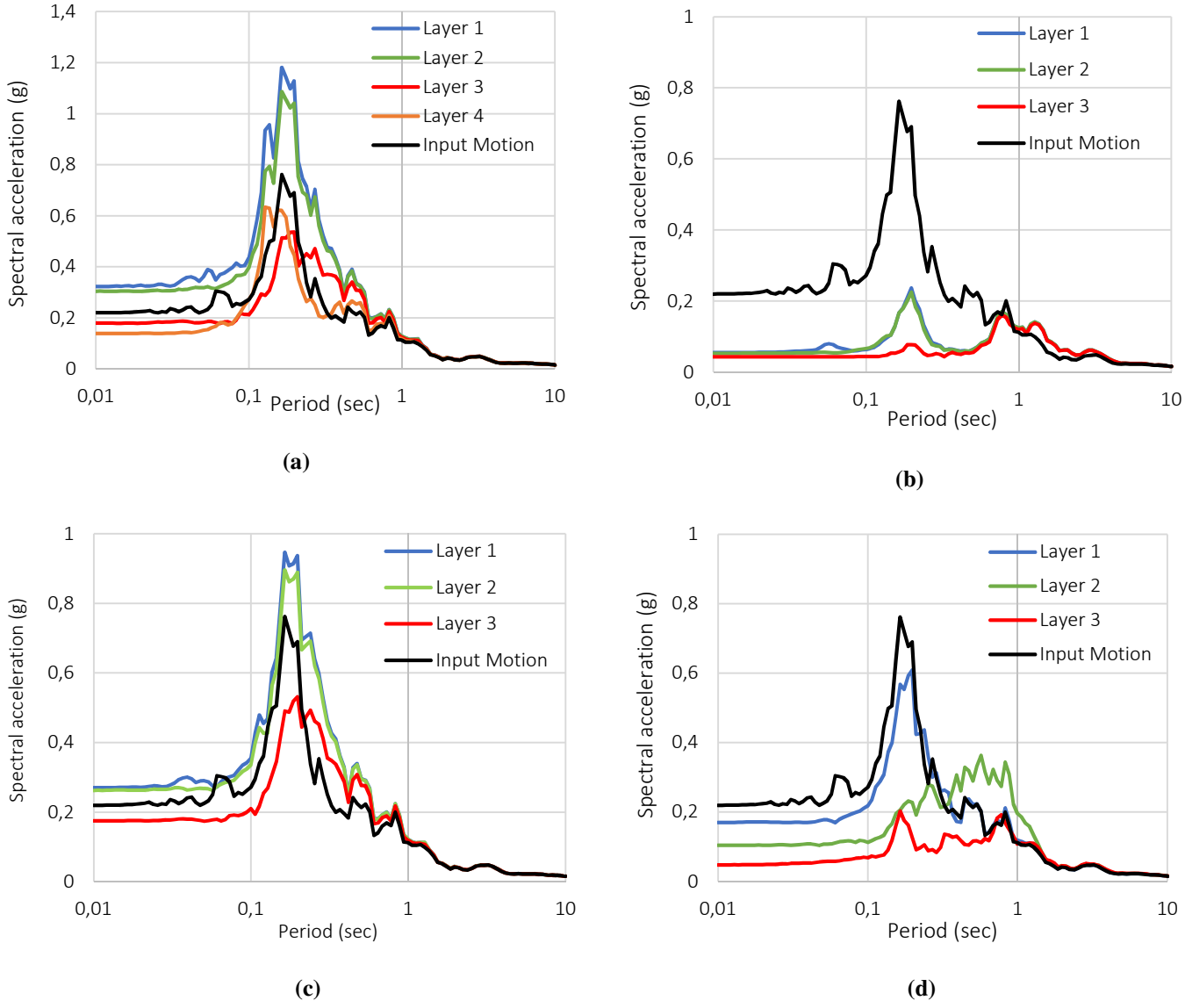

Figure 4. Site response spectra for a.BHI, b.BHII, c.BHIII and d.BHIV under Kocaeli Earthquake (NLA)

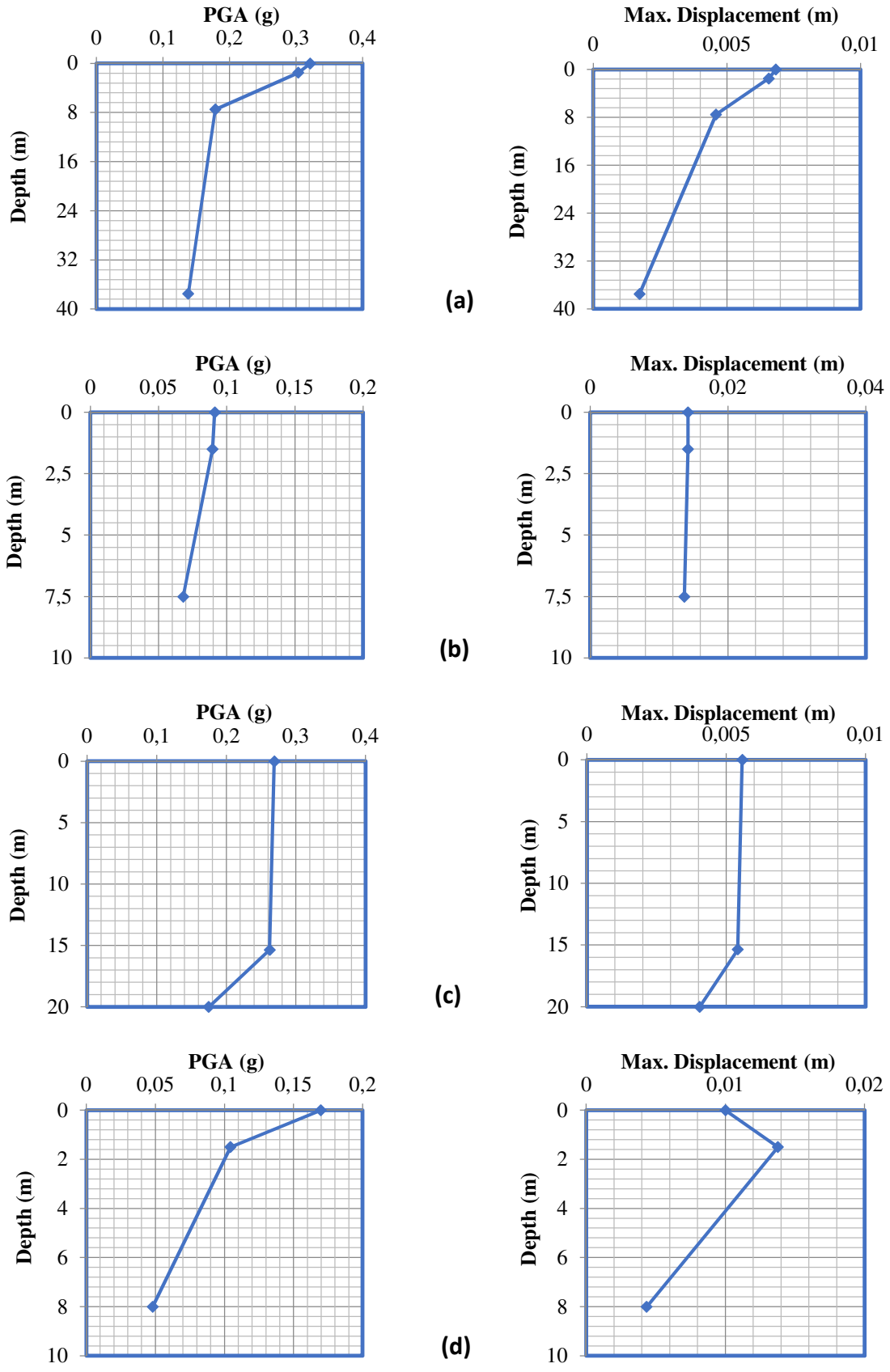

Figure 5. The variation of PGA values and maximum displacement with depth for a.BHI, b.BHII, c.BHIII and d.BHIV under Kocaeli Earthquake (NLA)

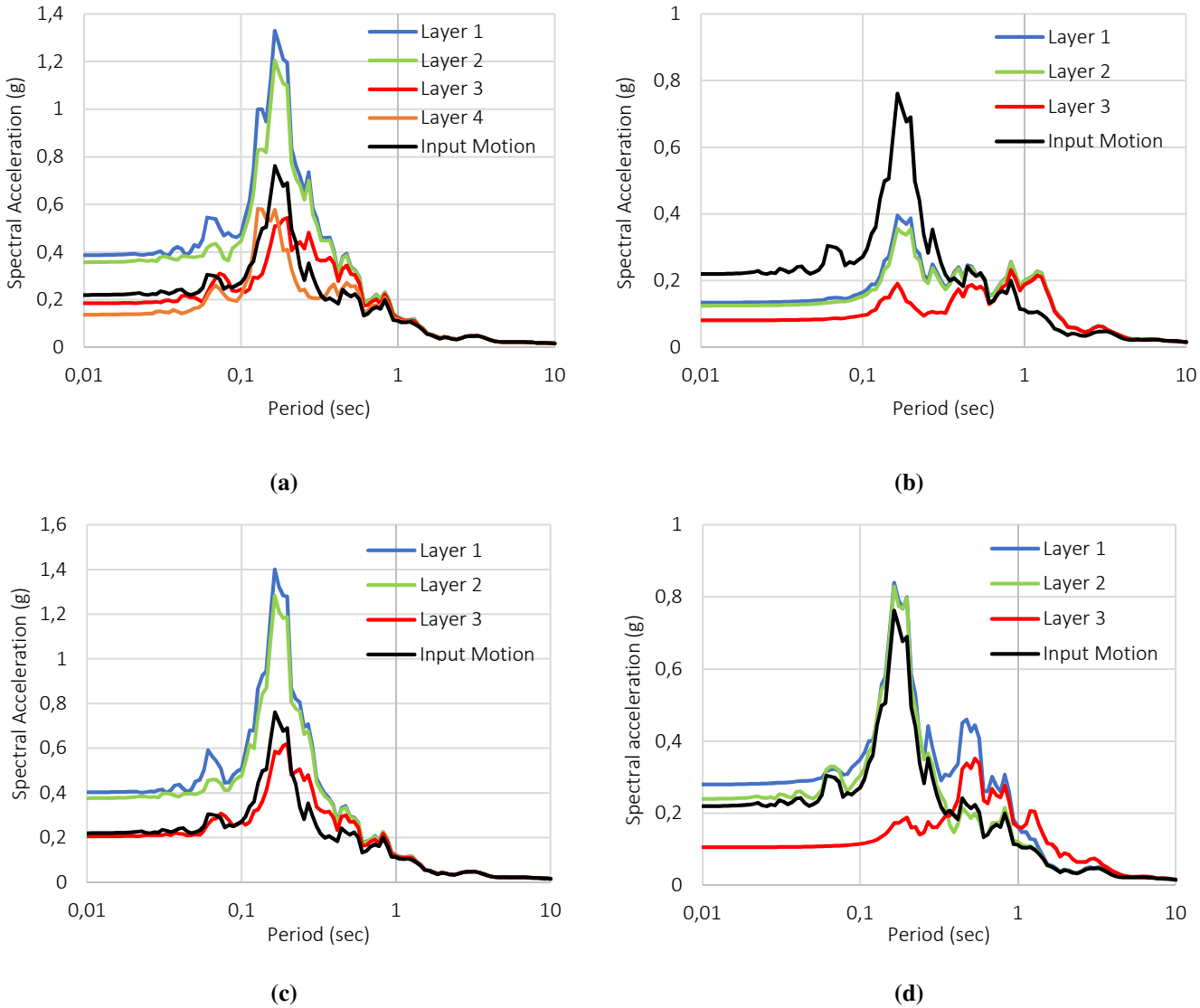

Figure 6. Site response spectra for a.BHI, b.BHII, c.BHIII and d.BHIV under Kocaeli Earthquake (ELA)

The results of the analyses are summarized in Table 3. The results obtained by both NLA and ELA demonstrate that the upper layers of the BHI and BHIII borehole logs amplified the accelerations, while the lower layers deamplified the seismic motion. There is a decrease of 45% and 22% in PGA values of BHI and BHIII obtained by NLA, respectively. The maximum deamplification observed by the lowest layer of BHII and BHIV borehole logs as 69% and 78 %, respectively. Considering the results of ELA, the seismic waves are amplified as 73% and 81% at surface layers of BHI and BHIII, respectively. The deamplification ratios observed by the BHIII borehole log from the lowest layer to the surface layer are 61%, 43% and 40% respectively. Inconsistent with the literature studies, the soil response of ELA using the total stress method demonstrates higher PGA values than of NLA which based on the effective stress method. This is due to the linear nature of ELA using only a single value of stiffness and damping for the entire duration of the ground motion. This over-predicted stiffness and under-predicted damping for shear strain greater than the effective shear strain leads to higher PGA values. Although it is known that ELA lacks the ability to exhibit the non-linear behavior of soils under seismic loading, it is widely used in literature studies with NLA due to its easy application. It was observed that the calculated maximum displacement values obtained by both approaches are very close to each other for all cases.

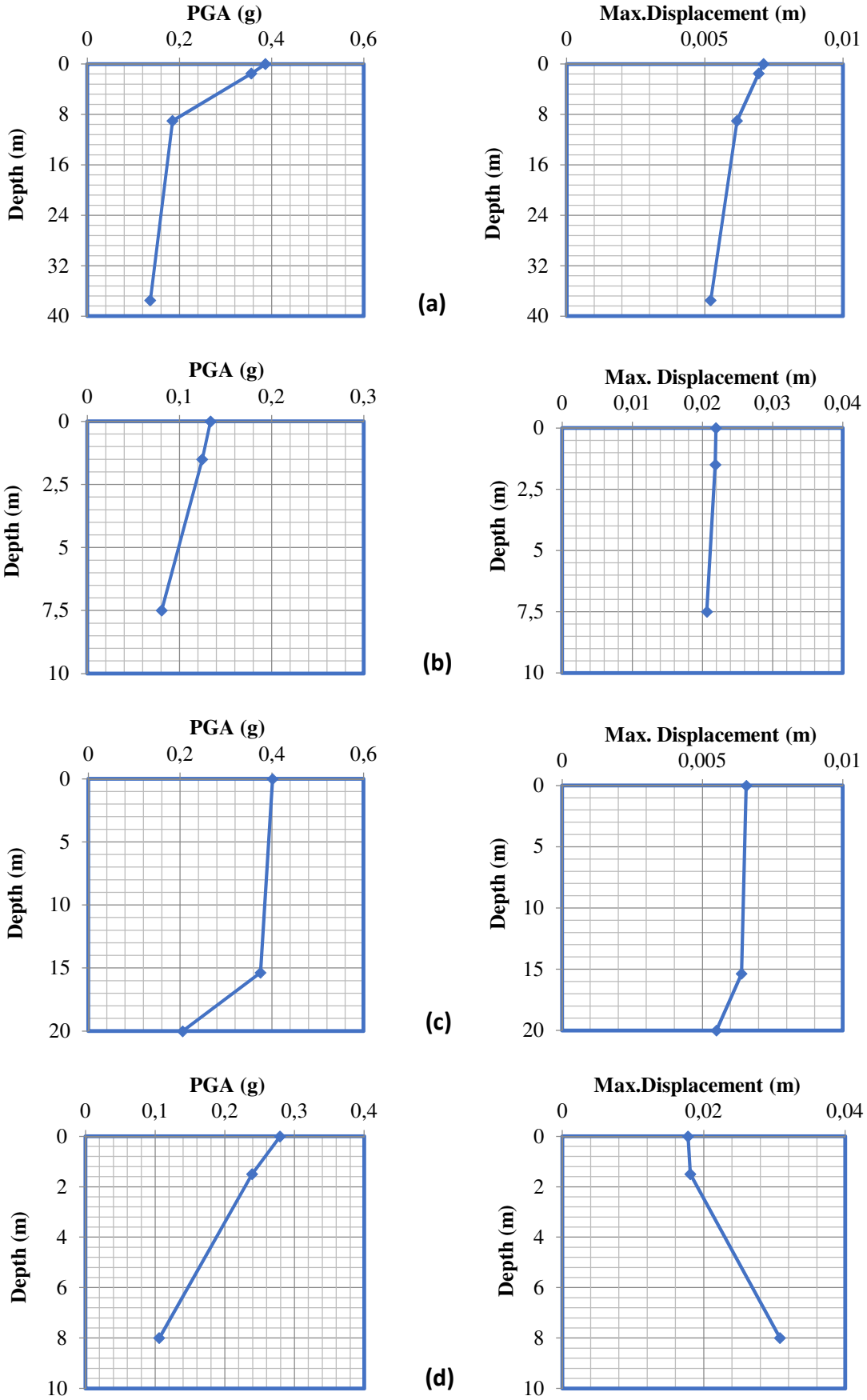

Figure 7. The variation of PGA values and maximum displacement with depth for a.BHI, b.BHII, c.BHIII and d.BHIV under Kocaeli Earthquake (ELA)

Table 3. Summary of the analysis results

Borehole	NLA			ELA		
	PGA (g)	Difference (%)	Displacement (m)	PGA (g)	Difference (%)	Displacement (m)
BHI	0,321078	45% ↑	0,006826	0,386095	73% ↑	0,007120
	0,303349	36% ↑	0,006559	0,355740	64% ↑	0,006943
	0,178422	19% ↓	0,004586	0,184802	16% ↓	0,006161
	0,137776	37% ↓	0,001726	0,136516	38% ↓	0,005206
BHII	0,091161	59% ↓	0,014195	0,133641	40% ↓	0,021923
	0,089528	60% ↓	0,014181	0,124590	43% ↓	0,021836
	0,067955	69% ↓	0,013662	0,080556	61% ↓	0,020628
BHIII	0,268959	22% ↑	0,005571	0,401524	81% ↑	0,006562
	0,262159	19% ↑	0,005410	0,375257	68% ↑	0,006392
	0,174588	21% ↓	0,004041	0,205297	9% ↓	0,005492
BHIV	0,169559	23% ↓	0,009995	0,279067	27% ↑	0,017765
	0,104224	53% ↓	0,013772	0,238967	9% ↑	0,018100
	0,047910	78% ↓	0,004337	0,105624	50% ↓	0,030765

* The red arrow reflects the amplification in PGA. The green arrow reflects the deamplification in PGA. The difference in PGA is calculated with respect to the input motion with PGA: 0.22g.

5.3. Liquefaction Analysis

In site response analysis studies, another issue that is as important as the effects of soils on the propagation of earthquake waves is the evaluation of the liquefaction potential of the soil under dynamic loadings. It is stated that the soil deposits with clay content may be evaluated as non-liquefiable [16]. It is indicated that soils having a liquid limit (LL) and the plasticity index (PI) lower than 30% and 10% respectively, are prone to liquefaction. The soils may liquefy if all of the following conditions are met; i. percent less than 5 mm < 15%, ii. LL < 35, iii. water content, Wn>0.9*LL [17]. The soil profiles mostly have LL higher than 35%. The natural water content of the tested specimens from the different depths of boreholes is below the limit values. Except for Case I, each of the investigated cases containing a considerably high amount of finer content of the soil. The plasticity index of the tested samples is well above 10%. The measured GWT of Case II, III and IV are varied between 14.60 to19.60 m. Since the location of BHI is close to the river, the GWT is measured as 2 m. However, considering all of the liquefaction susceptibility criteria for the investigated soil profiles, it is concluded that the examined soil profiles have no liquefaction potential (Table 4).

Table 4. Summary of the liquefaction evaluation of the soil profiles

Criteria	Case I	Case II	Case III	Case IV
LL<35 %	NP	62.3%	29-46%	57.9%
W_n>0.9*LL	NP	31.3%	8.6-24.8%	27.6%
Percent finer than 0.005 mm <15%	4.3%	96.3%	30-94%	62.7%
PI<10%	NP	34.3%	10-21.2%	32.9%
GWT<10 m	2	19.60	14.60	16

6. CONCLUSION

In this study, apart from rock units such as greywackes and limestone, the effects of soil conditions within the local geology of Istanbul on the propagation of seismic waves were investigated. 1D site response analyzes were carried out using real earthquake data with two different approaches namely; i. equivalent linear analysis, ii. non-linear analysis. The following conclusions have been drawn from the analysis conducted:

- The amplification of acceleration was observed by BHI and BHIII borehole logs (Layer 1 and 2). The observed amplification effect is attributed to the loose state of the upper layers. The deamplification of seismic waves observed by BHII and BHIV borehole logs is explained with the relatively dense and stiff layers.
- The non-linear analysis approach leads to lower PGA and spectral acceleration values compared to the equivalent linear analysis. This is due to over-predicted stiffness and under-predicted damping for shear strains greater than the effective shear strain.
- Since the liquefaction criteria are not met, the analyzed soil profiles do not pose a liquefaction risk even some of them are individually met by Case I.
- The behavior of the investigated soil units can also represent the behavior of soil profiles with similar characteristics in different regions.

The soil profiles for which seismic site response analyzes are performed belong to a large metropolis area. Therefore, it is not possible to model the entire area with a limited number of analyzes. However, the investigated soil profiles are typical soil formations encountered in various regions of Istanbul. In this sense, selected representative cases are important in predicting the behavior of areas with similar soil properties. It should also be stated that the amount of amplification and deamplification will vary with the input motion used.

Acknowledgement: The author would like to thank "DS-Mersa Proje Uluslararası Müh. ve Müş. Ltd. Şti." for their support.

REFERENCES

[1] Tezcan, S. S. and İpek, M. (1973). Long Distance Effects of the March 28, 1970 Gediz Turkey Earthquake, *Earthquake Engineering and Structural Dynamics,* 1, 203- 215.

[2] Hashash, Y.M.A., Phillipes, C. and Groholski, D. (2010). Recent Advances in Non-linear site response analysis, *5th International Conference on Recent Advances in Geotechnical Earthquake Engineering and Soil Dynamics*, San Diego, California, 1-21.

[3] Seed, H.B. and Idriss, I.M. (1969). Influence of soil conditions on ground motions during earthquakes, *Journal of the Soil Mechanics and Foundation Division (ASCE),* 95, 99-137.

[4] Idriss, I.M. and Sun, J.I. (1992). Shake91: A computer program for conducting equivalent linear seismic response analysis of horizontally layered soil deposits. *User's Guide, Center for Geotechnical Modeling, Civil Engineering Department*, UC Davis.

[5] Schnabel, P.B., Lysmer, J. and Seed, H.B. (1972). SHAKE-A computer program for earthquake analysis of horizontally layered sites, *Earthquake Engineering Research Center*, University of California, Berkeley, Report No. EERC 72-12.

[6] Park, D. and Hashash, Y.M.A. (2004). Soil damping formulation in nonlinear time domain site response analysis, *Journal of Earthquake Engineering*, 8(2), 249:274.

[7] Hashash, Y.M.A., Dashti, S., Romero, M.I., Ghayoomi, M., and Musgrove, M. (2015). Evaluation of 1-D seismic site response modeling of sand using centrifuge experiments, *Soil Dynamics and Earthquake Engineering*, 78, 19–31.

[8] Hashash, Y.M.A. and Park, D. (2001). Non-linear one-dimensional seismic ground motion propagation in the Mississippi embayment, *Engineering Geology*, 62(1-3), 185-206.

[9] Park, D.and Hashash, Y.M.A. (2008). Rate-dependent soil behavior in seismic site response analysis, *Canadian Geotechnical Journal,* 45(4), 454-469.

[10] Edinçliler, A. and Calikoglu, M. (2016). Comparison of Site Response of Unimproved and Improved Soils Using DEEPSOIL, *12th International Congress on Advances in Civil Engineering, ACE 2016*, Bogazici University, Istanbul, Turkey.

[11] Edinçliler, A. and Tuncay, G.S. (2018). Nonlinear and Equivalent Linear Site Response Analysis for the Bodrum Region, *Eurasian Journal of Civil Engineering and Architecture,* 2 (2), 59-68.

[12] Yıldırım, M., Tonaroğlu, M., Selçuk, M.E. and Akgüner, C. (2013). Revised stratigraphy of the tertiary deposits of Istanbul and their engineering properties, *Bulletin of Engineering Geology and the Environment*, 72(3-4), 413-420.

[13] Groholski, D.R., Hashash, Y.M.A., Kim, B., Musgrove, M., Harmon, J. and Stewart, J.P. (2016). Simplified Model for Small-Strain Nonlinearity and Strength in 1D Seismic Site Response Analysis, *Geotech. Geoenviron. Eng., ASCE 142*, 9.

[14] Darendeli, M.B. (2001). *Development of a new family of normalized modulus reduction and material damping curves*, Ph.D. dissertation, University of Texas at Austin.

[15] İyisan, R. (1996). Correlations between shear wave velocity and in-situ penetration test results, *Tech. J. Chamber Civil Eng.* Turkey, 7, 1187–99 (in Turkish).

[16] Youd, T.L., Idriss, I.M., Andrus, R.D., Arango, I., Castro, G., Christian, J.T., Dobry, R., Finn, L.W.D.,. Harder, L.F Jr, Hynes, M.E., Ishihara, K.J.P., Koester, S.S.C. Liao, W.F. Marcuson III, G.R. Martin, J.K. Mitchell, Y. Moriwaki, M.S. Power, P.K. Robertson, H.B. Seed, K.H. Stokoe. (2001). Liquefaction Resistance of Soils: Summary Report from the 1996 NCEER and 1998 NCEER/NSF Workshops on Evaluation of Liquefaction Resistance of Soils, *JGGE*, 127(10).

[17] Seed, H.B. and Idriss, I.M. (1982). Ground motions and soil liquefaction during earthquakes, EERI Monograph, Berkeley, CA.